EXPLORING THE MASTER CURVE PARAMETERS FOR EFFICIENT PERFORMANCE GRADING OF ASPHALT BINDERS FROM THE UNITED STATES OF AMERICA

By

SHIVANTHI PRABUDDHIKA DHARMARATHNA

A thesis submitted to the Graduate Program in Chemistry
in conformity with the requirements for the
Degree of Master of Science

Queen's University
Kingston, Ontario, Canada
(April, 2024)

Copyright © Shivanthi Prabuddhika Dharmarathna, 2024

Abstract

The importance of road infrastructure for national economic development is undeniable. However, countries like the United States of America (USA), with cold climates, face challenges in achieving long-term performance with asphalt pavements. Therefore, attention should be paid to the asphalt binder acceptance criteria used, and concerted efforts are required to develop and design test methods with high accuracy, sensitivity, repeatability, and reproducibility. Testing 39 asphalt binders from nine USA states across three different regions was representative of a wide range of binders. This study utilized Dynamic Shear Rheometer (DSR) testing to obtain rheological indicators such as $T_{\delta=30^\circ}$, $T_{\delta=45^\circ}$, Intermediate Temperature Performance Grade (ITPG), and master curve parameters under slow and fast cooling rates. Significant correlations between DSR indicators at different cooling rates were observed. Considering efficiency in time consumption, fast cooling emerges as the preferred method for DSR testing. The Extended Bending Beam Rheometer (EBBR) test is used to determine low-temperature cracking performance, and the Double-Edge-Notched Tension (DENT) test is used to measure the ductile strain tolerance. These tests are time consuming and require a larger sample quantity, even though they are rigorous and accurate. Hence, the study also evaluated the feasibility of using DSR indicators at different cooling rates as an alternative to the laborious EBBR and DENT tests. For this set of USA binders, $T_{\delta=30^\circ}$, $T_{\delta=45^\circ}$, and ITPG serve as viable alternatives for EBBR Limiting Low-Temperature Performance Grade (LLTPG). Grade loss from EBBR indicates thermo-reversible aging due to oil exudation in asphalt, surpassing DSR's capabilities, thus, DSR indicators cannot replace grade loss. The $T_{\delta=30^\circ}$, $T_{\delta=45^\circ}$, and ITPG demonstrated a reasonable correlation with the critical Crack Tip Opening Displacement (CTOD) obtained from the DENT test. Due to the wide variety of asphalt binders in the USA, the correlations for this set of USA binders deviated from those of previously tested Ontario binders, primarily because USA binders are harder while Ontario binders are softer. None of the master curve parameters proved sufficient substitutes for the EBBR or DENT test indicators. Black space diagrams were used to classify binders as thermo-rheologically simple or complex. The chemical characterization of asphalt binders was done using X-Ray Fluorescence (XRF), Nuclear Magnetic Resonance (NMR), and Fourier Transform Infrared (FTIR) spectroscopies. XRF detects recycled engine oil addition, NMR correlates low-temperature performance grade from the bending beam rheometer with the relative average length of the paraffinic internal methylene chain, and FTIR shows changes in quantity of functional groups with binder aging.

Acknowledgements

My earnest gratitude goes to my supervisor, Prof. Simon A. M. Hesp, for his immense support, guidance, and supervision throughout my studies at Queen's University. His generosity in providing me with this opportunity to study at Queen's University will always be in my heart. I am profoundly appreciative of the opportunity to work with and learn from him, and I value his welcoming personality and thoughtfulness throughout my study period.

I humbly express my gratitude to my supervisory committee, Prof. Gregory Jerkiewicz, Prof. Guojun Liu, and Prof. Robin A. Hutchinson, for their valuable suggestions and feedback, which significantly contributed to the successful completion of my master's degree program.

I extend my appreciation to Mr. Chanaka Nawarathna and Dr. Jianmin Ma for their immense support in gathering the data for my research work and for their guidance throughout my study period. I am also grateful to my colleagues, Ms. Pramodya Undugoda, Mr. Dariush Kokabi, and Mr. Hai Yuan, for their assistance in various ways.

Alberta Innovates and the Natural Sciences and Engineering Research Council are gratefully acknowledged for the financial support of this research project.

Lastly, I would like to express my heartfelt gratitude to my family. To my parents, Mr. K. P. Dharmarathna and Mrs. D. M. R. Dasanayake, my husband, Mr. Devaka Rajasekara, my sister, Miss. Lakshika Dharmarathna, my brother, Mr. Nipun Dharmarathna, and all my relatives for their support, encouragement, and unfailing love. Their faith in me has been a constant source of strength and inspiration.

This work would not have been possible without the contributions and support of each one of you.

Content

List of Figures

List of Tables

List of Abbreviations

AASHTO	American Association of State and Highway Transportation Officials
ASTM	American Society for Testing and Materials
BBR	Bending Beam Rheometer
CA	Christensen Anderson
CTOD	Crack Tip Opening Displacement
DCM	Dichloromethane
DENT	Double-Edge-Notched Tension
DSR	Dynamic Shear Rheometer
EBBR	Extended Bending Beam Rheometer
FTIR	Fourier Transform Infrared
GL	Grade Loss
HMA	Hot Mix Asphalt
HTPG	High Temperature Performance Grade
ITPG	Intermediate Temperature Performance Grade
LLTPG	Limiting Low-Temperature Performance Grade
LS	Laboratory Standard
LTPG	Low-Temperature Performance Grade
MTO	Ministry of Transportation of Ontario
NMR	Nuclear Magnetic Resonance
PG	Performance Grade
PAV	Pressure Aging Vessel
REOB	Recycled Engine Oil Bottom
RTFO	Rolling Thin Film Oven
SARA	Saturates, Aromatics, Resins, and Asphaltene
SATS	Saturation Aging Tensile Stiffness
SBS	Styrene Butadiene Styrene
SB	Styrene Butadiene
SHRP	Strategic Highway Research Program
TMS	Tetramethylsilane
USA	United States of America
WLF	Williams Landel and Ferry
XRF	X-Ray Fluorescence

List of Symbols

$\sigma_{net,5mm}$	Average net section peak stress
G^*	Complex modulus
β	Constant that describes the shape of the plastic zone
m_t	Creep rate
s_t	Creep stiffness
ΔT_c	Difference between limiting stiffness and m-value critical temperatures
ω_c	Crossover frequency
G_c	Crossover modulus
$\Delta T_{c\delta}$	Difference between limiting temperature at phase angle 45° and 30°
C_1	Empirical constants
C_2	Empirical constants
$W_{essential}$	Essential fracture work
T_g	Glass transition temperature
G_g	Glassy modulus
a_T	Horizontal shift factor
L	Length of the ligament
T_m	Limiting m-value temperature
T_s	Limiting stiffness temperature
$T_{\delta=30°}$	Limiting temperature at phase angle 30°
$T_{\delta=45°}$	Limiting temperature at phase angle 45°
G''	Loss modulus
T	Operational temperature
δ	Phase angle
$W_{plastic}$	Plastic work
f_r	Reduced frequency
T_{REF}	Reference temperature
R_m	Rheological index
α_T	Shift factor at a particular temperature
w_e	Specific essential work of failure
w_p	Specific plastic work of failure
w_t	Specific total work of failure
G'	Storage modulus
f	Tested frequency
B	Thickness of the specimen
W_{total}	Total energy
b_T	Vertical shift factor

Chapter 1

Introduction

1.1 Overview

In pavement construction, the asphalt binder serves as a glue that holds the aggregate and fines together and provides effective control of the various potential distresses under prevailing climatic and traffic conditions [1]. Asphalt binders play a pivotal role in the construction of durable and secure driving surfaces such as divided freeways, highways, secondary roads, and airport runways. The utilization of asphalt in road construction offers several advantages. Notably, hot mix asphalt (HMA) exhibits exceptional versatility, enabling its efficient placement to yield enduring road surfaces, both in busy urban areas and remote areas. Furthermore, once constructed, asphalt roads are easy to maintain and can be subject to multiple recycling cycles upon reaching their end of life. Adoption of asphalt in road construction can yield advantageous environmental outcomes, particularly with respect to greenhouse gas emissions [2].

The combination of oxidation and volatilization at high summer temperatures and structural rearrangement at cold temperatures in fall, winter, and spring (wax crystallization, asphaltene clustering, free volume shrinkage, and phase separation) collectively contribute to the deterioration of pavement serviceability. However, the implementation of an effective asphalt binder specification assures sustainable pavement performance, as pavement designs are optimized based on life cycle costs to the economy and environment. Incorporating more accurate, precise, and sensitive methods can substantially benefit both users and producers alike. While binder makes up only a minor part of the HMA, its rheological properties exert a predominant influence on performance, particularly in terms of cracking in the pavement [2, 3].

1.2 Chemistry of Asphalt

Asphalt contains bitumen as the predominant component that binds gravel, sand, and mineral powder [4, 5, 6]. According to the American Society for Testing and Materials (ASTM), bitumen is a general term for a group of amorphous, dark colored cementitious substances. Due to its capacity to adhere, bitumen serves as a binding component in asphalt concrete, which is then extensively utilized in a variety of applications in pavement designs including highways, roads, airport runways, and parking lots, producing a significant impact on the life span of its applications [5].

It is difficult to comprehend the chemistry of the asphalt binder since it has a very complex molecular structure. Examining the molecular interactions of asphalt is crucial for understanding the chemistry of asphalt [7, 8]. The chemistry, physical properties, and performance of asphalt binders are influenced by three main molecular interactions. They are London dispersion forces, polar and hydrogen bonds, and π-π forces [8]. London dispersion forces are the most common molecular interactions in asphalt, which govern the behavior of binders by temporarily induced dipoles. These interactions are most important for larger, non-polar molecules in asphalt binders. Polar and hydrogen bond interactions are significant for smaller molecules; they play a lesser role in larger bitumen molecules. Polar interactions are correlated with the asphalt binder's elastic stiffness component. The π-π forces, a third type of interaction, are caused by the delocalized π electrons in the molecules, which are unlimited [7, 8].

Asphalt binder is a complex blend that corresponds to the heaviest fraction obtained from the distillation of crude oil during refining. Since the composition of asphalt is dependent on the source of the crude oil, asphalt from two separate sources will likely have components with moderately varying percentage compositions [3, 9]. Since 90-95 % of asphalt's weight consists of carbon and hydrogen, it can be categorized as a hydrocarbon. A further 82-88 % of it is carbon, while 8-11 % of it is hydrogen. The remainder is made up of metals and heteroatoms. Common heteroatoms include sulfur (0-6 %), nitrogen (0-1 %), and oxygen (0-1.5 %) [10]. The peculiar chemical and physical properties of the asphalt molecule are caused by molecular interactions that result from the substitution of carbon atoms with heteroatoms. Vanadium, iron, and nickel are metals that are present in tiny amounts [8, 11].

Among various characterization techniques, chromatographic techniques can be used to separate and group asphalt into two major chemical groups, maltenes and asphaltenes [8]. The maltene fraction of asphalt binder is soluble in n-heptane, while asphaltene is insoluble in n-heptane. Depending on the solubilities in various solvents, soluble maltene is chromatographically divided into saturates, aromatics, and resins based on polarity [11]. These four fractions are often abbreviated as SARA, which is shown in Figure 1.1 [8]. However, Redelius and Soenen have mentioned that, although asphalt binder is frequently analyzed based on SARA fractions, the behavior of asphalt binder is not the sum of these fractions [3, 8].

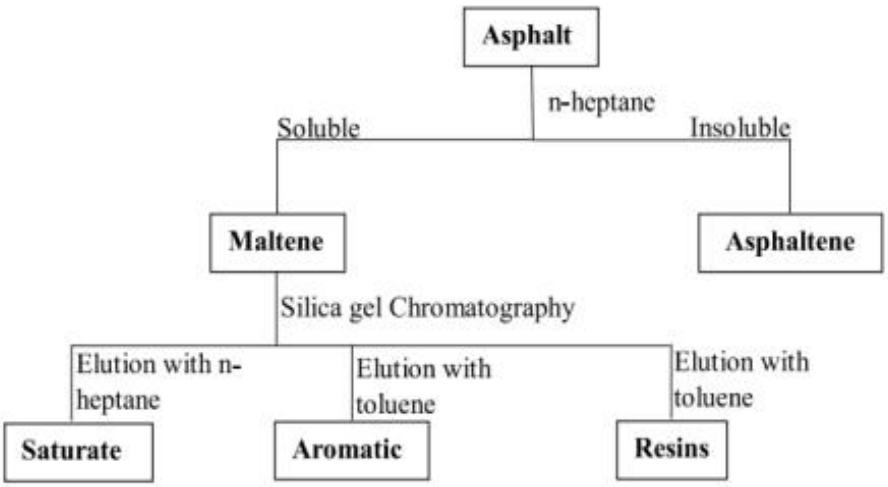

Figure 1.1: Schematic of SARA chromatographic method [10].

According to the conventional colloidal model, asphalt cement is a system of colloidal suspension made of high molecular weight asphaltene micelles dispersed in an oily medium with lower molecular weight maltenes. Maltenes form the continuous phase. Higher molecular weight polar resins operate as a stabilizing solvation layer by adhering to the surface of asphaltene particles and creating a sheath around them to prevent aggregation [10, 12]. The sol-type and gel-type are the two accepted boundary types of bitumen composition. Asphaltenes are completely distributed and mobile inside the maltenes in the sol model, which is illustrated in Figure 1.2. Adequate quantities of resins and aromatics will guarantee the necessary solvating power to fully peptize asphaltenes and maintain their dispersion in solution.

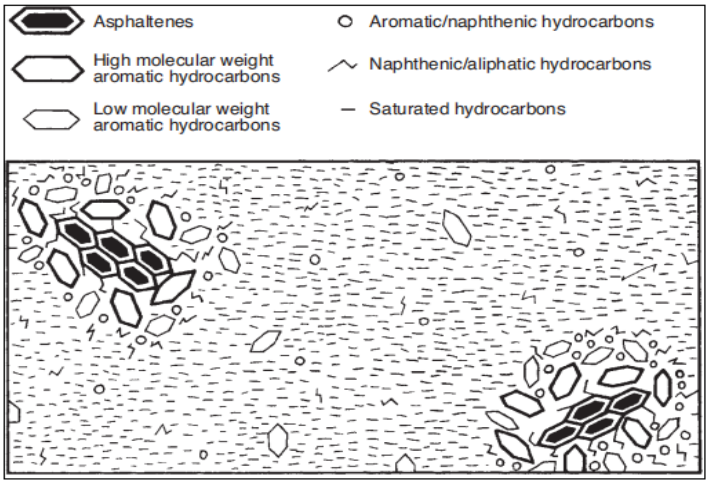

Figure 1.2: Schematic representation of a sol-type model [10].

In the gel model, the maltene fraction is insufficient for accomplishing asphaltene distribution. If the aromatic and resin fractions are not present in sufficient quantities to peptize the micelles or have insufficient solvating power, the asphaltenes can associate further, produce irregular, disconnected structures, and produce the gel-type depicted in Figure 1.3. Asphalt reduces gel behavior as it becomes heated. Most asphalt binders exhibit behavior that falls between the sol and gel types [8, 10].

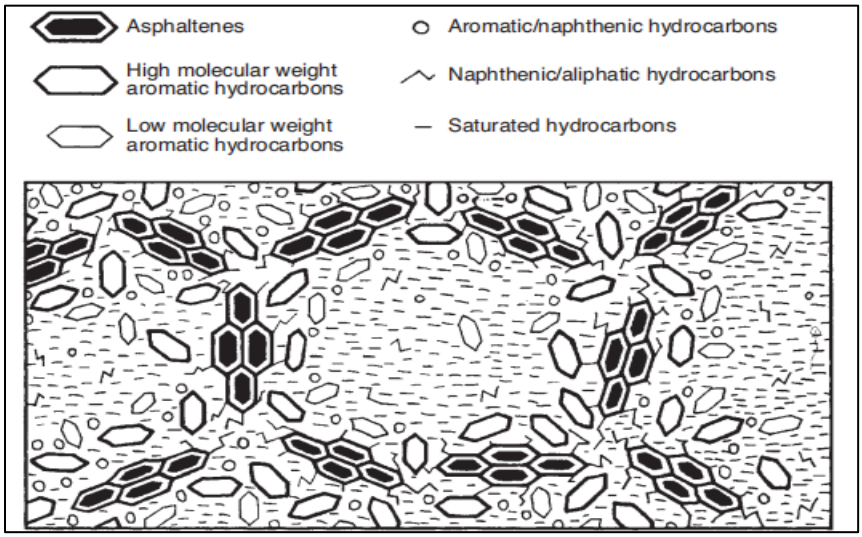

Figure 1.3: Schematic representation of a gel-type model [10].

1.3 Mode of Pavement Failures

Asphalt cement is typically chosen for many road construction applications due to its durability and resilience. Researchers and designers of pavements have discovered that some roads have longer service lifespans than others [13]. Poor building methods, constant traffic loading, and prolonged exposure to harsh climatic conditions can reduce the lifespan of asphalt pavements [14]. Rutting, fatigue, cracking, and moisture damage are the four most typical types of pavement failures. Efforts are constantly made to mitigate above pavement failures [2].

1.3.1 Rutting

Rutting is a common pavement distress that affects the service life and safety of the highway. This is non-recoverable and mainly depends on slow traffic at high temperatures, repeated traffic loads, and weather conditions. The quality of the mixture and construction also affects rutting performance [15, 16, 17]. Asphalt binders become less viscous at high temperatures. This leads to the formation of ruts or tracks on the pavement surface due to the easy flow of the binder under heavy traffic loads, as shown in Figure 1.4. Superpave specifications define and place

the necessity of a rutting factor, G*/sin δ, which represents a measure of the rutting resistance of the asphalt binder. This can be determined from the complex modulus (G*) and phase angle (δ) obtained from the Dynamic Shear Rheometer (DSR) experiment [10]. Higher G* values and lower δ values are considered favorable factors for rutting resistance [18]. Hence, highly stiff and more elastic binders have higher rutting resistance. By using proper aggregate gradations, rutting is effectively controlled [2].

Figure 1.4: Rutting on asphalt pavement [19].

1.3.2 Fatigue Cracking

Recurrent or fluctuating stress that has a maximum value of less than the tensile strength of the material causes fatigue cracking, which is a fracture that is shown in Figure 1.5 [10]. Caused by repetitive heavy traffic loading at moderate temperatures between 15 °C and 30 °C and by construction techniques [1, 6, 20]. Other than that, fatigue cracking is affected by poor subgrade drainage, improper pavement layer design, and inadequate compaction. Fatigue cracking has three stages. Crack initiation is the point at which microcracks begin to form. During crack propagation, microcracks increased in size into macrocracks with stable crack growth. In the end, at the stage of disintegration, an entire loss of fatigue life takes place. Hesp and his coworkers stated that “crack initiation and propagation processes depend on the loading mode in terms of frequency, rest periods, and temperature for a given material composition since fatigue failure involves both energy dissipation and healing” [1]. Fatigue cracks may either initiate at the top or bottom of the asphalt layer and then spread upward or downward [21]. Using the G* and δ discovered by the DSR experiment, the fatigue resistance factor G*sin δ, of the asphalt binder can be evaluated [2, 6, 21, 22].

Figure 1.5: Fatigue cracking on the pavement [23].

1.3.3 Thermal Cracking

Thermal cracking (transverse cracking) is a common form of pavement failure experienced in colder regions like Canada, the United States of America (USA), and other areas in extreme northern and southern latitudes [1, 24]. Thermal cracking of asphalt pavements is attributed to thermal stresses that occur during cooling. When the stress is equal to or higher than the tensile strength of the pavement, a microcrack may be initiated on the surface of the pavement, and, after additional low-temperature cycles, this crack will spread downward through the pavement [25]. Figure 1.6 shows the thermal cracking of a pavement [24].

Thermal cracking is composed of three distinct processes. The first process is referred to as single event thermal cracking. It is the outcome of one catastrophic drop in temperature below a critical value at which the thermal stress generated exceeds the tensile strength of the pavement. The second process is related to the effect of repeated thermal stresses below the critical value, which will eventually weaken the mix and cause it to fail even though the expected critical stress was not achieved. The third process is the impact of recurrent loading caused by regular vehicles and heavy truck traffic. Freeze-thaw cycles are potentially significant in the occurrence of additional transverse cracks during later cold spells [24].

The effect of several different types of factors, such as environmental, material, and pavement structure factors, on the low-temperature behavior of asphalt pavements has been recognized. Binder consistency parameters of materials such as stiffness, viscosity, penetration, and softening point have a strong impact on the thermal cracking of asphalt mixtures. Thermal cracking may lead to poor ride quality, reduced service life, and increased costs for the maintenance of roads [25]. According to Superpave specifications, a Bending Beam Rheometer (BBR) is used to examine thermal cracking, which occurs at low temperatures [24].

Figure 1.6: Thermal cracking of a pavement [24].

1.3.4 Moisture Damage

Moisture damage occurs when asphalt binder is stripped from the aggregate due to the passage of water molecules through the porous asphalt pavement because of rain, snow, and the absorption of groundwater [26]. The intrusion of water can cause a loss of cohesion within the asphalt binder itself or weaken or break bonds between asphalt binders and aggregates, leading to a reduction or loss of adhesion. Figure 1.7 shows a pavement that has undergone moisture damage. The damage is not caused directly by moisture, but its presence increases the extent and severity of already existing distresses such as rutting and cracking. Moisture sensitivity of asphalt mixtures is influenced by factors such as pavement material (chemical composition of asphalt and surface texture of aggregates), mixture design (thickness, air void level, and permeability), environmental factors, and pavement age [27]. Using highly viscous asphalt binder, adhesiveness can be increased and the interference of water with the bonding decreased. Moisture damage can be controlled by proper compaction and by using additives such as antistripping agents [14]. The additives reduce the stripping by increasing the physicochemical bond between the asphalt binder and aggregate and improving the wetting by reducing the surface tension of the binder [27]. The moisture sensitivity of compacted asphalt mixtures was measured using the Saturation Aging Tensile Stiffness (SATS) test.

Figure 1.7: Moisture damage to pavement [14].

1.4 Asphalt Specification Properties

The specification of asphalt should include details on its capacity to withstand stress in a traffic environment, how the material functions in specific geographic environments, and how it behaves in various climatic circumstances [6]. Initially, conventional specifications were established, however, due to the limitations of conventional methods, Superpave specifications were introduced. As a further development, the Ministry of Transportation of Ontario (MTO) innovated new test methods and modified some Superpave tests to meet the actual pavement performance.

1.4.1 Conventional Specifications

The most popular conventional test procedures that have been in use since the 1900s are penetration, viscosity, softening points, and Fraass breaking point. However, these test methods cannot be utilized to assess certain engineering characteristics of asphalt, such as strain and stress. Moreover, there is no connection between the conventional test results and the service performance of roads [6]. Both the viscosity and penetration procedures are empirical, meaning that performance experience on the pavement is needed before the test findings to provide insightful information [6]. Other than that, the complete range of temperatures is not covered by either the viscosity or penetration tests. The elastic behavior of asphalt at low-temperatures cannot be predicted with conventional methods. A detailed explanation of penetration, viscosity, softening point, and Fraass breaking point tests are given below.

The penetration test is the oldest technique. In this method, the characterization and grading of asphalt binders were determined by measuring the extent to which asphalt could be penetrated. Since the penetration test is based on hardness, it indicates the stiffness of the asphalt. The term "soft" refers to asphalt binders with high penetration values, whereas the term "hard" refers to asphalt binders with low penetration values [28]. It is an empirical test. Today's society views penetration grading as insufficient for performance prediction [28]. Decimilimeters, abbreviated as “dmm”, are used to measure penetration.

The viscosity test is based on how the asphalt sample flows at 60 °C. Viscosity is an indicator of the material's resistance to flow. The asphalt substance in viscosity grade bitumen becomes soft at high temperatures and tough at low-temperatures. This relationship between asphalt viscosity and temperature is used to estimate bitumen's adhesion, rheology, durability, and application temperatures [29]. The testing temperature of 60 °C was chosen since it approximates the maximum temperature of paved surfaces in the USA [28].

The softening point test can be used to determine the temperature at which asphalt tends to flow during service. Asphalt gradually softens and reduces viscosity at high-temperatures because it is a viscoelastic substance with no clearly defined melting point [30]. The temperature at which a bitumen sample can no longer withstand the weight of a 3.5 g steel ball is known as the softening point. The apparatus required for this test consists of a Ring-and-Ball apparatus and a thermometer. Temperatures between 30 °C and 157 °C are used to conduct the test [29].

Asphalt's behavior at very low-temperatures is evaluated using the Fraass breaking point test [10]. Fraass breaking point is the temperature at which bitumen first becomes brittle and is measured by the formation of fractures when a thin film of bitumen on a metal plaque is cooled and flexed under specific conditions. The Fraass breaking point of solid and semisolid bitumen can be found using the breaking point apparatus [10].

1.4.2 Superpave Specifications

To develop specifications that fully characterize asphalt binders based on their performance parameters, the USA government funded the Strategic Highway Research Program (SHRP) which developed the Superpave performance grading system [10, 31]. The Superpave system consists of a new and enhanced set of asphalt binder and mixture test techniques as well as concurrent specifications [29]. A binder receives a performance grade from Superpave testing procedures using instruments such as a Rolling Thin Film Oven (RTFO), Pressure Aging Vessel (PAV), DSR, and BBR [10]. According to the Superpave specification, asphalt cement is ranked according to the degree to which it performs in various environmental conditions in the field [31]. In line with the performance grading system, a binder must pass several tests at various temperatures that are chosen based on the climate, load on the pavement (traffic conditions), and aging concerns. A detailed discussion of Superpave specifications is given in section 2.2.

1.4.3 Ministry of Transportation of Ontario (MTO) Specifications

The MTO has investigated certain issues with the Superpave specifications which lead to actual performance failing to meet the expected performance of the pavements. Thus, research was conducted to investigate the premature deterioration of the pavements. This led to the development of new and modified test methods to effectively predict the performance of asphalt, such as the Extended Bending Beam Rheometer (EBBR) test and the Double-Edge-Notched Tension (DENT) test [32]. A detailed discussion of MTO specifications is given under section 2.3.

1.5 Objectives

Roads constitute the backbone of having a highly functional transport network and keeping them well maintained is crucial for economic growth and stability. Consequently, a significant amount of effort is invested in enhancing the performance and durability of asphalt mixtures [3]. To enhance their durability and performance, scientists have mainly focused on improving the specifications of asphalt binders, as it is necessary to know whether the physical response of an asphalt mixture is suitable for road operations [3].

Specifically, the investigation involves a comparative analysis of rheological indicators derived from the DSR test obtained under two different conditioning times: 1-hour (slow cooling), and 10-minute (fast cooling). To achieve this, all the rheological indicators obtained under the slow and fast cooling rates with the DSR are systematically compared. Then the impact of cooling rates on the sensitivity and magnitude of different DSR indicators are examined. This investigation contributes to the understanding of asphalt binder characteristics under varying conditioning times, thereby enhancing the precision and applicability of rheological assessments in practical applications and specification development.

Currently, both the EBBR and DENT tests are used for determining resistance of asphalt to low-temperature cracking and assessing asphalt failure at intermediate temperatures respectively. However, notable limitations of this methodologies are the extensive time consumption and the high quantity of samples required. Here the potential substitution of EBBR and DENT tests with the DSR test is explored. This substitution could offer benefits by enabling the prediction of low and intermediate temperature performance in a shorter timeframe with reduced sample requirements [2]. Thus, rheological indicators obtained from the DSR tests are utilized to investigate potential correlations present between EBBR and DENT test indicators. The primary focus is to recognize which indicators are most appropriate, practical, and accurate for future specifications testing. The goal is to identify properties that are effective in the control of road cracking, with practicality defined in terms of simplicity, speed, precision, and cost effectiveness. A comparison between different rankings and the effect of cold conditioning is focused here. This work may contribute to seeking valuable insights into the selection of optimal asphalt binder properties for enhanced testing efficiency and the development of future specifications. To implement the most suitable, practical, accurate, and precise specification, the repeatability and reproducibility of the testing protocol need to be validated [33]. The assessment of repeatability and reproducibility has considerable significance in

ensuring the reliability of the testing methodology. When a measurement is accurate, it is close to the true value. Precision, on the other hand, is a measure of the extent to which measurements done repeatedly under the same conditions can provide identical results. Precision is related to repeatability and reproducibility. It is noteworthy that a system can be accurate but lacking in precision, precise but inaccurate, or neither accurate nor precise, and conversely, it can exhibit both qualities [34]. Repeatability is frequently used to characterize the variation in successive measurements of the same variable acquired under the same conditions such as the same observer, location, instrument, and procedure in a short period [34, 35, 36]. Reproducibility provides insights into the broader applicability and reliability of the testing protocol, offering a comprehensive evaluation of the method's consistency and robustness across varying experimental conditions.

Another principal objective of this research initiative is to establish correlations between the chemical structure of asphalt polymer and its corresponding behavior. This investigation employs advanced spectroscopic techniques, namely X-Ray Fluorescence (XRF), Nuclear Magnetic Resonance (NMR), and Fourier Transform Infrared (FTIR). The analytical framework takes into careful consideration the origin of the binder, recognizing its potential influence on the chemical composition and performance characteristics.

Chapter 2

Literature Review

2.1 Rheological Properties of Asphalt Binder

Rheology is the study of the properties of a material or its flow behavior under various deformation conditions. The name "rheology" was developed by Professor Eugene C. Bingham while he was studying the qualities of materials that exhibited both the elastic properties of solids and the flow characteristics of liquids [10]. It is crucial to discuss the rheological properties of the asphalt binder because those properties significantly impact how asphalt pavements behave [1, 10]. These rheological properties determine the viscoelastic behavior of asphalt binders. The viscoelasticity of asphalt has a huge impact on pavement performance, specifically its ability to resist permanent deformation and cracking [10, 37].

The viscous and elastic properties of the binder determine the recovery response for each state of deformation. To effectively model pavement response and predict pavement performance, it is mandatory to accurately predict the stress-strain response of the binder over a broad range of temperatures, loading times, and stresses or strains [38]. Stress is the deformation force per unit area, and strain is the degree of deformation due to stress. To specify the stress-strain behavior of materials, shear tests are used in the laboratory. Shear tests are conducted under controlled stress or controlled strain conditions. Materials having a linear stress-strain behavior largely independent of time and temperature can be productively characterized by the elastic (Young's) modulus. On the other hand, Newtonian fluids can be characterized through the viscosity coefficient [38]. Viscoelastic materials, such as asphalt, must be characterized with test methods that account for the loading time and the loading temperature. The creep test is a simple test used for characterizing the stress-strain response of a material [38]. In this test, a constant load is applied to a material between time t_0 and time t_i, and then the load is removed. The inherent strain responses for elastic, viscous, and viscoelastic materials are readily apparent, as shown in Figure 2.1 [38].

The ability to store deformation energy is determined by the elasticity of the binder. Ideal solids exhibit elastic behavior by regaining their original shape and properties when a force or stress is removed. Most solid materials are elastic, and the response to very small stresses causes a strain that is precisely proportional to the stress, which is known as Hooke's law. When an elastic material is loaded in creep, it will immediately deform to a constant strain. When the load is removed, the material will immediately return to its initial shape (Figure 2.1 (a)) [10, 38].

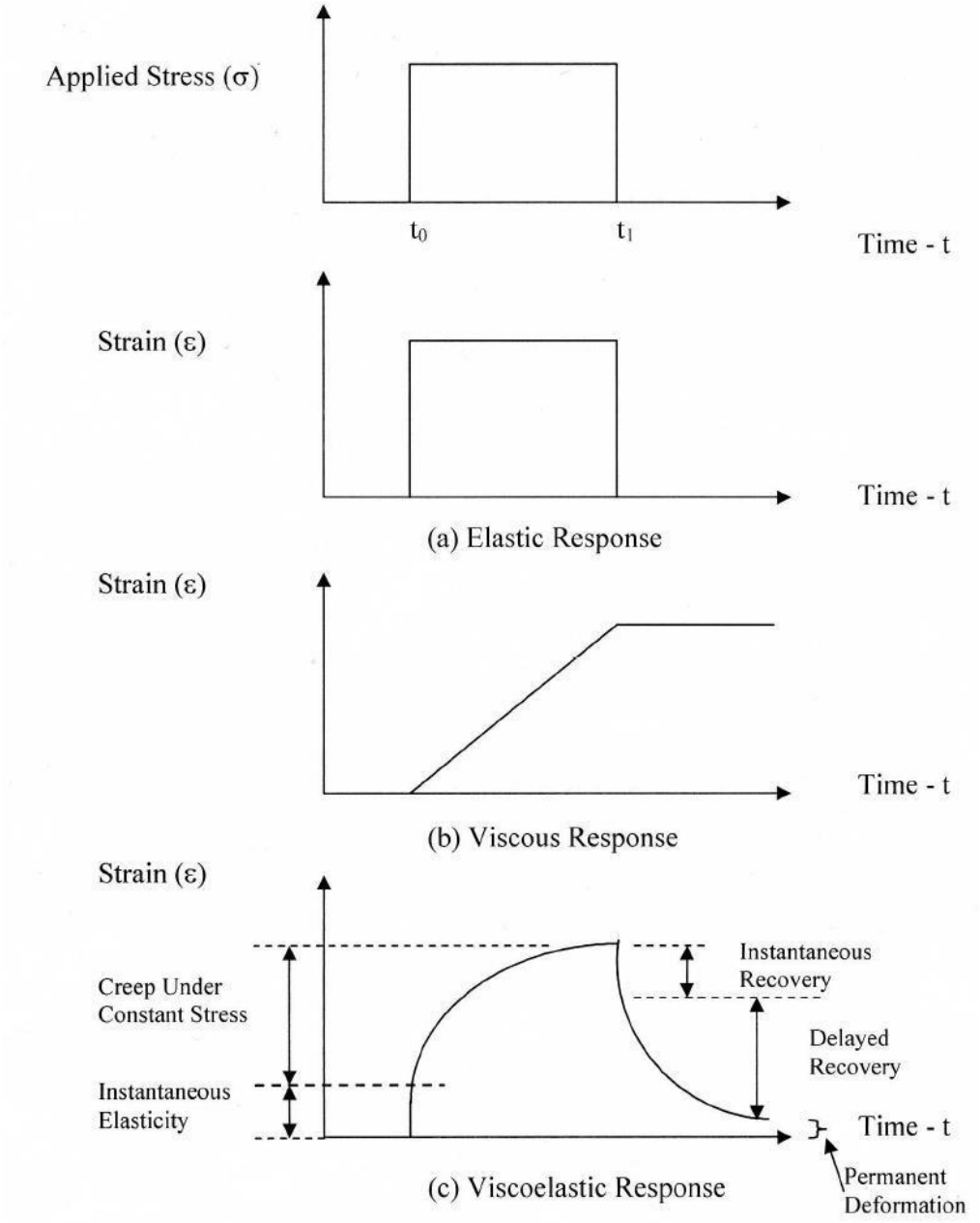

Figure 2.1: Idealized response of a) Elastic, b) Viscous, and c) Viscoelastic materials under creep loading [28].

The viscosity evaluates its ability to resist flow. This reflects the dissipation of deformation energy through flow. Liquids act in a viscous manner and are not able to recover their original shape after loading. In a viscous fluid, the stress is proportional to the rate of strain. On the other hand, viscous material will deform at a constant rate when the load is exerted at t_0. Deformation will continue at the same rate until the load is removed at t_i. After t_i, there was no further deflection or recovery as shown in Figure 2.1 (b) [10, 38].

Between two ideal elastic and viscous states, materials can display viscoelastic behavior, in which the reaction to stress is partially viscous and partially elastic. It is possible to quantify the degree to which a material exhibits viscoelastic behavior. Marcus Reiner, a professor at the Israel Institute of Technology, proposed the Deborah number (De) as a measure of a material's viscoelasticity [10]. The viscoelasticity of a material describes its mechanical characteristics depending on the temperature and the period of loading. Viscoelastic materials behave as a glass like elastic solid at low-temperatures and/or during short loading and as a viscous fluid at high-temperatures and/or during slow loading [10]. A viscoelastic material, as shown in Figure 2.1 (c), has both elastic and viscous components of response. When loaded in creep, there is an instantaneous deformation, corresponding to the elastic response, followed by a gradual time dependent deformation until the load is removed. This time dependent deformation may further be classified into a purely viscous component and a delayed elastic component. After removing the load at t_i, the viscous flow ceases, and none of this deformation is recovered (residual permanent viscous strain remains). However, the delayed elastic deformation is recovered, but not instantly as with purely elastic deformation. Instead, once the load is removed, the delayed elastic deformation is slowly recovered at a decreasing rate [38].

2.2 Superpave Testing for Asphalt

The USA government funded the SHRP, which created Superpave, to provide standards that effectively characterize asphalt binders based on their performance parameters. The goal of this five-year research project was to enhance the performance, durability, protection, and efficiency of the nation's highway system [6, 39]. The American Association of State Highway and Transportation Officials (AASHTO) accepted Superpave tests. These methods of testing were developed to assess how well and accurately an asphalt binder performs under the various temperature conditions that pavements are subject to [28, 35, 38]. Utilizing the Superpave tests, performance grades were determined for high-temperature, intermediate-temperature, and low-temperature [14].

2.2.1 Performance Grade (PG)

PG for asphalt cement is indicated as PG XX-YY, where XX denotes the maximum working limitations of asphalt binder while YY denotes its minimum working limits [14]. For instance, the first digits, 64, in PG 64-22 have been referred to as the "high-temperature grade". This indicates that the binder would be physically capable of resisting rutting up to 64 °C. This implies a high pavement temperature that corresponds to the actual climate where the

binder is intended to function. The second number (-22) is frequently referred to as the "low-temperature grade" and denotes that the binder would have sufficient physical characteristics to resist thermal cracking at least down to a low of -22 °C [26].

2.2.2 Simulating the Oxidative Aging of Asphalt in the Laboratory

It is significant to note that asphalt oxidation occurs in two stages. The first stage refers to the complete processes that the asphalt must undergo when producing an asphalt mixture, from extraction to road construction. Throughout its service life is the second phase. During these two stages, asphalt hardens for two key reasons. They are losses of volatile and alterations to the chemical makeup brought on by the reaction with oxygen [37, 40]. The establishment of specifications based on the asphalt's performance requires mimicking this hardening condition in a laboratory. Through accelerated laboratory methods, it is possible to precisely replicate the effects of aging in the real world. Many of these simulation protocols involve prolonged heating of asphalt binder or asphalt mix at high temperatures, which speeds up oxidation. Of the several procedures proposed, the RTFO and PAV processes have been the most employed over the years because the key bitumen specifications, such as AASHTO M320 (2017) (Bitumen and Bituminous Binders Specifications for Paving Grade Bitumen) and European standard EN 12591:2009 (Standard Specification for Performance Graded Asphalt Binder), both recommended their use. Both RTFO and PAV mimic the age oxidation effect that occurs in bitumen during short and long term aging, respectively [9].

2.2.2.1 Rolling Thin Film Oven (RTFO)

Division of Highways of the State of California Department of Public Works developed the RTFO test in 1963. Utilizing the RTFO approach, short term aging is simulated. The type of aging attained with this technique is the same type that happens when HMA is mixed, transported, and placed in a plant. During this test, eight cylindrical glass containers, each holding 35 g of asphalt binder, are mounted to a shelf that rotates vertically. Figure 2.2 shows the testing equipment. When hot air is intermittently ejected into each glass jar during the test, the asphalt binder flows constantly around the inside surface of each container, generating a rather thin film. This process makes sure that all the binder is exposed to heat and air, and continuous movement guarantees that no skin forms to shield the asphalt binder.

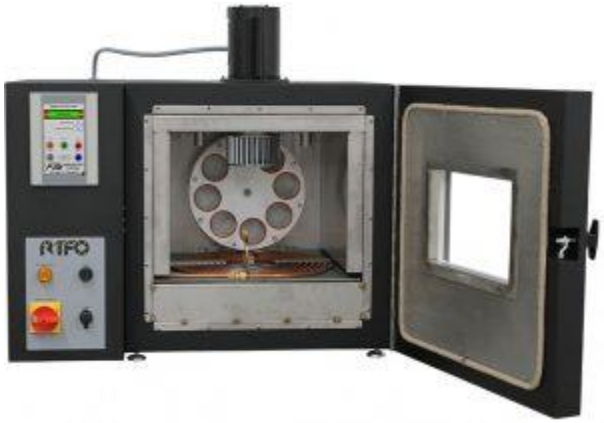

Figure 2.2: Rolling Thin Film Oven [10].

The RTFO test quantifies oxidative and evaporative changes. Typically, a difference in the mass of the specimen before and after the test will be observed. Mass loss indicates the presence of volatile substances in the asphalt binder. However, as a result of the reaction with oxygen, the mass of the specimen frequently increases during the test [10]. RTFO aged samples are further tested for physical properties [9].

2.2.2.2 Pressure Aging Vessel (PAV)

Simulating the long term aging of asphalt binders has been attempted on numerous occasions throughout the last years. However, this has turned out to be very challenging due to numerous factors, including void content, mixture type, and aggregate type, that influence binder aging. The SHRP stated the PAV as an aging method that simulates long term field oxidative aging of six to ten years of the pavement service life [9, 41]. The PAV is used to mimic the aging process that occurs after an asphalt pavement is constructed due to various climate factors and recurrent traffic loads. To accurately depict asphalt that has experienced hot mixing and placing, the binder to be PAV aged should have already been RTFO aged [14].

The samples that will be PAV aged are poured into pans on a rack [38]. The pans are heated for 20 hours at temperatures between 90 °C and 110 °C with an air pressure of 2.08 MPa [42] inside the PAV as shown in Figure 2.3. The overall climatic conditions of the region should be concerned with the choice of aging temperature. The residual is then used for BBR and DSR tests to evaluate the performance at low and intermediate temperatures, respectively [9, 10].

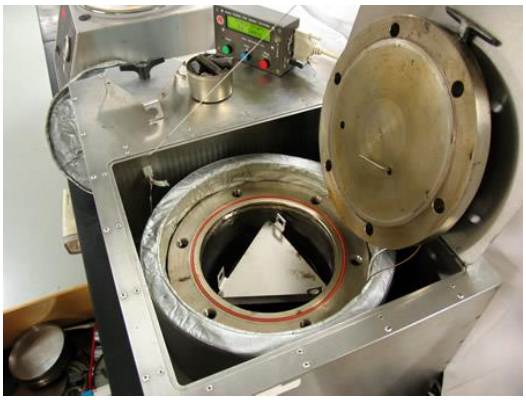

Figure 2.3: Pressure Aging Vessel viewed from the top with the pan holder inserted [43].

2.2.3 Dynamic Shear Rheometer (DSR)

DSR test determines the flow behavior of asphalt. The viscous and elastic behavior of asphalt can be explained and measured using the DSR [38]. The test can be performed on unaged, RTFO aged, and PAV aged samples, and the test parameters are used to identify the high and intermediate grades of asphalt binders.

The sample is positioned between two parallel plates of known geometry that are the same size as shown in Figure 2.4. The intermediate-temperature range DSR tests are performed using an 8 mm parallel plate design, and the high-temperature range DSR tests are performed using a 25 mm parallel plate. The specific type of geometry used should offer the ideal range of required strain or stress. The oscillating upper plate is called the rotor, while the fixed lower plate is the stator [10, 44].

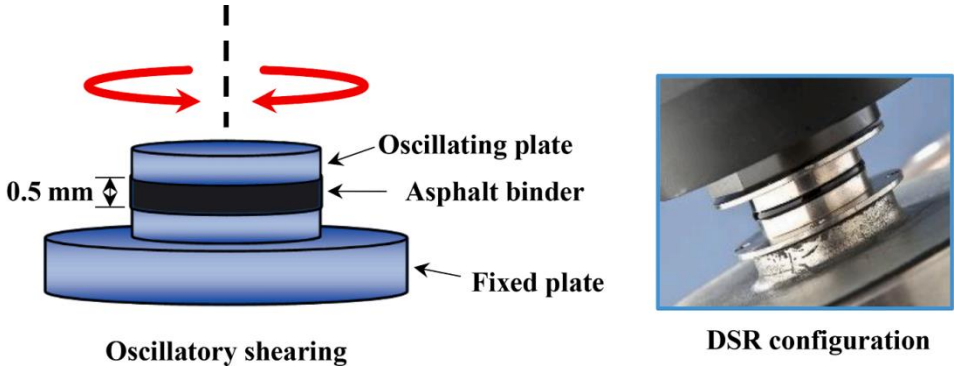

Figure 2.4: Schematic diagram of parallel plate geometry of DSR plates [1].

At a predetermined temperature, sinusoidal oscillatory shear stress or strain is exerted at a frequency of 10 radians per second [10, 44]. Using a transmitter, it is possible to determine how the upper plate oscillates around its own axis to shear the asphalt and how the asphalt reacts to the applied shear force as a function of frequency [28, 45].

The spindle oscillates on its own axis, point "O," during the test, with the radial line moving from point "A" to point "B", reversing to point "C" through "A," and then returning from "C" to "A" as shown in Figure 2.5 [26]. The temperature of the sample is regulated during the DSR test by the temperature chamber along with the nitrogen vessel, while the compressor regulates the motor and bearing system. The computer with the DSR software provides the results.

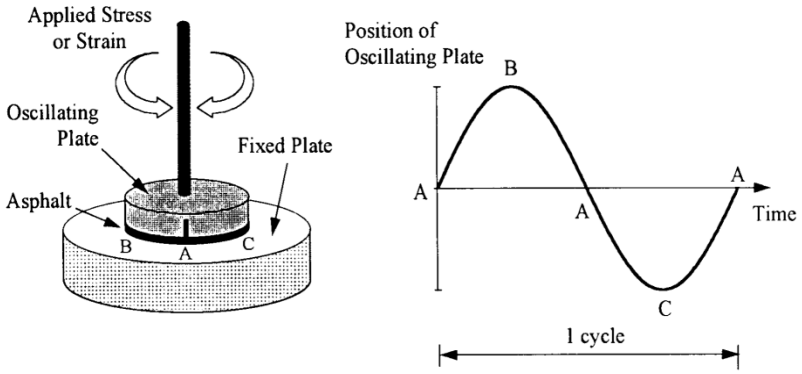

Figure 2.5: Schematic representation of DSR operation [26].

A single test run of the DSR test method can be employed to determine rheological parameters, including the G* and the δ, at various temperatures and frequencies [45, 46]. These two factors represent the linear viscoelastic rheological characteristics of asphalt binders [47]. The results of the DSR testing yield parameters like G*/sin δ and G*sin δ, which can be utilized to assess rut resistance and fatigue cracking, respectively [28]. The minimum G*/sin δ specifications are 1.0 kPa for the unaged binder and 2.2 kPa for the RTFO aged binder. When G*/sin δ is set to its minimum value, the binder has sufficient elastic stiffness to prevent permanent deformation. To resist rutting, the binder should be stiff (higher G*) and elastic (lower δ). The intermediate-temperature performance grade (ITPG) for the PAV aged binder is the temperature at which G*sin δ has a maximum value of 5000.0 kPa [2, 18]. When the G*sin δ is set to its maximum value, the sample exhibits sufficient viscous flow to prevent the binder from fracturing [44].

2.2.3.1 Complex Modulus (G)*

The G* measures the stiffness or overall resistance of an asphalt binder to deformation when exposed to repeated pulses of shear stress. G* can be defined as the ratio of maximum shear stress to maximum strain as given in equation 1 [6, 44, 46, 48]. The G* was first divided into two components by Brodnyan and coworkers. The storage

modulus (G′) is the elastic component, and the loss modulus (G″) is the viscous component [2, 10]. The viscous component is non-recoverable, although the elastic component is [38]. The relationship between G′ and G″ is shown in equation 2 [44, 49]. Variations in the viscous component and the elastic component of polymers with the temperature are shown in Figure 2.6.

$$\text{Complex modulus} = \frac{\text{Peak shear stress}}{\text{Peak shear strain}} \qquad \text{Equation 1}$$

$$G^* = \sqrt{((G')^2 + (G'')^2)} \qquad \text{Equation 2}$$

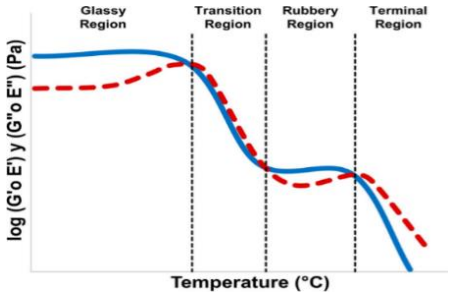

Figure 2.6: Variations in the viscous component (red dotted line) and the elastic component (blue continuous line) as a function of temperature in polymers [37].

2.2.3.2 Phase Angle (δ)

In harmonic oscillation, the δ is the difference in time or phase between the applied shear stress and the resulting shear strain [6, 46, 47, 48, 50] as shown in Figure 2.7. The δ is crucial to describing the viscoelastic qualities of an asphalt binder [38]. Pure elastic materials have a δ of 0° while pure viscous materials have a δ of 90°. For viscoelastic materials, the δ ranges from 0° to 90°. Simply, asphalt binder tends to become more viscous at higher δ and more elastic at lower δ [10, 38, 50].

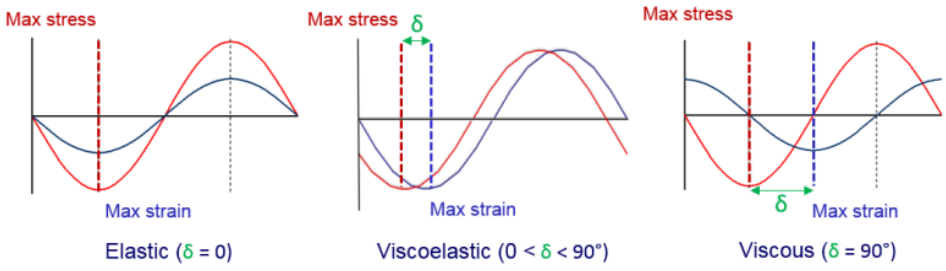

Figure 2.7: Stress and strain response during oscillatory testing for pure elastic, viscoelastic, and pure viscous materials [48].

The δ is defined as the ratio of the viscous over the elastic modulus as shown in equation 3 [38, 46]. Figure 2.8 illustrates how the δ connects the elastic and viscous components to the G* [38, 44, 49].

$$\tan \delta = \frac{G''}{G'} \qquad \text{Equation 3}$$

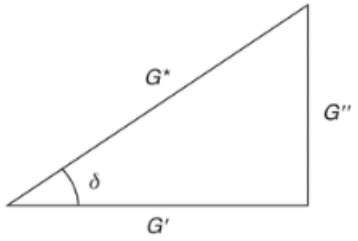

Figure 2.8: Relationship among complex modulus (G), storage modulus (G'), loss modulus (G''), and the phase angle (δ)* [28].

The loss tangent, tan (δ) which is linked to δ, is an indicator of the sol and gel properties of asphalt binder. tan (δ) is therefore examined as a substitute for a performance indicator for thermal cracking because it closely relates to how well a material can relax stress [51, 52]. Using phase angles, limiting phase angle temperatures were determined for the performance ranking of asphalt binders.

2.2.3.3 Limiting Phase Angle Temperatures

The limiting phase angle temperatures, $T_{\delta=30^\circ}$ and $T_{\delta=45^\circ}$, at which the phase angles reached 30° and 45°, respectively, were determined by interpolation after polynomial fitting of each tested binder. Based on the difference between the limiting phase angle temperatures at 30° and 45°, an empirical index $\Delta T_{c\delta}$ can be derived, as shown in equation 4. The term "$\Delta T_{c\delta}$" refers to the slope of the phase angle master curve throughout a temperature range that is significant for thermal cracking, around the freeze-thaw domain range of temperatures. According to the binder's capacity to relax stress at service temperatures, the "$\Delta T_{c\delta}$" index measures the degree of solid like behavior. If the asphalt binder is aged to an acceptable degree prior to rheological testing, "$\Delta T_{c\delta}$" can rank the performance of asphalt pavement in service [1].

$$\Delta T_{c\delta} = T_{\delta=45^\circ} - T_{\delta=30^\circ} \qquad \text{Equation 4}$$

2.2.3.4 Master Curves

To display the complete rheological profile of the asphalt, master curves can be constructed from a series of frequency sweeps collected at various temperatures [10, 38]. The master curves employ the time temperature

superposition principle to depict viscoelastic parameters such as the complex modulus or phase angle against reduced frequency on a log-log (or semi-log) scale as shown in Figure 2.9 [38, 53]. The set of complex modulus or phase angle measurements at a given temperature is called an isotherm [54, 55].

Since master curves can be employed to analyze the viscoelastic characteristics over a broad range of temperature or frequency range [56] there are several benefits of creating master curves. Once the master curve is constructed, interpolated values of a property can be derived for any combination of temperature or time of loading (frequency) inside the measurement range. The ability to create master curves eliminates the limits of laboratory tests by enabling the results to be extrapolated to more practical circumstances [9]. Additionally, this allows for the comparison of data from two laboratories that used various sets of test circumstances, such as frequencies and temperatures [57]. Although single point measurements were ultimately accepted for SHRP specifications for asphalt binders, recent research indicates that master curve based parameters may more accurately reflect the cracking resistance of asphalt binders than the current parameters [54].

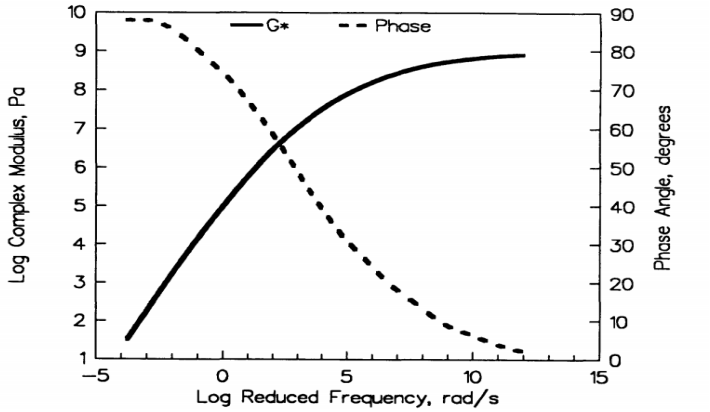

Figure 2.9: Complex modulus and phase angle master curves [38].

All binders experienced varying degrees of phase angle reduction in the frequency domain with aging [1]. When the phase angle is examined as a function of log frequency, the general shape is sigmoidal [38]. At very low frequencies, the phase angle is almost 90°, and at very high frequencies, it is almost 0° [38]. The asphalt binder has a low viscosity and fluid like behavior at high temperatures or low loading frequency. Asphalt binders have glassy and solid like qualities when subjected to higher loading frequencies or lower temperatures [22]. To capture the variety of mechanical behavior, Christensen and Anderson presented the Christensen Anderson (CA) model based on the

shape of the relaxation spectra to create the master curves [9]. The CA model links the crossover frequency (ω_c), glassy modulus (G_g), and rheological index (R_m) to the frequency dependence of G* [58].

The dynamic mechanical data acquired so far on the SHRP asphalts and the literature analysis on the linear viscoelastic properties of asphalt cement have made it evident that four key criteria are required to adequately characterize the linear viscoelastic properties of any asphalt cement [38]. They are ω_c, G_c, G_g, and the R_m.

• ***Crossover Frequency (ω_c)*** - The frequency at which the plots of G′ and G″ intersect is referred to as the crossover frequency (ω_c), or the frequency at which the δ is 45° [37, 38]. At the ω_c since G′ equals G″, tan (δ) is 1. At ω_c equal contributions from the elastic and viscous components of G* are observed [22]. ω_c serves as a frequency dependent transition point from viscous (fluid like) to elastic (solid like) dominated behavior since it designates the point at which the storage and loss moduli are equal [22, 54]. The reciprocal of the crossover time is denoted as the ω_c [38]. It can be conveniently obtained through graphical or statistical methods [38]. The ω_c acts as the location parameter for the master curve and serves as a good indicator of the overall hardness of asphalt. Importantly, ω_c is considered an asphalt specific property [38, 58]. The harder the asphalt, the lower the ω_c at a given temperature [58]. The ω_c declines and the R_m value rises as asphalt binders age due to oxidation [54].

• ***Crossover Modulus (G_c)*** - One of the three variables in the CA model is the G_c. The modulus at the intersection of the storage modulus master curve and the loss modulus master curve is known as the G_c [58]. The G_c corresponds to the G* at ω_c [22]. G_c is occasionally employed as a measure of polydispersity in research on the viscoelastic characteristics of polymers [58]. Although the correlation depends on the asphalt, the relationship between oxygen uptake (mass %) and the inverse of the log of the G_c is approximately linear. G_c reduces with oxidative aging. Consequently, log G_c reduces when stiffness, total oxygen, or carbonyl increase [58]. The G_c is regarded by Christensen and Anderson as a parameter related to asphalt structure and how it evolves with aging [58]. Both frequency and temperature have no effect on G_c. G_g and ω_c decline with the aging of a binder, while crossover temperature rises [8].

• ***Glassy Modulus (G_g)*** - The G* reaches a limiting value at high frequencies, which is the G_g. It is the plateau that is reached by the value of the G* of binders at very high frequencies (or very low temperatures) [22, 38] or short loading times. When frequency tends to be infinite ($f \rightarrow \infty$), G_g is the highest modulus, which is also known as the vitreous modulus. In shear loading, the G_g for most asphalt cement is typically quite close to 1 GPa [37, 38].

• ***Rheological Index (R_m)*** - The R_m is the difference between the logarithmic values of G_g and G_c [22, 38, 55, 58]. The R_m value introduced by Christensen and Anderson is an indicator of asphalt binder cracking potential [18, 54]. The R_m value is the shape parameter in the CA model [58], so the R_m value indicates the shape (width or broadness) of the relaxation spectrum [22]. The R_m value is also used to identify the type of rheology [38, 58]. A stiffer, more brittle behavior is indicated by higher R_m values. R_m values for binders aged with an RTFO test followed by 20 hours of aging in a PAV are tentatively allowed to range from 1.5 to 2.5, whereas R_m values for binders aged with an RTFO followed by a 40 hours PAV range from 2.0 to 3.2 [21]. R_m is a measurement of the asphalt cement's shear rate dependence because it reflects the modulus change with frequency or loading time. R_m is asphalt specific and is not a measure of temperature [38]. Phase angle at any given modulus value will be lower for binders with higher R_m values, this leads to the important finding that overall healing potential will decrease with increasing R_m values [21]. Higher R_m values indicate that the binder has been heavily oxidized. Moreover, higher R_m values will always reduce the strain tolerance of a binder, even when it is polymer modified [21].

2.2.3.5 Time Temperature Superposition (TTS)

According to certain studies, the effects of temperature and loading time on the process of mechanical relaxation in viscoelastic materials are equal. Particularly, the mechanical properties of viscoelastic materials at low temperatures are equivalent to those acquired with short loading times (higher frequency), according to the TTS principle [56]. The TTS principle, often known as the method of reduced variables, is applied when creating master curves. Dynamic data over a range of temperatures and frequencies is initially gathered before employing TTS. A standard reference temperature must then be chosen. Using a horizontal shift factor (frequency scale shift factor) a_T and a vertical shift factor b_T, the principle of TTS can transform a viscoelastic function at various temperatures into a viscoelastic master curve at the reference temperature. The data at all other temperatures are shifted with respect to frequency until the curves merge into a single, smooth function as shown in Figure 2.10. If there is only a horizontal shift factor, the substance can be categorized as a simple thermo-rheological substance. Asphalt and asphalt mixtures are generally categorized as simple thermo-rheological materials or adhere to the "thermo-rheologically simplified" hypothesis [38, 53, 56, 59].

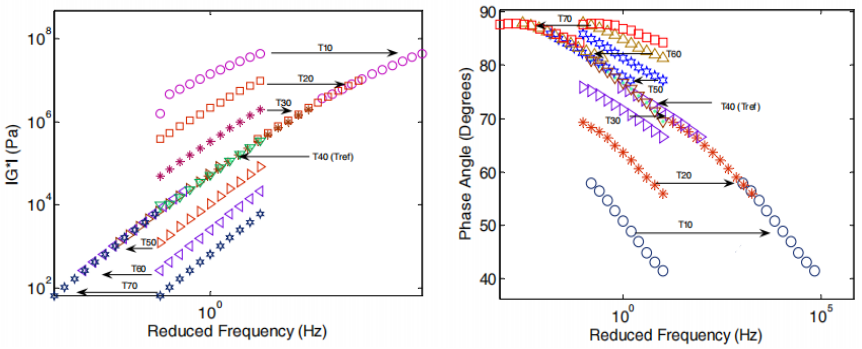

(a) *(b)*

Figure 2.10: Schematic representation of how the shift factors at different temperatures are used to construct the a) G and b) δ master curves at a particular reference temperature* [46].

Constrained shifting and free shifting are the two primary techniques for shifting the isotherms of viscoelastic functions along the frequency or time axis to produce a master curve. Constrained shifting involves forcing the master curve or the shift factors to fit a predetermined function [53, 54]. Shift factors are used to indicate how bitumen's viscoelastic behavior is affected by temperature and are expressed as shown in equation 5. The a_T is the shift factor, f is the tested frequency, and f_r is the reduced frequency at a reference temperature [46, 57]. At the reference temperature, the shift factor $a_{T0} = 1$ or $\log a_{T0} = 0$.

$$a_T = \frac{f_r}{f} \qquad \text{Equation 5}$$

The Williams Landel and Ferry (WLF) equation is one of the constrained shifting methods for creating master curves using TTS [46, 55]. The link between a_T and temperature of asphalt binders has been described using the WLF equation [53, 55, 57, 59]. The empirical WLF equation implies that the shift factor has a temperature dependence in the form displayed in equation 6 [57]. T is the operational temperature, T_{REF} is the reference temperature, and C_1, C_2 are empirical constants [53, 55, 56]. The limitation of the WLF equation is it has an operational temperature range relative to the glass transition temperature T_g ($T_g < T < T_g$+100 °C) [55, 56, 57].

$$\log a_T = \frac{-C_1(T-T_{REF})}{C_2+(T-T_{REF})} \qquad \text{Equation 6}$$

Numerous studies have shown that the function of asphalt is governed by a unique thermally activated relaxation process that is simple. However, some studies have demonstrably shown that the impacts of thermo-reversible

aging can significantly contribute to the additional complexity of asphalt binder [2]. When the structure of asphalt binder is complex, it cannot be considered a simple thermo-rheological material. Thus, highly structured asphalt binders following high degrees of polymer modification and/or oxidative aging demonstrate a deviation from thermo-rheological simplicity [46]. Zhan and Wang explained that most ordinary asphalt and styrene–butadiene–styrene (SBS) modified asphalt satisfy the simple thermo-rheological time temperature superposition at temperatures less than 70 °C [56].

2.2.3.6 Black Space Diagrams

Various aspects of the rheological behavior of asphalt binder can be highlighted using a variety of graphical representations. Among them, researchers have highlighted the high sensitivity of the Black space diagram for recognizing minute changes in the performance of asphalt binders with aging [8]. The logarithm of G* is plotted against the δ in the Black space diagram without any mathematical shifting (TTS) [1, 8]. Due to the removal of frequency and temperature from the plot, all the dynamic data can be displayed in a single plot without the requirement to perform TTS on the raw data [1].

Black space can offer insightful information about the failure mechanisms linked to extremely aged bitumen. Previous studies have emphasized the significance of evaluating the development of the age induced cracking performance of bitumen based on its placement in Black space [9, 14]. Before creating rheological master curves, Black space diagrams can be used to determine whether TTS is applicable [1]. A smooth curve in a Black space diagram symbolizes the validity of TTS. A disjointed curve in a Black space diagram indicates the breakdown of the TTS and may indicate the presence of a high asphaltene structured bitumen, a high wax content bitumen, or a high polymer modified bitumen [10]. Very little information about the field performance of different modified asphalt binders could be obtained from the Black space diagram [1, 8]. Black space offers a better method of evaluating data at high temperatures. It also allows one to estimate the pure elastic component of the G* at very low temperatures [53].

2.2.4 Bending Beam Rheometer (BBR)

The SHRP presented the BBR test method to the engineering field to examine the Low-Temperature Performance Grade (LTPG) of asphalt binders [60]. It assesses the asphalt's resistance to low-temperature cracking and the degree to which the binder relaxes load induced stresses [61]. The BBR is the ideal solution for the above tasks since it has

all the necessary qualities, including availability, user friendly calibration verifications, and accurate measurements of low temperature creep stiffness [2, 8, 9, 38].

The rheometer is composed of the loading frame unit, a liquid bath with temperature control, and a computer based data collection system [38]. Figure 2.11 depicts the testing setup schematically. A three-point bending test [9] is performed on an asphalt beam with dimensions of approximately 125 mm in length, 12.5 mm in width, and 6.25 mm in depth [9]. As per standard specifications, the asphalt beam is preconditioned in an ethanol bath for an hour at temperatures between +10 ℃ and +20 ℃ above the designated low pavement temperature. At these temperatures, asphalt acts as an elastic solid [6]. The constant load is applied at the center of the beam, which is placed in an ethanol bath at a specified low payment service temperature, and the beam's deflection is monitored during the 240 second test [22, 38, 44, 51]. The deflection is greatest at the center of the beam.

Figure 2.11: Bending Beam Rheometer [62].

At test completion, a polynomial curve fit is used to generate a mathematical representation of the log-log plot of flexural creep stiffness (s_t) versus time (Figure 2.12) to determine the slope (m_t) of the master curve at particular times. m_t is known as creep rate [44, 51, 60]. Both s_t and m_t of aged asphalt binders are measured at 60 s [2, 8, 9, 22].

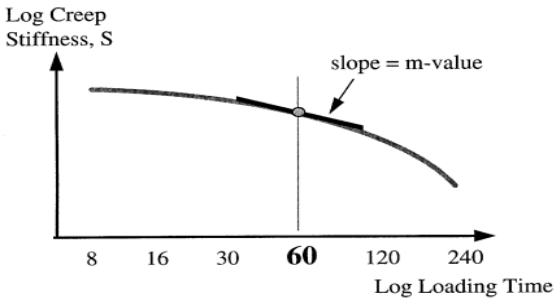

Figure 2.12: Plot of flexural creep stiffness versus time [51].

s_t provides a measure of the resistance of the bitumen to the thermal stresses that occur at low temperatures during cracking under constant load [2, 8, 9]. s_t is calculated by equation 7. In the below formula, P is the applied constant load (N), L is the distance between the beam supports (102 mm), b is the beam width (12.5 mm), h is the beam thickness (6.25 mm), s_t is the creep stiffness at time t, and δ_t is the deflection at time (t) [38].

$$S_t = \frac{PL^3}{4bh^3\delta_{(t)}} \qquad \text{Equation 7}$$

Measuring the m_t provides a representation of the asphalt's capacity for stress relaxation [9, 38]. A maximum s_t of 300 MPa and a minimum m_t value of 0.3 are the specifications for BBR [44]. An asphalt sample that is more brittle and prone to thermal cracking has a lower m_t and a higher $s_t$value than the standard limits [51]. If either $s_{(60)}$ or $m_{(60)}$, or both specifications fail, then the asphalt cement needs to be modified or substituted, or it can only be used in a warmer climate [51].

The corresponding temperature when the maximum s_t is less than 300 MPa is defined as the limiting stiffness temperature (T_s). Similarly, the corresponding temperature when the minimum m is greater than 0.3 is the limiting m-value temperature (T_m) [9, 18, 22]. By the difference between the T_s and T_m of BBR, critical cracking low-temperature spread, ΔT_c, can be determined [2, 8, 18, 21, 22].

$$\Delta T_c = T_s - T_m \qquad \text{Equation 8}$$

ΔT_c is correlated to low-temperature cracking by quantifying the cracking resistance of the binder. It is the temperature at which induced thermal stress will cause asphalt to crack [63]. The binder is S-controlled when ΔT_c is positive (less negative) and m-controlled when ΔT_c is negative. It is preferred that the binder be S-controlled

because flexural stiffness regulates the performance rather than the relaxation properties [8]. The BBR curve flattens and ΔT_c shifts more and more negatively as asphalt binder ages. The limiting values were proposed for ΔT_c to denote the potential risk of cracking ($\Delta T_c \leq -2.5°C$) and for more urgent remediation ($\Delta T_c \leq -5°C$) [9]. ΔT_c serves as a physical indicator for the durability and quality of binders [22]. It gives an indication of how near the substance is to becoming gelled and ceasing to flow [2]. ΔT_c is highly dependent on the rheological index and temperature susceptibility parameters [9].

Using the $s_{(60)}$ and $m_{(60)}$ obtained from the BBR, the rheological index can be simply determined using the equation 9 [21]. Because the Christensen Anderson rheological index (R value) and ΔT_c are directly connected, the rheologic type of the binder has a considerable impact on thermal cracking independent of low-temperature stiffness [21]. Binders with higher R values or highly negative ΔT_c values have a higher tendency to fail prematurely than binders with lower R values or highly positive ΔT_c values [21].

$$R=\log(2)\frac{\log(^{S_{(60)}}/_{3000})}{\log(1-m_{(60)})} \qquad \text{Equation 9}$$

During BBR premature failure may be observed frequently because the specimen is in a non-equilibrium state as a result of the short conditioning time. Due to this, poor performance materials benefit since they are less structured, gelled, and phase separated during the test, relative to degradation over months or years at cold temperatures [9, 35]. Moreover, premature failure is significant when a binder is graded to a lower temperature than it should be [21]. Hesp and coworkers have pointed out that the lack of sensitivity of the BBR test is due to the short conditioning period. To address these issues related to physical hardening during the BBR test, the EBBR was suggested [9, 21].

2.3 Methods by the Ministry of Transportation of Ontario

The Superpave specification system has some issues. According to the MTO, some of these issues are related to the actual application. The following are the main issues with the Superpave specification system: inadequate aging in the RTFO and PAV, inadequate conditioning in the BBR, and a lack of fracture and failure tests for the brittle and ductile states [13]. The Hesp Research Laboratory at Queen's University's Chemistry Department has worked with the MTO to develop new and improved testing procedures in response to these difficulties. These tests are the EBBR and DENT test [51] that exhibit strong reproducibility within the laboratory conditions [2].

2.3.1 Extended Bending Beam Rheometer (EBBR)

Low quality asphalt pavements consolidate their wax/asphaltene structure over the winter as a result of prolonged conditioning, which makes them unable to relax thermal stresses. Thus, the 1-hour conditioning time required by a typical BBR approach is insufficient to precisely simulate the behavior of the binder at low temperatures, which is what pavements experience in the real world. This issue with the original BBR approach led to the creation of the LS 308 EBBR test procedures, which were used to predict binder performance at extended conditioning. Thus, EBBR produces conditions for long term physical hardening that are similar to those developed when asphalt pavement is exposed to significant amounts of low temperatures, especially in the winter [6]. When compared to the normal BBR technique, field performance appears to be substantially better correlated with the EBBR test. Evaluation of asphalt binder susceptibility to thermo-reversible aging is one objective of EBBR testing [2, 64].

Binders are conditioned and tested after 1, 24, and 72 hours in the EBBR test [2, 9]. Two temperatures, 10 °C and 20 °C higher than the low-temperature grade, are employed to condition the samples. In this, duplicate or triple beams that undergo identical conditioning and testing procedures are used. With this approach, a great level of accuracy as well as confidence can be attained. A Limiting Low-Temperature Performance Grade (LLTPG), Grade Loss (GL), ΔT_c (1 hour and 72 hours), and R (1 hour, 72 hours) were determined after the test completion to provide accurate measures of durability [2, 20]. Also, the limiting temperatures (T_m and T_s) corresponding with instances when the m-value approaches 0.3 and creep stiffness reaches 300 MPa were determined [2]. By plotting the grades on a semi-logarithmic scale, the limiting grades can be calculated using extrapolation or interpolation. According to EBBR, the worst grade loss needs to be less than 6 °C compared to the regular BBR test after the EBBR test with 72 hours of conditioning time. In predicting the low-temperature behavior of asphalt binders, the EBBR is a trustworthy test.

This specification's main drawback is that it consumes an extended period and requires a higher quantity of sample. The DSR, in which binders are tested after short periods of conditioning in between steel plates, does relatively well in determining $\Delta T_{c\delta}$ compared to the EBBR, where binders are conditioned for an extended period. EBBR probably penalizes binders through exudative hardening by leaching lighter oils into the ethanol bath [1] through the additional time, which is problematic [9]. Thus, relating the EBBR test to other simpler tests is a crucial concern. For example, it is probable that the R value in the CA model and the level of physical hardening in the EBBR test

are related. This would make it possible to develop a quicker and simpler specification while also identifying binders susceptible to extreme physical hardening [21].

2.3.2 Double-Edge-Notched Tension (DENT) Test

The DENT test was created as an enhanced ductility test to assess the fracture toughness of asphalt binders [2]. It serves as one of the few fracture test methods applicable close to the brittle-ductile transition. Thus, the fracture property characterization of both asphalt binders and HMA mixtures has been satisfactorily evaluated using the DENT test. It was discovered that the DENT test and fatigue cracking performance were correlated [32]. Many engineers and researchers have used this test, which has been standardized by the MTO as test method LS-299 [39]. A schematic of the DENT specimen is provided in Figure 2.13 [31].

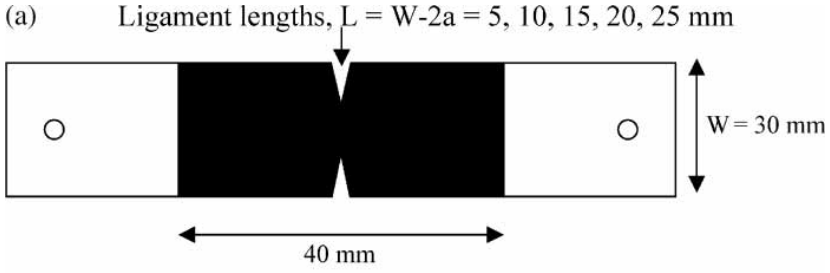

Figure 2.13: Schematic of DENT specimen design [31].

The load and energy to failure of the specimen are measured after it has been loaded at a steady deformation rate until failure. A total of three sets of specimens are usually produced, each with a different ligament length (the ligament length is the gap between the two notches at the specimen's centre. The testing conditions for the DENT test are specified as 15 °C and 50 mm/min in the current Ontario LS-299 standard. To determine essential and plastic works of failure, the critical Crack Tip Opening Displacement (CTOD), DENT test is used [35, 39, 65]. The area under the force-displacement curve obtained from the DENT test is used to determine the total energy, W_{total} (J), which is divided into two parts, as shown in Equation 10. Essential fracture work $W_{essential}$ (J), is the energy required for the fracture process and plastic work $W_{plastic}$ (J), also called non-essential fracture energy, is the energy needed for the plastic deformation outside the fracture zone [35, 39, 66]. $W_{essential}$ depicts the total work necessary to separate two failure surfaces in a localized area of a specimen under high constraints. Cracks in an asphalt mixture are often highly localized in between large aggregate particles. Hence, plastic work, $W_{plastic}$, which is the work dissipated away from the failure zone, is less significant in the failure of an asphalt mixture [39].

$$W_{total} = W_{essential} + W_{plastic} \quad \text{Equation 10}$$

The essential component is surface related and creates new surfaces, while the plastic component is volume related and may consist of single or possibly various dissipation mechanisms [66]. The first to postulate that the specific essential work of failure scales with the cross-sectional area of the ligament (LB) and the specific plastic work of failure, which scales with the volume around the ligament ($\beta L^2 B$) were Cotterell and Reddel. Mathematically, the relationship becomes equation 11 [35, 39, 65, 66], where L (m) is the length of the ligament, B (m) is the thickness of the specimen, w_t (J/m^2) is the specific total work of failure, w_e (J/m^2) is the specific essential work of failure, and w_p (J/m^3) is the specific plastic work of failure. β is a constant that describes the shape of the plastic zone [39, 66].

$$W_{total} = w_t \times LB = w_e \times LB + w_p \times \beta L^2 B \quad \text{Equation 11}$$

The renowned essential work of failure expression is given by dividing equation 11 by the cross-sectional area (LB) on either side [35, 39].

$$w_t = w_e + w_p \beta \times L \quad \text{Equation 12}$$

Using the above relationship, when the specific total work of failure, w_t, is plotted as a function of ligament length L straight line is produced. The intercept provides the specific essential work of failure w_e, which is an indicator of the material's intrinsic fracture toughness. The slope of the plot represents the specific plastic work of failure, w_p times the β constant [35, 39, 66]. The w_e property is a measure of strength and toughness [35, 39]. For thin sheets (i.e., plane stress conditions), the specific essential work of fracture changes with thickness [66]. (w_e and βw_p, measures of strength and toughness) [35, 39, 66]. By dividing the essential work of failure, w_e by the average net section peak stress for the 5 mm ligament (smallest) specimen, the CTOD is determined as in equation 13 [35, 39, 65].

$$CTOD = w_e/\sigma_{net,5mm} \quad \text{Equation 13}$$

CTOD has been demonstrated to be notably correlated to cracking performance because it is a failure property that assesses strain tolerance in the ductile state under intense confinement close to the brittle state [2, 35, 39, 65]. It reveals the extent to which a binder can stretch prior to suffering tensile damage [32]. Higher CTOD values should increase fatigue life since they allow the pavement to flex more before failing [65]. Laboratory, an accelerated loading facility, and actual pavement performance have all been used to validate the CTOD [35]. The CTOD is sensitive to the quality of the asphalt cement and rapidly deteriorates when undesirable additives are introduced (e.g. recycled engine oil bottoms (REOB), wax, air blown residues, reclaimed asphalt) [39, 65]. Despite being a viable

test for assessing the fatigue performance potential of asphalt binders, the DENT has two critical drawbacks. They are the complexity and duration of testing six different samples and the quantity of supplies needed to make these specimens.

2.4 Tests to Determine the Chemical Structure of Asphalt

2.4.1 X-Ray Fluorescence (XRF) Spectroscopy

This test is designed to determine whether waste engine oil was applied to the asphalt binder as an additive or modifier. The primary benefit of adding this modifier to asphalt cement is that it causes partial precipitation of the asphaltene portion once the base asphalt is mixed with this largely paraffinic material [67]. The discovery of zinc and molybdenum content in asphalt binders provides proof of this addition [67]. Zinc is present in engine oil as zinc dialkyldithiophosphate (ZDDTP) [51]. It serves as both an anti-wear additive and a universal antioxidant [29, 61]. Massive quantities of metals are present in engine oil, which negatively affects field performance by catalyzing the chemical oxidation of asphalt.

The surface of the material is exposed to high energy X-rays by the XRF instrument, which causes heavy metals to release their inner K-shell electrons [39, 67]. The electrons from the exterior L and M shells replace the resulting empty spaces. When electrons leave the outer shells, they emit low energy X-rays that are characteristic of the element being detected. Schematic of the X-ray Fluorescence process is shown in Figure 2.14. When the emitted radiation is detected by the XRF analyzer, a plot of the intensity versus the X-ray energy generated offers both qualitative and quantitative data on the existence of a variety of heavy elements. Peak heights within the spectrum provide a quantitative representation of the metal's existence; however, calibrations for every metal are required to allow for absolute comparisons among metals because fluorescence yields changes between various elements [68].

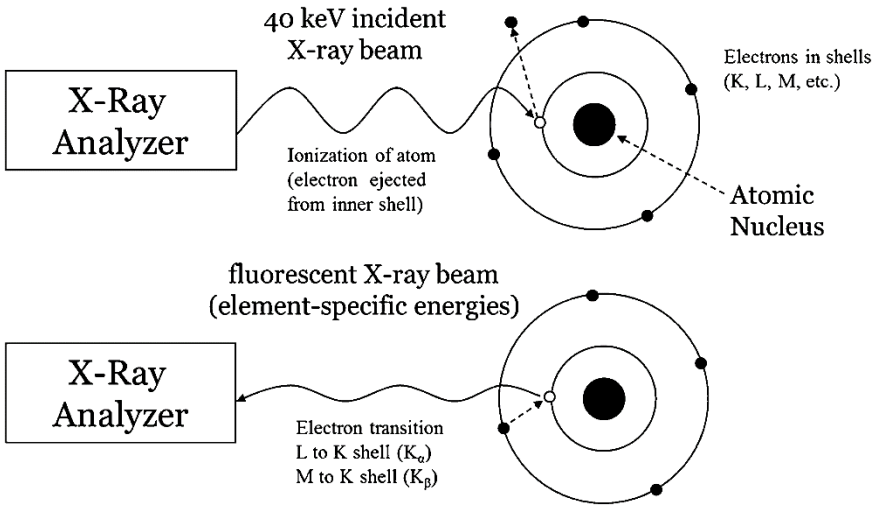

Figure 2.14: Schematic of the X-ray Fluorescence process [39].

2.4.2 Nuclear Magnetic Resonance (NMR) Spectroscopy

NMR spectroscopy can reveal details on the proportion of various hydrogen, carbon, or other atom types in a molecule as well as the chemical environment to which these atoms are exposed. The chemical shift is represented by the abscissa of the NMR spectrum, while the ordinate represents the intensity of the resonance absorption peak, whose peak area is proportional to the quantity of such nuclei in the molecule. The peak of tetramethylsilane (TMS) is typically used as a reference for comparison because the absolute value of the chemical shift of the general atomic nucleus is relatively small, and the relative change value is presented as ppm (parts per million). For blends like asphalt, NMR conveys average structure details about the entire sample. This understanding will help to characterize and distinguish the chemical properties of various asphalts as a whole [69].

^{13}C and DEPT-135 (Distortionless Enhancement by Polarization Transfer) NMR spectra can be used to successfully determine the types of carbon present in complex mixtures. The hydrocarbon chemistry and degree of branching, including branch-ethyl, terminal-methyl, branch-methyl, and bulk methylene configurations, are revealed by the ^{13}C NMR spectra, which also directly reveal the molecular carbon skeleton. The method is quite useful for pinpointing spectral regions that contain aromatic and olefinic carbons, aliphatic carbons, and certain oxygen bound carbon functions and provides insight into the elucidation of chemical structures in complicated mixtures like petroleum [70]. DEPT-135 experiments can be used to differentiate among the methyl (CH_3), methylene (CH_2), and methine (CH) groups. Thus, they were utilized to elucidate the aliphatic region of ^{13}C spectra by making a general characterization of the aliphatic region. The typical DEPT-135 spectrum will display the methyl (CH_3) and methine

(CH) carbons as positive signals, whereas the methylene (CH_2) carbons are "down", or negative signals [71]. The native asphalt binders and their oxidized residues were characterized by liquid state NMR spectroscopy [69].

2.4.3 Fourier Transform Infrared (FTIR) Spectroscopy

One of the main reasons for asphaltic pavement failure is oxidative aging, which occurs during mixing, transport, and compaction as well as in use over time in pavement construction [40, 72]. The binder stiffens and becomes more brittle because of this oxidative impact. Asphalt oxidizes when exposed to air due to an interaction between reactive oxygen, carbon, and sulfur. As a result, carbonyls and sulfoxides form and chemical composition is altered [37, 73]. FTIR spectrophotometer (Figure 2.15) is employed to characterize different functional groups found in the asphalt mix. It is an effective analytical method used to assess how oxidative aging affects the chemical composition of asphalt [37, 40, 72, 73]. The degree of oxidation that develops following short term RTFO aging and long term PAV aging will be predicted using the functional groups carbonyl, sulfoxide, aromatic, butadiene, and styrene. FTIR aids in predicting the origin and history of the asphalt and provides an understanding of the additives used to modify the asphalt. The radiation absorbance and concentration can be determined via Beer Lambert's law. Transmission mode and reflection mode are the two most frequently applied FTIR concepts for characterizing asphalt [20].

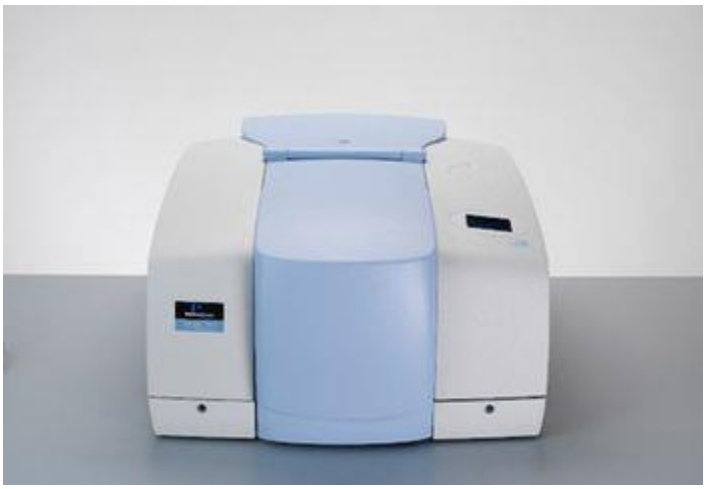

Figure 2.15: FTIR spectrophotometer [28].

Chapter 3

Materials and Experimental Methods

3.1 Materials

Asphalt binders used in this project were supplied from nine agencies in the USA, representing the West, Mid-West, and North-East regions. A, B, C, and D were indicative of four agencies from the West region, while E, F, G, and H denoted four agencies from the Mid-West region. The North-East region was represented by I. The binders obtained from the tank prior to mixing in plants were referred to as tank samples, while those recovered from loose mix were known as recovered samples. Table 3.1 presents the performance grades for the 39 asphalt binders used in this research.

Table 3.1: Performance grades respective to the sample code of asphalt binders.

Performance grade	Sample code
58-28	A1, A3, A4, A6, F2
64-28	A2, A5, B2, B3, B4, C1, C2, C6, H3, I1, I2
76-28	A7
58-34	B1, C3, C4, C5, F1, F3, F4, G1, G2
64-40	D1, D2, D3, D4
70-22	E1, E2, E3, E4, E5, E6, E7
64-22	H1, H2

3.2 Extraction and Recovery of Asphalt Binders

Each asphalt mix was soaked in dichloromethane (DCM) in a sealed, clean container and allowed to stand overnight. The 2 - 4 L DCM was used as a solvent to recover the asphalt binder present in the 4 - 8 kg asphalt mix. After allowing the DCM soaked sample to stand overnight, it was decanted into a clean bottle and washed with excess DCM to ensure the recovering maximum possible amount of binder from the mix. Next, the dissolved asphalt in DCM was allowed to undergo high speed centrifugation twice and stand to ensure some sediments settled, and the extract was collected to a clean labeled bottle. The essence of double centrifugation was to ensure the purity of the extract and to keep sediments to the barest minimum.

The binders were recovered from the extract using the Buchi R-210 rotary evaporator, as shown in Figure 3.1, under a dry nitrogen atmosphere. It was assumed that the properties of the recovered asphalt binder are similar to those of

the original asphalt binder, although slight changes may occur as a result of exposure to high temperatures and other contaminants. However, these changes are insignificant. The rotary evaporation process was carried out at a condensation temperature between 50-80 °C and an aspirator pressure of 450 mbar to remove the solvent. Once no more solvent was visibly being distilled, the temperature of the silicone oil bath was slowly raised to the final temperature of 160 °C at 20 °C intervals. Once the disappearance of condensed solvent dropped out, that means when the system was stabilized, the pressure was decreased below 100 mbar at 160 °C for an additional hour to ensure all solvent had been removed. The recovered binder was transferred into a clean beaker, with a small portion being poured into a silicone mold for further testing [2, 6, 20].

Figure 3.1: Rotary evaporator [28].

3.3 Aging of Asphalt Binder

3.3.1 Rolling Thin Film Oven (RTFO)

An electrically heated convection oven is used in the RTFO test procedure. Samples were heated to 160 °C in the oven for 15 minutes to melt the material for easy pouring. Next, 35 g of each sample was weighed out into clean, labeled RTFO tubes (Figure 3.2 (a)) The tubes were horizontally positioned on a cooling rack and allowed to

condition for an hour at room temperature. After the conditioning, tubes containing samples (8 samples per one turn) were transferred into the preconditioned RTFO carousel (Figure 3.2 (b)), which was reading 160 °C, and rotated at 15 RPM for 85 minutes. Throughout this period, the temperature of the oven was held at 160 °C, and the airflow into the tubes was retained at 4000 mL/min.

(a) *(b)* *(c)*

Figure 3.2: RTFO aging a) Loading the glass tube b) Placing horizontally in RTFO c) Coated tube after aging [14].

3.3.2 Pressure Aging Vessel (PAV)

A total of 50 g of RTFO aged samples were weighed into labeled 140 mm stainless steel PAV pans to provide the standard thickness of a 3.2 mm asphalt binder layer, as shown in Figure 3.3 (a). The samples were organized on a rack, as shown in Figure 3.3 (b), and inserted into the PAV (Figure 3.3 (c)). To prevent any air pressure leaks and temperature loss, the PAV was covered and firmly sealed. PAV aging was carried out for 20 hours at a temperature of 100 °C and a pressure of 2.08 MPa.

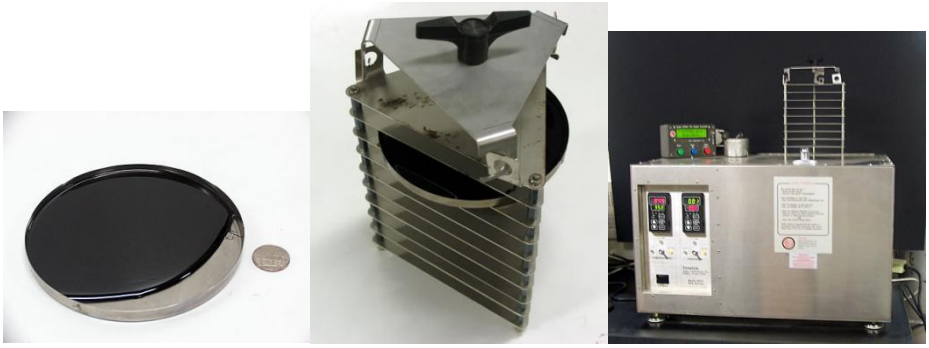

(a) *(b)* *(c)*

Figure 3.3: a) PAV pan with sample b) Pan holder with PAV sample inserted c) Pressure Aging Vessel [14].

3.4 Dynamic Shear Rheometer (DSR) Testing

The DSR frequency sweep tests were used to examine the rutting and fatigue cracking resistance at high and intermediate temperatures to assess the binder performance. The Discovery Hybrid 1 (DHR-1) and Discovery Hybrid 2 (DHR-2) TA instruments were used for all the tests. To prepare the samples, binders were heated in an oven at 160 °C until they were pourable. PAV aged samples were poured into thin, disc shaped silicon molds with an 8 mm geometry for the intermediate temperature frequency sweep DSR testing, as shown in Figure 3.4. The mold was used to ensure reasonable measurement of the amount of sample required for the test and to facilitate easy handling. The precalibrated DSR instrument with an 8 mm parallel plate configuration was then loaded with the asphalt binder thin layer. The standard procedure was followed. The loading temperature was 64 ℃, and the tests were conducted from 64 ℃ to -2 ℃ at an interval of 6 ℃. The testing was initiated at a frequency of 0.1 rad/sec to 10 rad/sec with appropriately chosen torque and strain values. At this point, the software automatically measures and produces the δ and the G* data after carrying out the cycles of the procedure. Tests were conducted for all the samples at both slow and fast cooling rates.

Figure 3.4: DSR samples in silicon molds [14].

3.4.1 Master Curve Generation and Time Temperature Superposition

Dynamic data gathered using DSR testing at a range of temperatures and frequencies was used in order to construct a master curve. A standard reference temperature must then be selected. In this study, 34 °C was used as the reference temperature. The data for every other temperature were then shifted relative to time until the curves converged into a single smooth curve. On a log-log scale, the complex modulus and the phase angle were plotted

against frequency. The viscoelastic functions will shift into continuous functions if the time temperature superposition is valid**.** Master curves were generated for all the samples that were tested using both slow and fast cooling methods.

3.4.2 Black Space Diagrams

For all the samples tested with DSR in both methods, slow and fast cooling Black space diagrams were generated. The G* and δ belonging to all the temperatures for different frequencies were considered. Then, log G* values were plotted versus δ.

3.5 Bending Beam Rheometer (BBR) Testing

The regular BBR test, which is in accordance with the AASHTO M 320 standard test procedure, was used to determine how effectively asphalt binders operate at low temperatures [20]. The BBR test measures the propensity of the PAV aged asphalt binder to undergo physical hardening and thermal cracking. Each sample was heated for about 30-45 minutes at about 150 °C and poured into a silicone mold with definite dimensions (125 mm × 12.5 mm × 6.25 mm) to form a beam. For the samples to take the shape of the mold, they had to cool for about an hour.

After being sufficiently cooled and taking on the shape of the mold, the asphalt binder beams were immediately trimmed. Following trimming, the beams were preconditioned for 1-hour at T_{design} + 10 °C and T_{design} + 20 °C in an ethanol bath before testing. The beams were then tested in the BBR instrument (Figure 3.5) at T_{design} + 10 °C and T_{design} + 16 °C. The equipment automatically measured the creep stiffness and the creep rate after obtaining a graph of the load and deflection versus time, as shown in Figure 3.6. Using the creep stiffness and the creep rate of tested asphalt binders, the LTPG was investigated [14].

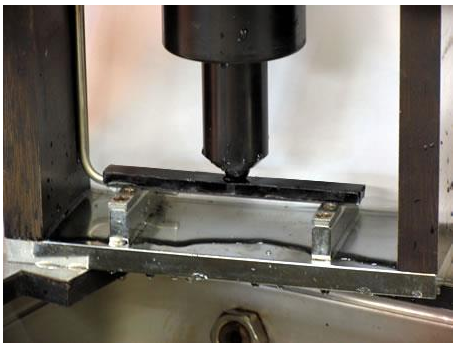

Figure 3.5: BBR beam ready to be tested [14].

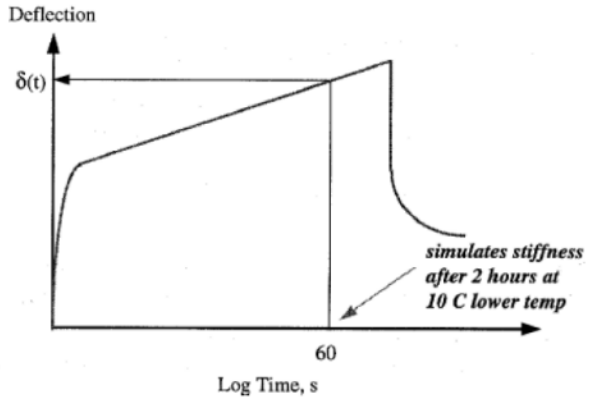

Figure 3.6: A typical graph of change in deflection with time [20].

3.6 Extended Bending Beam Rheometer (EBBR) Testing

The EBBR test was established to determine the degree to which an asphalt binder can physically harden when stored at low temperatures for extended periods of time. In order to conduct the EBBR tests, the beams were preconditioned in an ethanol bath at T_{design} + 10 °C and T_{design} + 20 °C. The beams were then evaluated in the BBR apparatus as usual after 1-hour and again after 24 and 72 hours.

Creep stiffness and the creep rate of the asphalt binders were then recorded. An interpolation of the data was carried out using a pass/fail temperature per AASHTO M320 to determine the grade of the asphalt binder [14]. The LLTPG and worst GL were determined after 72 hours. One major difference between the regular BBR and EBBR is the extended conditioning time.

3.7 Double-Edge-Notched Tension (DENT) Test

The DENT test has been developed as an improved test of ductility [2]. To enable free flow and homogenization for this test, materials were heated in an oven to a temperature of 160 °C. As illustrated in Figure 3.7, the samples were subsequently poured into three distinct notched silicon molds with varied ligament lengths (5 mm, 10 mm, and 15 mm). The asphalt binders were allowed to cool off at room temperature for an hour. The essence of the aforementioned is to get it solidified and to allow easy removal from the silicone mold to take the shape of the mold. After conditioning in a water bath at 15 °C for an hour, the thickness of each of the molded samples was measured. To assess the asphalt binder's ductile failure resistance, tests were conducted in a water bath at a constant speed of 50 mm/min at a temperature of 15 °C until the samples were torn apart. An Excel sheet was used to process the test data and determine the CTOD, essential work of fracture, and plastic work of fracture [14].

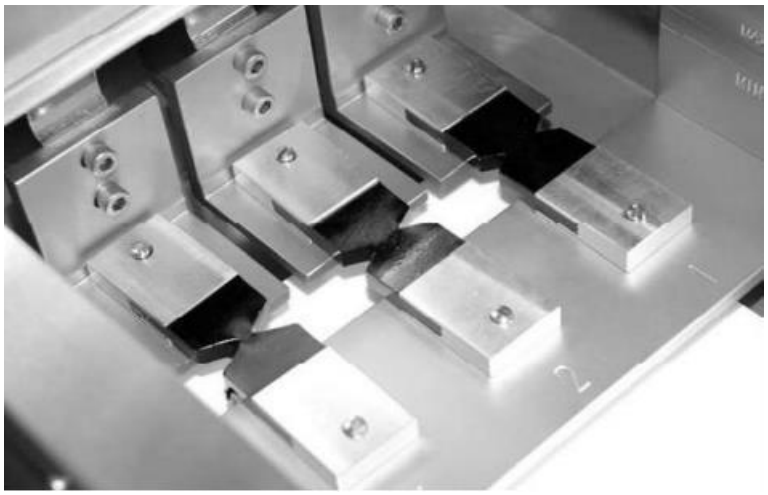

Figure 3.7: Samples loaded for DENT test [21].

3.8 X-Ray Fluorescence (XRF) Spectroscopy

An Epsilon I analyzer, which is shown in Figure 3.8 (a), was used to acquire XRF data for the samples of asphalt binder. The purpose of this test is to determine whether waste engine residue was introduced to the asphalt binder as a modifier or additive. The discovery of zinc and molybdenum levels in asphalt samples serves as confirmation of this.

(a) *(b)*

Figure 3.8: a) XRF spectrometer and b) Sample holders [74, 75].

For the asphalt to be in liquid form, the sample was melted in the oven for 1-hour. After being poured into the little plastic container (Figure 3.8 (b)), it was sealed with a thin transparent film on top and a circular piece of plastic at the bottom. The XRF instrument was calibrated prior to loading the sample. The sample spent about 5 minutes in the XRF machine. High energy X-rays from the XRF device were used to irradiate the material's surface. The emitted

radiation was detected by the XRF analyzer, and a plot of intensity versus X-ray energy offered qualitative and quantitative data on the presence of a variety of heavy elements [29].

3.9 Nuclear Magnetic Resonance (NMR) Spectroscopy

The asphalt binder was dissolved in the solvent $CDCl_3$ inside a glass bottle. Using a dropper, the prepared sample was transferred to the NMR tube. The Bruker NMR Spectrometer Auto 400 (Figure 3.9) was used for the analysis by obtaining H-NMR, ^{13}C NMR, and DEPT-135 NMR spectra. TMS was used as an internal standard. The chemical shift was represented by the abscissa of the NMR spectrum, while the ordinate represented the intensity of the resonance absorption peak, whose peak area was proportional to the quantity of such nuclei in the molecule.

Figure 3.9: Bruker NMR Spectrometer Auto 400.

3.10 Fourier Transform Infrared (FTIR) Spectroscopy

The presence and proportion of functional groups in all unaged, and PAV aged samples were assessed in this analysis using a Perkin Elmer Spectrum TM 400 FTIR spectrometer. To calibrate the spectrometer, a background scan was run on it under software control. A tiny amount of the sample was smeared with a hot spatula on the KBr disc surface that had been preheated at 140 °C for 3 minutes in order to create the thin film of the sample. Then a KBr disc with the sample was placed in the spectrometer (Figure 3.10), and over a wavenumber range of 4000 cm^{-1}

to 400 cm^{-1}, a sixteen scan was carried out on the test sample. The functional groups of interest and their proportions present in the sample were identified using peak area and peak height data from the scan. The FTIR functional groups with their respective wavelength ranges are shown in Table 3.2, and the FTIR spectrum of an asphalt binder with various functional groups of interest is shown in Figure 3.11.

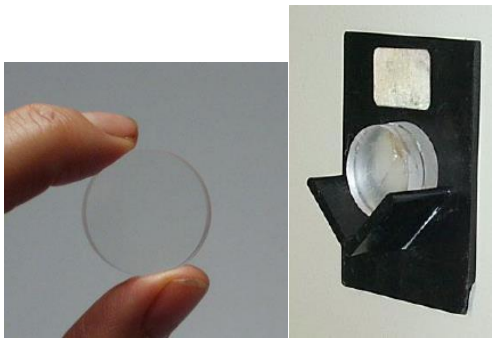

Figure 3.10: KBr disk and cell holder [76].

Table 3.2: FTIR functional groups with their respective wavelength range [28].

Functional Group	**Wavenumber Range**
Carbonyl	1760 cm^{-1} - 1655 cm^{-1}
Sulfoxides	1070 cm^{-1} - 985 cm^{-1}
Aromatics	1650 cm^{-1} - 1535 cm^{-1}
Butadiene	983 cm^{-1} - 955 cm^{-1}
Styrene	710 cm^{-1} - 696 cm^{-1}
CH_3	1400 cm^{-1} - 1300 cm^{-1}
CH_2	3121 cm^{-1} - 2746 cm^{-1}

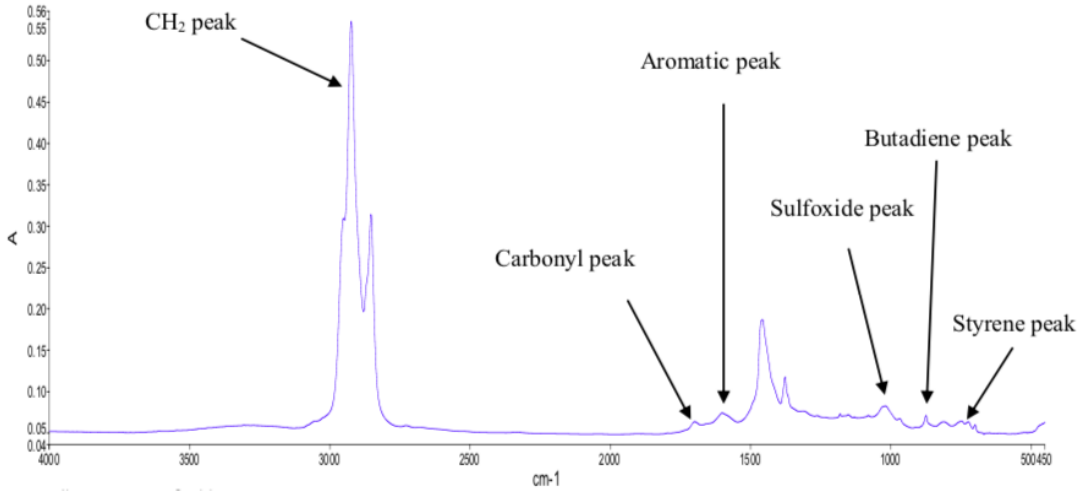

Figure 3.11: FTIR spectrum of an asphalt binder with various functional groups of interest [28].

Since CH_2 is less susceptible to chemical oxidation than CH_3, it was used as an internal standard (reference peak). The index of each individual functional group was then calculated by dividing the peak area of the specific functional group by the peak area of CH_2.

Chapter 4

Results and Discussion

4.1 Correlation and Sensitivity Analysis

Indicators obtained from DSR under slow cooling and fast cooling conditions are plotted against each other in section 4.2 to determine the most suitable DSR testing method. Meanwhile, in sections 4.3 and 4.4, parameters obtained from DSR under slow cooling and fast cooling conditions are plotted against EBBR and DENT test indicators. The aim is to identify the possibility of replacing the EBBR and DENT test indicators with the DSR test indicators. In section 4.2, DSR indicators obtained from slow cooling are considered the ordinate (y-axis). In contrast, indicators obtained from fast cooling are considered the abscissa (x-axis). Under sections 4.3. and 4.4, the indicators obtained from DSR are considered ordinates, while the indicators obtained from EBBR and DENT tests are considered abscissas of the graphs. To determine the goodness of the correlations present between the indicators on the y and x axes, the correlation coefficient (R^2) is used. Meanwhile to compare the sensitivity of indicators in the y and x axes the gradient (slope) is considered.

The R^2 value obtained from the graph is a good indication of the relationship between the indicators in the ordinate and abscissa. If the R^2 is one, it is a perfect correlation. Conversely, when the R^2 is zero, there is no correlation. Depending on the R^2 value between zero and one, the goodness of the correlation between the considered indicators can be predicted. Thus, R^2 is a good factor in evaluating the relationship between indicators obtained from DSR under slow and fast cooling conditions. In addition to that, R^2 is a significant factor in deciding the possibility of replacing EBBR and DENT indicators with DSR indicators.

However, a strong correlation between two indicators is not the only deciding factor to be considered here. Concern should be paid to the sensitivity of indicators, and in this case, the gradient, also known as the slope, has been monitored. A positive gradient indicates that as the indicator in the x-axis increases, the indicator in the y-axis also increases (direct relationship). A negative gradient implies that as the indicator in the x-axis increases, the indicator in the y-axis decreases (inverse relationship). The gradient measures how much the indicator in the y-axis changes for a unit change in the indicator in the x-axis. Based on the behavior of the gradient, the sensitivity of indicators has been analyzed. When the gradient is greater than one, the range of the indicator in the y-axis is higher than the range of the indicator in the x-axis, which means the indicator in the y-axis has higher sensitivity. If the gradient is equal to

one, the ranges of the indicators in both axes are the same, and the sensitivity of the indicators in the y and x axes is equal. When the gradient is less than one, the range of the indicator in the y-axis is lower than the range of the indicator in the x-axis, which means the indicator in the y-axis has lower sensitivity. Having a gradient extremely close to one recommends replacing the EBBR and DENT test indicators with the DSR test indicators in terms of sensitivity. If the gradient is greater than one, which means the sensitivity of DSR test indicators is higher than the sensitivity of EBBR and DENT test indicators, then indicators can be replaced by each other in terms of sensitivity, but the precision of the test indicators has to be considered when replacing each other.

4.2 Correlation and Comparison of DSR Data for Different Conditioning Times

The G* and the δ, which are related to the elastic and viscous responses of the PAV aged binders, were measured using the DSR instrument. This data indicates the stiffness and relaxation capacity of the binder. The DSR is used to determine the limiting temperatures, ITPG, and master curve parameters, namely ω_c, G_c, G_g, and R_m. There were two conditioning times in each temperature used for the test: 10-minutes (fast) and 1-hour (slow). Concerning rheological characteristics derived from DSR, the acquired data were utilized to assess the impact of fast and slow cooling.

The equation of the trendline obtained will be a good tool to determine whether the slow and fast cooling rates affect the magnitude of the DSR indicator. In the ideal condition, all the data points should align on the equal line y=x, resulting in an R^2 value of one, implying that cooling rates do not affect the magnitude of the DSR indicator. However, in the non-ideal condition, if the trendline, which is exhibiting a strong correlation with an R^2 value closer to one, deviates from the equal line y=x (either above or below), it means that the cooling rate affects the magnitude of the DSR indicator.

4.2.1 Correlation and Comparison with Limiting Temperatures

The quality of asphalt binder can be determined by analyzing the phase angle values of asphalt samples derived from DSR data. The asphalt binder has a relatively high phase angle at high temperatures and low frequencies because of its fluid like characteristics. Because asphalt behaves like an elastic solid at low temperatures and high frequencies, it exhibits a smaller phase angle value. Therefore, when stiffness increases, the phase angle of asphalt binder lowers. It is well known that good points for ranking asphalt binder performances are the limiting phase temperatures at phase angles 45° and 27° (27° has been rounded to 30°) [6, 9, 35].

4.2.1.1 Limiting Temperature at Phase Angle 45° ($T_{\delta=45^\circ}$)

The elastic (G′) and viscous (G″) moduli equalize when the phase angle of the sample reaches 45°, signifying that the elastic and viscous components of G* contribute equally. As a result, the $T_{\delta=45^\circ}$ denotes a change in viscoelastic behavior from being more solid like to more fluid like, as well as a balance between G′ and G″. Asphalt pavements function in a broad temperature range, and when the pavement is beyond $T_{\delta=45^\circ}$, the binder is more likely to flow under stress rather than crack because of the predominant impacts of the G″ component. The probability of pavement temperatures rising above $T_{\delta=45^\circ}$ decreases as $T_{\delta=45^\circ}$ increases. Asphalt samples that have a lower $T_{\delta=45^\circ}$ exhibit stronger resistance to fatigue and thermal cracking due to their ability to relax stresses. High $T_{\delta=45^\circ}$ asphalt samples exhibit stiffness and more susceptibility to cracking under load.

According to Figure 4.1, $T_{\delta=45^\circ}$ between slow and fast cooling rates shows a strong correlation with an R^2 value of 0.99. Since the trendline deviates from the equal line (y=x), the cooling rate affects the magnitude of the $T_{\delta=45^\circ}$. Worthy of note is the gradient of the graph. Since the gradient is almost equal to one (0.99 ± 0.02), it can be concluded that $T_{\delta=45^\circ}$ under slow cooling has a similar sensitivity when compared to $T_{\delta=45^\circ}$ for fast cooling. Due to higher correlation coefficient values and since sensitivity is almost the same, both methods are recommended to determine $T_{\delta=45^\circ}$.

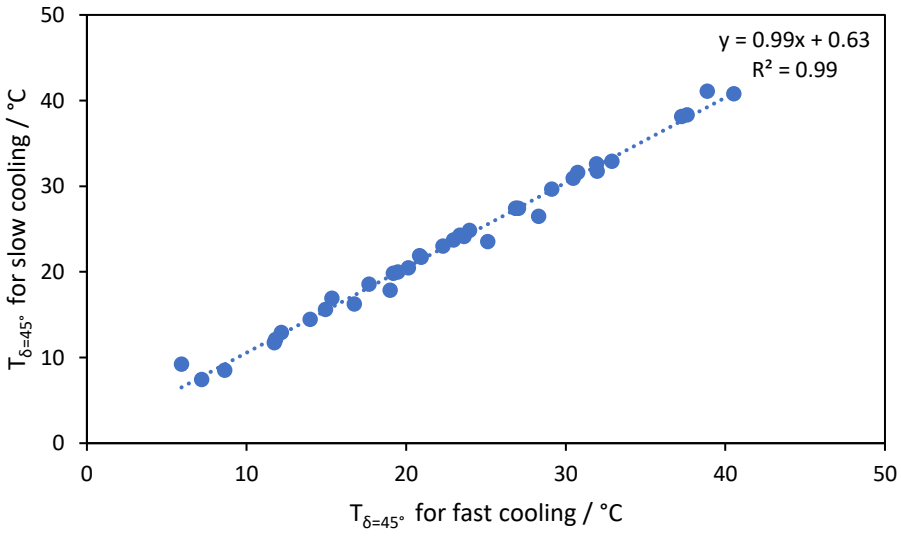

Figure 4.1: Correlation of $T_{\delta=45^\circ}$ for slow cooling with $T_{\delta=45^\circ}$ for fast cooling.

4.2.1.2 Limiting Temperature at Phase Angle 30° ($T_{\delta=30°}$)

Since most binders used in northern regions, such as those in North America and Northern Europe, achieve their phase angle at 27° at temperatures around 0 °C, limiting temperatures around phase angles 27°-30° ($T_{\delta=30°}$) are similarly crucial. This makes it an effective metric for ranking binder cracking performances. The pavement moves a lot at this point, known as the "freeze-thaw point." Water freezes beneath the layer of pavement at night and melts again during the day, causing significant damage to the surface of the road. Stiffer asphalt binders have a high $T_{\delta=30°}$, which indicates that at high temperatures, the binder phase angle becomes 30°. Thus, these binders with a high $T_{\delta=30°}$ are unable to relax tension and are prone to cracking. Binders with a low $T_{\delta=30°}$ value are softer and exhibit fluid like behavior even at relatively low temperatures. They can relax stresses and have greater resistance to cracking.

As shown in Figure 4.2, $T_{\delta=30°}$ for slow and fast cooling rates exhibits a higher correlation of R^2 0.98. Because the trendline deviates from the equal line (y=x), the cooling rate has an effect on the magnitude of the $T_{\delta=30°}$. Since the gradient of the graph is almost equal to one (0.99 ± 0.02), the $T_{\delta=30°}$ for slow cooling has the same sensitivity as $T_{\delta=30°}$ for fast cooling. Due to strong correlation and the same sensitivity, both slow and fast cooling methods are suitable for measuring $T_{\delta=30°}$ from DSR. The strength of the correlation and sensitivity obtained for $T_{\delta=30°}$ at different cooling rates are the same as for $T_{\delta=45°}$, which is described in Figure 4.1.

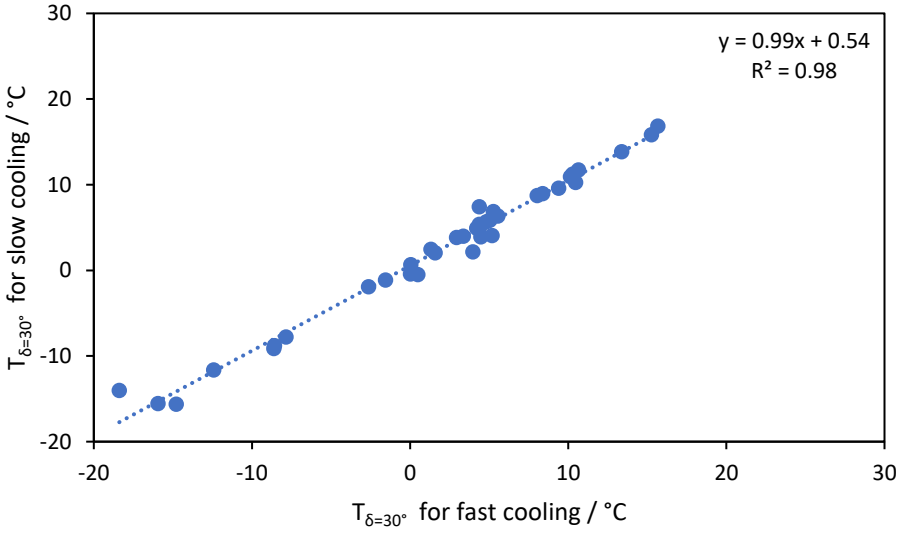

Figure 4.2: Correlation of $T_{\delta=30°}$ for slow cooling with $T_{\delta=30°}$ for fast cooling.

4.2.1.3 Difference in Limiting Temperature ($\Delta T_{c\delta}$)

The $\Delta T_{c\delta}$ could give an insight into whether a sample is a gel or sol. Because $\Delta T_{c\delta}$ is a DSR parameter, it can be obtained at a higher temperature and faster equilibration, giving it an advantage over the EBBR procedures [20]. The $\Delta T_{c\delta}$ for slow cooling and fast cooling are presented in Figure 4.3. There is a strong correlation with an R^2 value of 0.97 between $\Delta T_{c\delta}$ for slow and fast cooling rates. Since the trendline deviates from the equal line (y=x), the cooling rate has an effect on the magnitude of the $\Delta T_{c\delta}$. The sensitivity is the same for slow and fast cooling as the gradient is nearly equal to one (0.95 ± 0.03). Considering the higher correlation and same sensitivity, both methods are suitable to determine $\Delta T_{c\delta}$. Even though the R^2 value is high for $\Delta T_{c\delta}$ at slow and fast cooling conditions, it is less compared to that of $T_{\delta=45^\circ}$ (Figure 4.1) and $T_{\delta=30^\circ}$ (Figure 4.2).

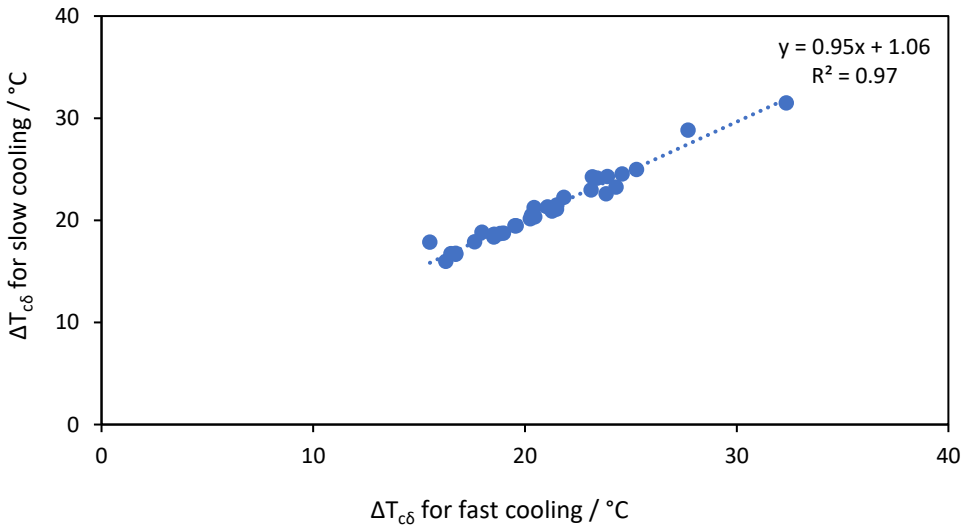

Figure 4.3: Correlation of $\Delta T_{c\delta}$ of slow cooling with $\Delta T_{c\delta}$ of fast cooling.

4.2.2 Correlation and Comparison with ITPG

The impact of cooling circumstances on the fatigue cracking character of PAV aged samples at intermediate temperatures was assessed using the DSR technique. The temperature at which the fatigue cracking resistance factor (G*sin δ) for PAV aged samples is equal to 5,000 kPa determines ITPG. The ITPG of PAV aged samples was used to address the susceptibility of the binder to fatigue distress at a long term age, in accordance with the Superpave binder specification as per AASHTO M 320. Higher ITPG values of binders make them more prone to fatigue cracking. The lower the ITPG of the asphalt binder, the less susceptible it is to fatigue cracking [6,14].

As depicted in Figure 4.4, there is a strong correlation with an R^2 value of 0.96 between ITPG for slow and fast cooling rates. Since the trendline deviates from the equal line (y=x), the cooling rate has an effect on the magnitude of the ITPG. The sensitivity of ITPG for slow cooling can be considered equal to fast cooling, as the gradient is 0.94 ± 0.03. Due to the equal sensitivity, and considering the high correlation between slow and fast cooling conditions, both methods are accepted to determine ITPG. The correlation coefficient value obtained for ITPG is relatively less compared to the correlation coefficient values obtained for both the limiting phase angle temperatures for slow and fast cooling, as shown in Figures 4.1 and 4.2.

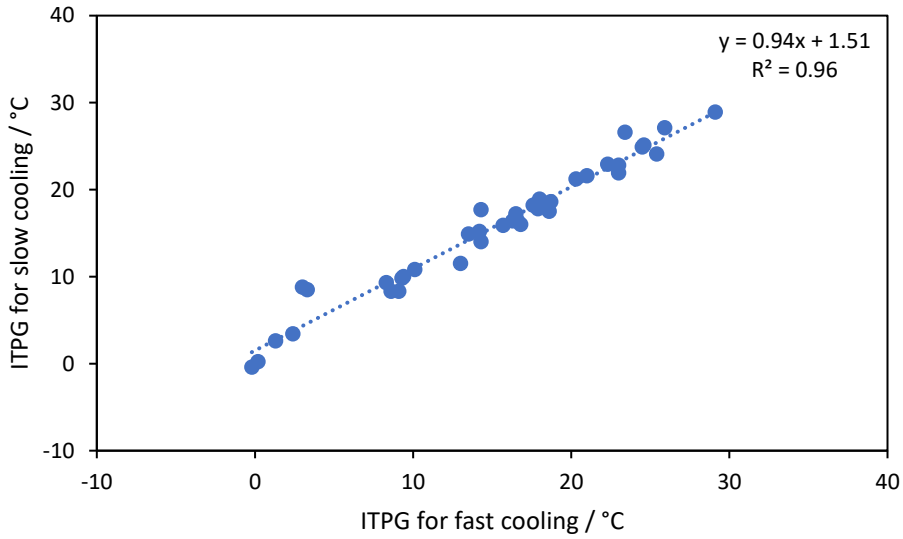

Figure 4.4: Correlation of ITPG for slow cooling with ITPG for fast cooling.

4.2.3 Correlation and Comparison with Master Curve Parameters

4.2.3.1 Crossover Frequency (ω_c)

As per Figure 4.5, there is a strong correlation between log ω_c for slow and fast cooling rates with an R^2 of 0.98. Because the trendline deviates from the equal line (y=x), the cooling rate influences the magnitude of ω_c. From the gradient of the graph, which is 0.99 ± 0.02, it can be inferred that log ω_c has almost the same sensitivity for both slow and fast cooling conditions. Both methods are considered appropriate for DSR tests due to their high correlation coefficient values and identical sensitivity to determining log ω_c.

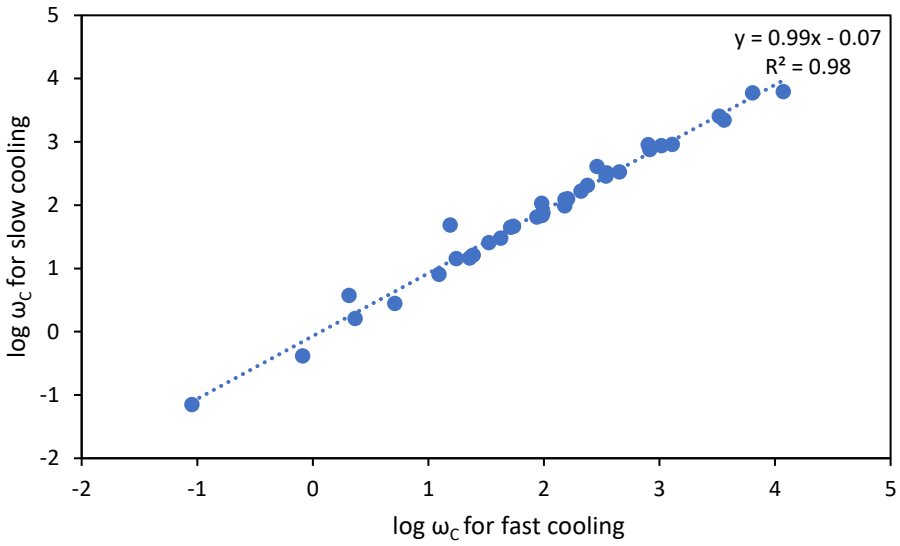

Figure 4.5: Correlation of log ω_c for slow cooling with log ω_c for fast cooling.

4.2.3.2 Crossover Modulus (G_c)

As indicated in Figure 4.6, there is a high correlation between log G_c for slow and fast cooling rates with an R^2 of 0.81. Since the trendline deviates from the equal line (y=x), the cooling rate has an effect on the magnitude of the G_c. It can be deduced that log G_c exhibits lesser sensitivity during slow cooling as compared to fast cooling, a fact further substantiated by a gradient of less than one, which is 0.84 ± 0.08. Given the high value of the correlation coefficient, both cooling methods are suitable for determining the G_c. However, due to the high sensitivity of the fast cooling method, it is more suitable for conducting DSR tests to determine the master curve parameter G_c.

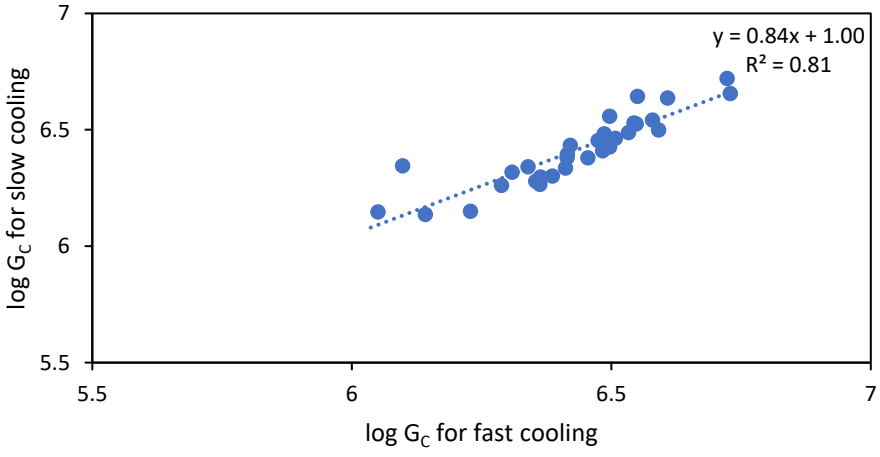

Figure 4.6: Correlation of log G_c for slow cooling with log G_c for fast cooling.

4.2.3.3 Glassy Modulus (G_g)

A high correlation with an R^2 value of 0.79 exists between log G_g for slow and fast cooling rates, as seen in Figure 4.7. Since the trendline deviates from the equal line (y=x), the cooling rate influences the magnitude of the G_g. Notably, the gradient of the graph is 0.90 ± 0.09. From this, it may be inferred that log G_g is less sensitive to slow cooling than to fast cooling. Both techniques are appropriate for DSR testing due to the high correlation coefficient values. However, due to the high sensitivity of fast cooling, it is more convenient to obtain the master curve parameter, G_g from the fast cooling DSR test. Other than that, it is important to note that the R^2 values of log ω_c and log G_c between slow and fast cooling conditions are higher than the R^2 values of log G_g for slow and fast cooling conditions.

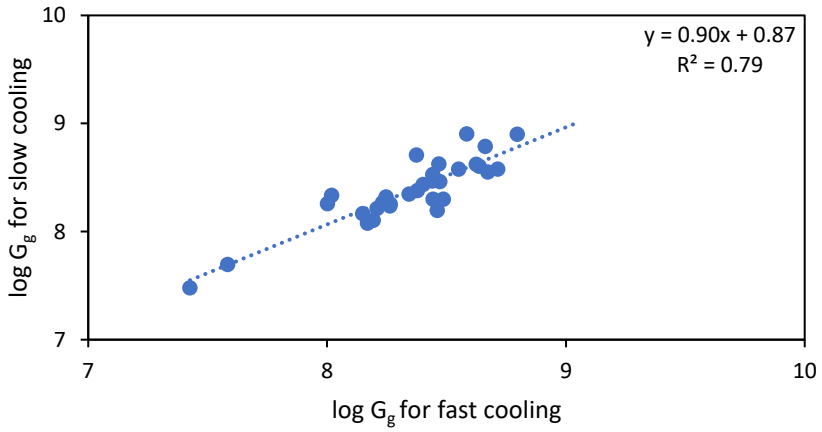

Figure 4.7: Correlation of log G_g for slow cooling with log G_g for fast cooling.

4.2.3.4 Rheological Index (R_m)

There is a strong association between R_m for slow and fast cooling rates, with an R^2 of 0.92, as observed in Figure 4.8. Because the trendline deviates from the equal line (y=x), the cooling rate has an effect on the magnitude of the R_m. The gradient of the graph is 1.02 ± 0.06, indicating the sensitivity of R_m for slow and fast cooling conditions is nearly the same. Both cooling conditions can be used for conducting DSR tests to determine R_m because of their high correlation coefficient values and equal sensitivity.

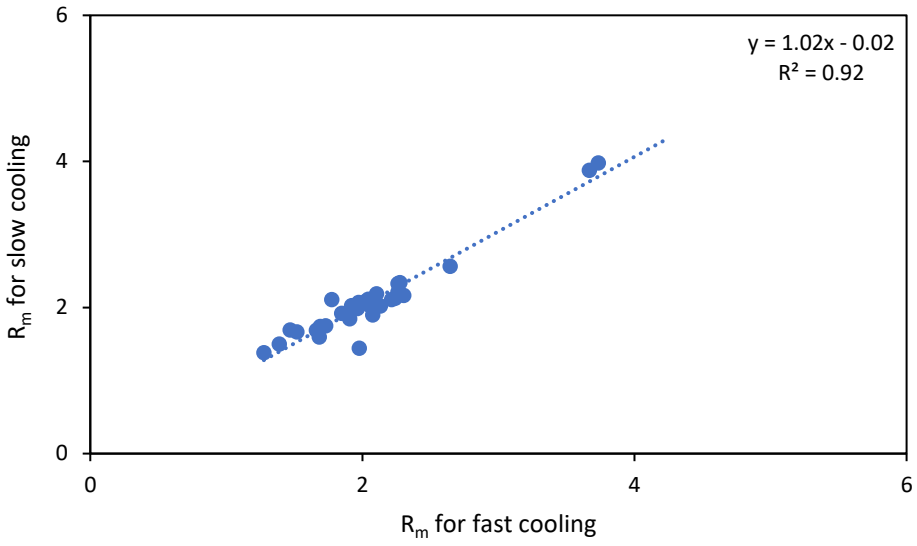

Figure 4.8: Correlation of R_m for slow cooling with R_m for fast cooling.

4.3 Correlation Analysis of Rheological Results from DSR and EBBR

The EBBR approach is essential for thermal cracking research because it can explain the physical hardening phenomena that occur when asphalt binders are exposed to extremely low temperatures for prolonged periods. Over time, researchers have examined how asphalt gradually changes in consistency at constant low temperatures. They have concluded that the presence of paraffinic waxes in asphalt mixtures made with unstable binders causes a phase separation that results in the formation of a rigid gel like structure. Due to this, ductility is decreased, and the material is more likely to crack early at low temperatures [28]. Using the EBBR test, the LLTPG and the worst GL are identified [14].

GL is the difference between the low-temperature grades obtained at 1 hour and 72 hours of cold conditioning. To predict how asphalt binders will react to physical hardening and thermal stress, GL can be used. In simple terms, it is beneficial to understand or anticipate the in-service performance of the asphalt binders. During the EBBR test, liquid oily components were expelled from the asphalt beam into the ethanol bath through exudation or syneresis, resulting in a GL. Utilizing the GL indicator from the EBBR test enables the monitoring of thermo-reversible aging in asphalt binders, consequently increasing their brittleness and susceptibility to cracking. Thermo-reversible aging results in a rise in the asphaltene fraction in the binder. During this process, asphaltene molecules agglomerate into interpenetrating networks, a phenomenon known as "paraffinic demixing," which decreases the stability of the

colloid system. Distinctive phase separation occurs as nonpolar oils separate from the polar asphaltene precipitate during exudation [77]. In comparison to asphalt binder samples with higher grade loss, those with lower grade loss have good resistance to physical hardening and can relax thermal stresses that occur in the asphalt pavement more quickly. As a result, there will be reduced or no stress during the "spring thaw," which will reduce or eliminate cracking [14]. Production faults, including overheating and the use of low quality binders, are other reasons that may impact the GL. Grade losses are highly sensitive to the presence of deleterious additives (waxes, air-blown residues, pitches, acids, and bases) [29]. LS 308 states that following the EBBR test with 72 hours of conditioning time, the worst GL should be less than 6 °C when compared to the standard BBR test [78, 79].

The EBBR test requires more labor, time, and samples, in contrast with the DSR test. Hence, replacing EBBR indicators with DSR is more beneficial. Thus, in this investigation, EBBR test indicators were correlated with the DSR test indicators for USA binders from three regions under two cooling rates (slow and fast).

4.3.1 Correlation of Limiting Temperatures with EBBR Data

Phase angle measurement could be carried out easily with a small amount of sample and in less time using the DSR. Therefore, phase angle measurement could be a viable alternative to the EBBR test in characterizing the low-temperature performance of binders. Here, limiting temperatures obtained from different cooling conditions from DSR are correlated with LLTPG obtained from the EBBR method.

Figure 4.9 shows the correlations of both limiting phase angle temperatures, $T_{\delta=30^\circ}$ and $T_{\delta=45^\circ}$, with LLTPG for both slow cooling and fast cooling conditions. $T_{\delta=30^\circ}$ for both slow and fast cooling conditions show a strong correlation with LLTPG, in which R^2 values are 0.94 and 0.92, respectively, as shown in Figure 4.9 (a). The gradient of fast cooling (1.15 ± 0.06) is higher than the gradient of slow cooling (1.05 ± 0.05), which indicates that $T_{\delta=30^\circ}$ of fast cooling is more sensitive than $T_{\delta=30^\circ}$ of slow cooling. In addition to that, since both gradients are greater than one when compared with the LLTPG, the $T_{\delta=30^\circ}$ is more sensitive.

As shown in Figure 4.9 (b), $T_{\delta=45^\circ}$ for both slow and fast cooling conditions shows a higher correlation with LLTPG with the same R^2 value of 0.89. The gradient of fast cooling (1.12 ± 0.07) is higher than the gradient of slow cooling (1.06 ± 0.07), which indicates that $T_{\delta=45^\circ}$ of fast cooling is more sensitive than $T_{\delta=45^\circ}$ of slow cooling. In addition to that, both gradients for slow and fast cooling for variation of $T_{\delta=45^\circ}$ with LLTPG are greater than one. Thus, when compared with the LLTPG, the $T_{\delta=45^\circ}$ is more sensitive.

When comparing the association of two limiting phase angle temperatures with LLTPG at different cooling conditions, $T_{\delta=30^\circ}$ of slow cooling has the highest correlation. The R^2 values for $T_{\delta=45^\circ}$ are less compared to the $T_{\delta=30^\circ}$ for both slow and fast cooling. The sensitivity of slow cooling is almost the same for $T_{\delta=30^\circ}$ and $T_{\delta=45^\circ}$ as gradients are very close to each other (1.05 and 1.06, respectively). The sensitivity of fast cooling for both $T_{\delta=30^\circ}$ and $T_{\delta=45^\circ}$, is higher since the gradient values of fast cooling (1.15 and 1.12, respectively) are higher than those of slow cooling. It is worth noting that the sensitivity of both $T_{\delta=30^\circ}$ and $T_{\delta=45^\circ}$ is higher compared to LLTPG at both cooling conditions. Due to strong correlations, either limiting phase angle temperatures or LLTPG are suitable for low-temperature performance grading for this set of USA binders recovered from loose HMA. These findings may not directly apply to Ontario binders due to differences in hardness and stiffness. In prior Ontario binder studies, LLTPG showed a high correlation with $T_{\delta=30^\circ}$, while $T_{\delta=45^\circ}$ was not highly correlated with LLTPG [2].

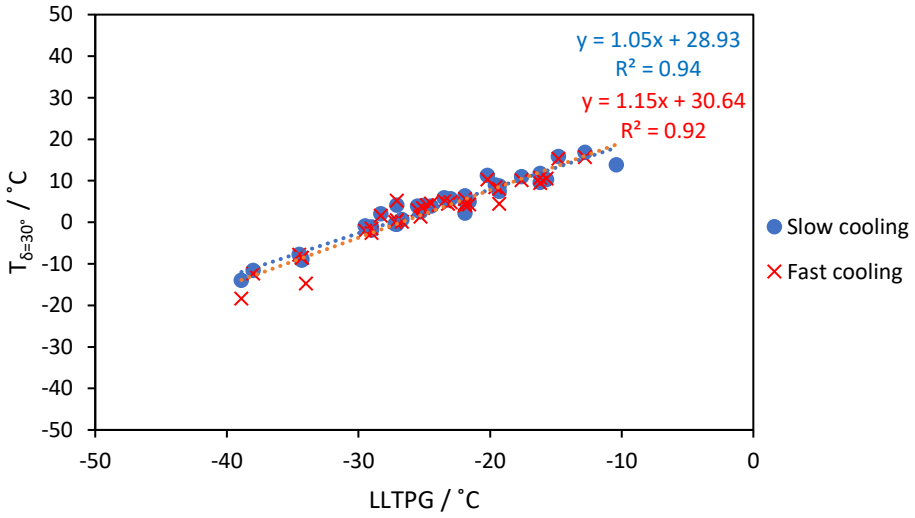

(a)

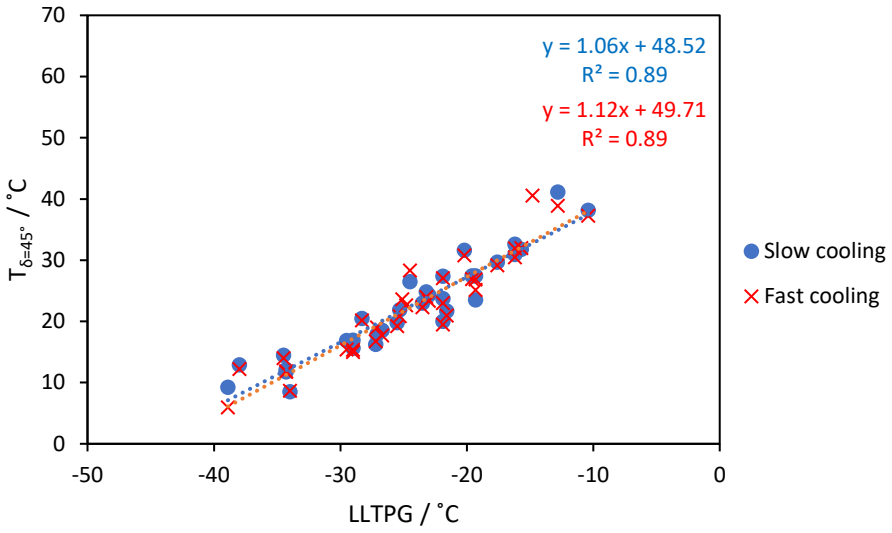

(b)

Figure 4.9: Limiting phase angle temperature correlation with LLTPG for both slow and fast cooling a) $T_{\delta=30^\circ}$, b) $T_{\delta=45^\circ}$.

Figure 4.10 shows the correlations of both limiting phase angle temperatures $T_{\delta=30^\circ}$ and $T_{\delta=45^\circ}$ with grade loss obtained from the EBBR method for both slow cooling and fast cooling conditions. $T_{\delta=30^\circ}$ for both slow and fast cooling conditions show a weak correlation with grade loss, in which R^2 values are 0.30 and 0.41, respectively, as shown in Figure 4.10 (a). Due to the weak correlations, $T_{\delta=30^\circ}$ is unsuitable to replace grade loss.

As shown in Figure 4.10 (b), $T_{\delta=45^\circ}$ for both slow and fast cooling conditions shows a moderate correlation with grade loss with the same R^2 value of 0.52. The gradient of fast cooling (2.49 ± 0.41) is less than the gradient of slow cooling (2.64 ± 0.44), which indicates that $T_{\delta=45^\circ}$ of slow cooling is more sensitive than $T_{\delta=45^\circ}$ of fast cooling. In addition to that, since gradients for variation of $T_{\delta=45^\circ}$ with grade loss for slow and fast cooling are greater than two, compared with grade loss, $T_{\delta=45^\circ}$ is sensitive more than two times. However, further testing might be required to confirm the use of $T_{\delta=45^\circ}$ instead of grade loss, as R^2 values show a moderate correlation. Grade loss cannot be replaced by DSR indicators since DSR cannot predict thermo-reversible aging in cold conditions.

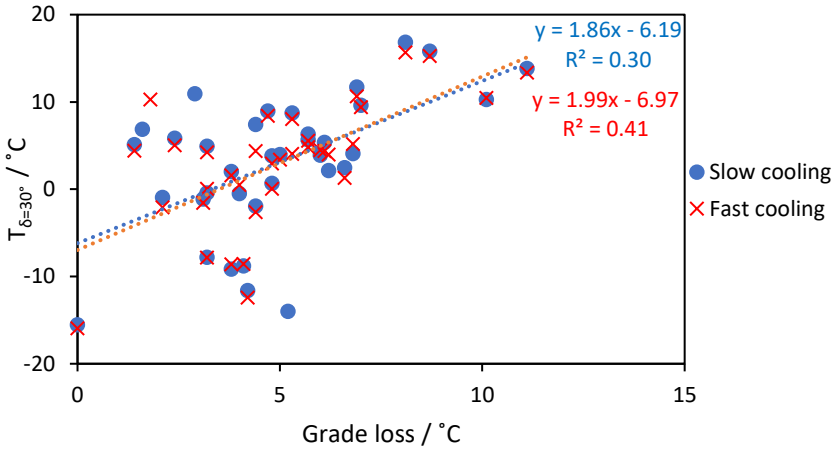

(a)

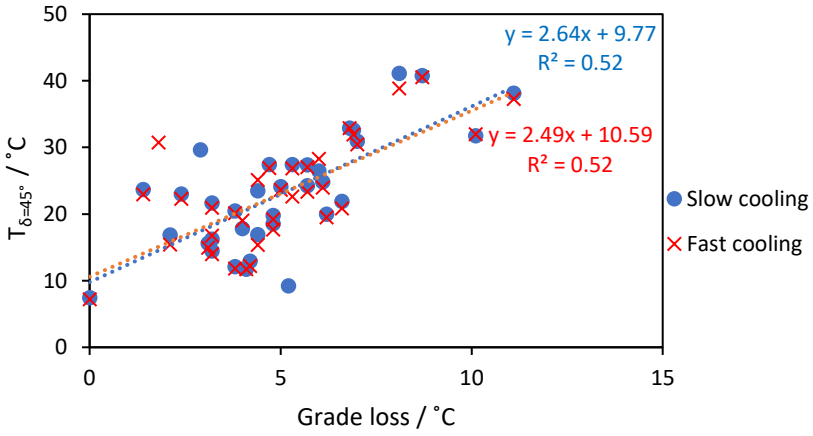

(b)

Figure 4.10: Limiting phase angle temperature correlation with grade loss for both slow and fast cooling a) $T_{\delta=30°}$, b) $T_{\delta=45°}$.

4.3.2 Correlation of ITPG with EBBR Data

According to Figure 4.11, ITPG for both slow and fast cooling conditions shows a strong correlation with LLTPG, in which R^2 values are equal to 0.90 and 0.88, respectively. The gradient of fast cooling and slow cooling is equal to 1.02 ± 0.06, which indicates that the ITPG of slow and fast cooling has the same sensitivity. Since the gradients for ITPG for slow and fast cooling with LLTPG are almost equal to one (1.02), it indicates that LLTPG and ITPG have almost the same sensitivity at both cooling conditions. Due to higher correlations and the same sensitivity, both the ITPG for slow and fast cooling and the LLTPG have equal opportunities for low-temperature performance grading for this set of USA binders recovered from loose HMA. These findings may not directly apply to Ontario binders

due to differences in hardness and stiffness. In prior Ontario binder studies, ITPG was not highly correlated with LLTPG.

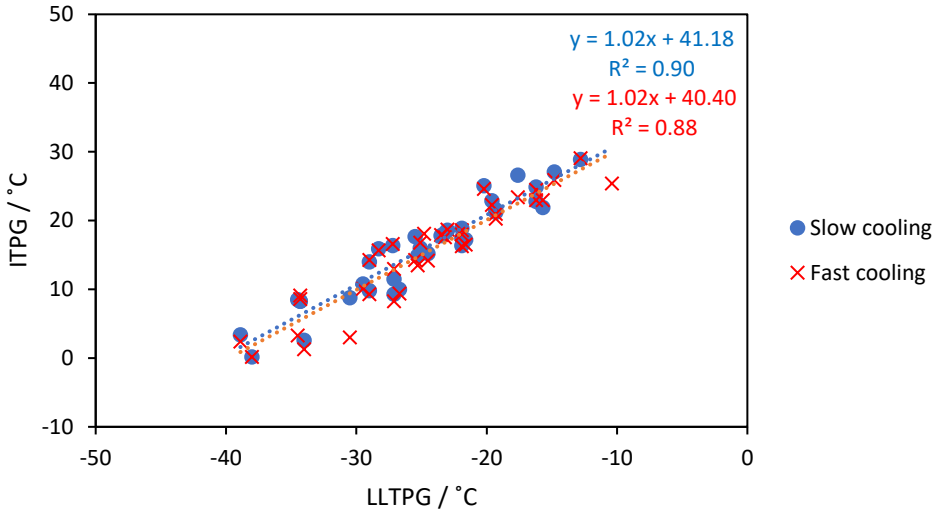

Figure 4.11: ITPG correlation with LLTPG for both slow and fast cooling.

ITPG for both slow and fast cooling conditions shows no correlation with grade loss, in which R^2 values are very low, according to Figure 4.12. Due to the lack of correlations, ITPG is not suitable to replace grade loss. Grade loss cannot be replaced by DSR indicators since DSR cannot predict thermo-reversible aging in cold conditions.

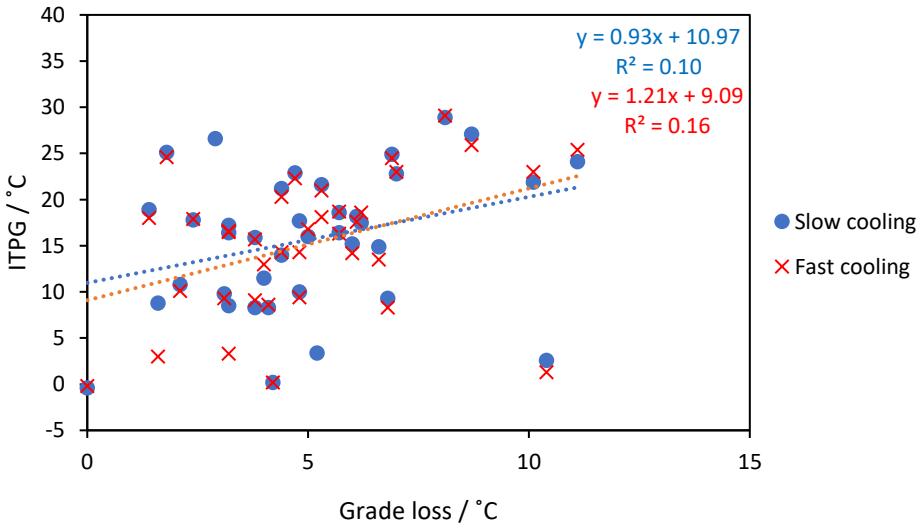

Figure 4.12: ITPG correlation with grade loss for both slow and fast cooling.

4.3.3 Correlation of Master Curve Parameters with EBBR Data

4.3.3.1 Crossover Frequency (ω_c)

Figure 4.13 shows the correlations between log ω_c and LLTPG for both slow and fast cooling conditions. The log ω_c for the slow cooling condition correlates more with LLTPG, with R^2 values of 0.86. The correlation coefficient for fast cooling is 0.82. The gradient of slow cooling and fast cooling is equal to 0.12 ± 0.01, which indicates that the log ω_c of slow and fast cooling have the same sensitivity. Since the gradients of both slow and fast cooling are less than one (0.12), the log ω_c is less sensitive at both cooling conditions compared to LLTPG. The log ω_c has an inverse relationship with LLTPG as the gradients are negative. Even though higher correlations are available for slow and fast cooling for log ω_c with LLTPG, sensitivity is less for log ω_c compared to LLTPG.

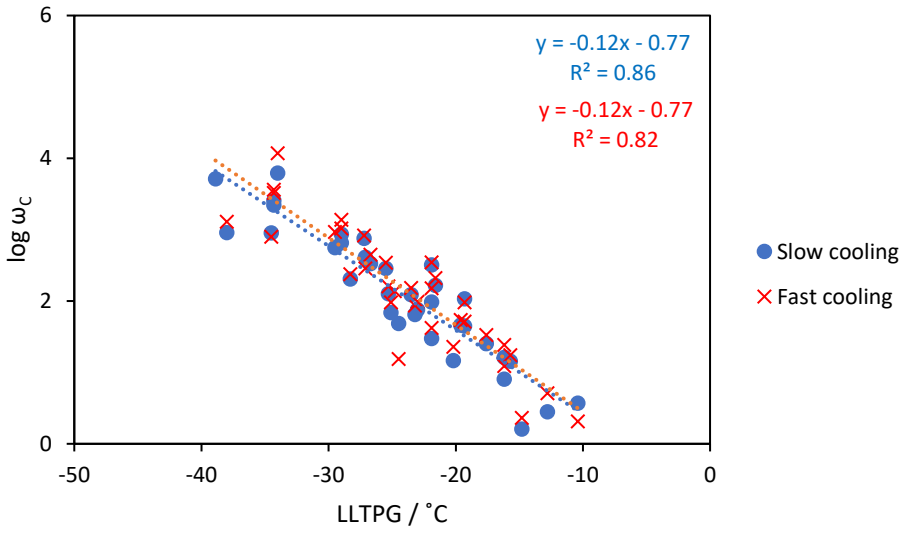

Figure 4.13: log ω_c correlation with LLTPG for both slow and fast cooling.

The relationships between log ω_c and grade loss for both slow and fast cooling conditions are displayed in Figure 4.14. The log ω_c for both slow and fast cooling conditions show a moderate correlation with grade loss, with R^2 values of 0.56 and 0.57, respectively. It is important to note the gradients of both slow and fast cooling, which are less than one, which indicates that when compared with the grade loss, the log ω_c is less sensitive at both cooling conditions. The gradients of slow cooling (0.27 ± 0.04) and fast cooling (0.28 ± 0.04) are almost the same, which indicates that the log ω_c of slow and fast cooling have almost the same sensitivity. The log ω_c has an inverse relationship with grade loss as the gradients are negative. Even though the presence of R^2 values with moderate

correlations for slow and fast cooling for log ω_c with grade loss due to the gradient lower than one log ω_c is less sensitive compared to grade loss.

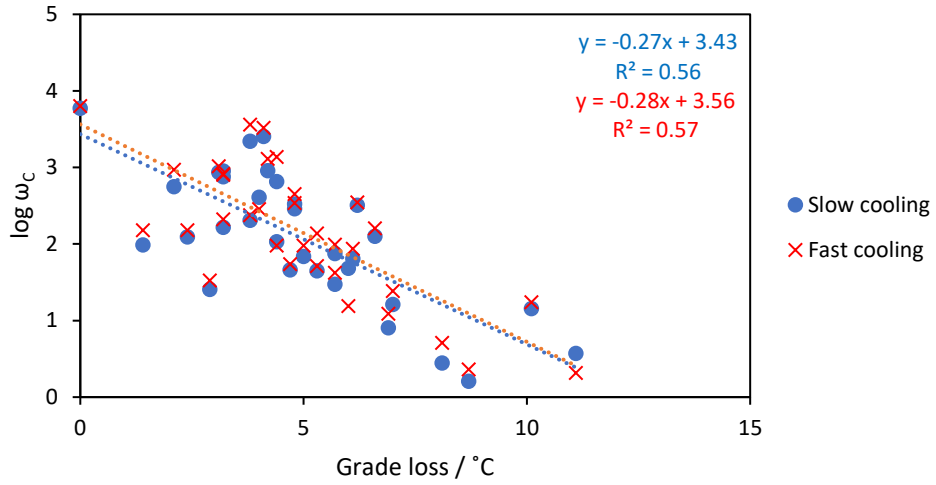

Figure 4.14: log ω_c correlation with grade loss for both slow and fast cooling.

4.3.3.2 Crossover Modulus (G_c)

Figure 4.15 shows the correlations between log G_c and LLTPG for both slow cooling and fast cooling conditions. The log G_c for both slow and fast cooling conditions shows no correlation with LLTPG with extremely low R^2 values.

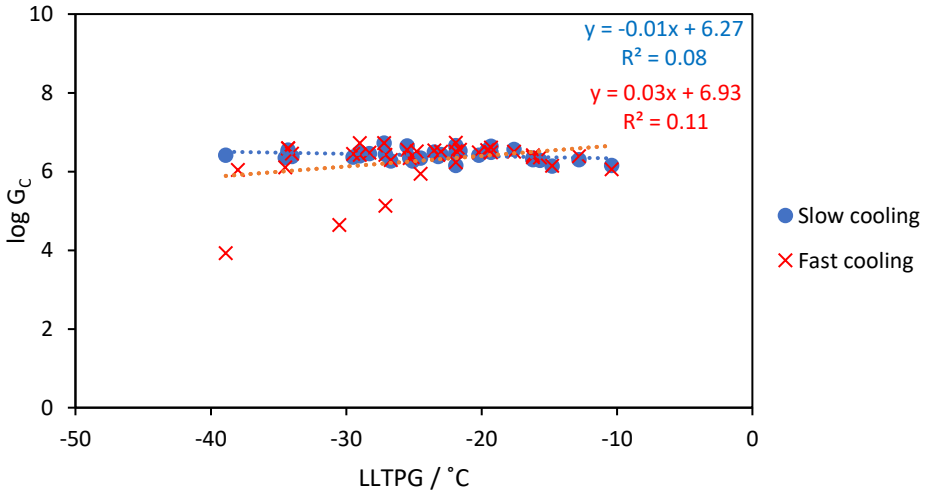

Figure 4.15: log G_c correlation with LLTPG for both slow and fast cooling.

According to Figure 4.16, log G_c with grade loss for slow cooling shows a very low correlation with R^2 of 0.32. Meanwhile, the fast cooling condition shows no correlation with grade loss, with zero R^2 values.

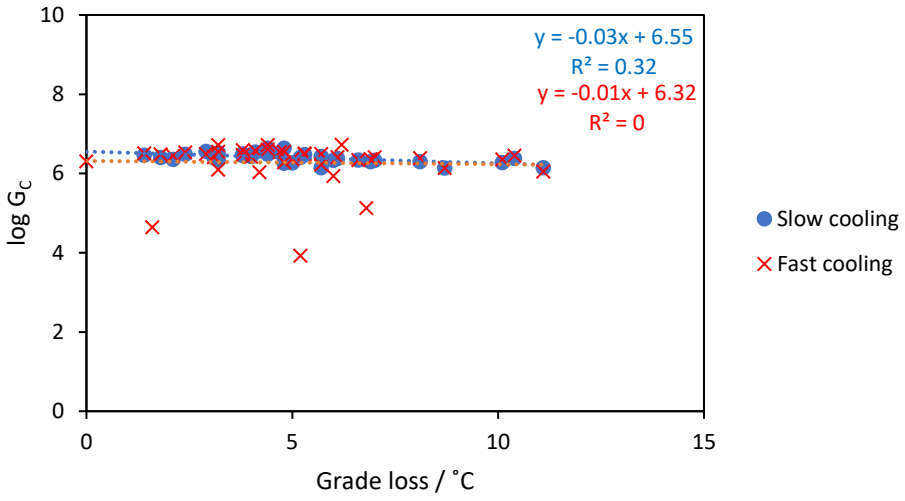

Figure 4.16: log G_c correlation with grade loss for both slow and fast cooling.

4.3.3.3 Glassy Modulus (G_g)

Figure 4.17 shows that log G_g does not have correlations with LLTPG for slow cooling conditions since the R^2 value is zero. However, for fast cooling conditions, there is a lower R^2 value of 0.33, which indicates log G_g has a minor correlation with LLTPG. Hence, replacing the LLTPG with log G_g is not effective in both cooling conditions due to a lack of strong correlations.

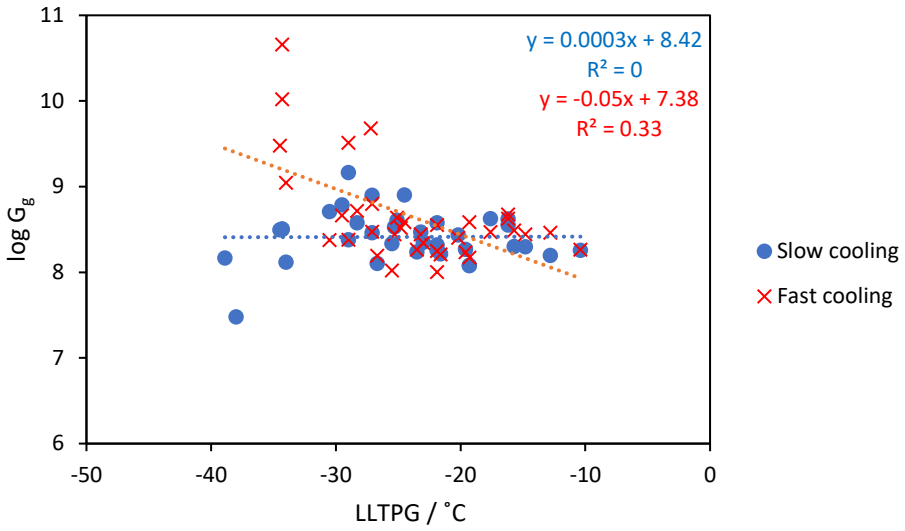

Figure 4.17: log G_g correlation with LLTPG for both slow and fast cooling.

According to Figure 4.18, log G_g for both slow and fast cooling conditions shows no correlation with grade loss since R^2 values are very low. Due to the lack of correlations, log G_g is unsuitable to replace grade loss. Further testing might be required to confirm this.

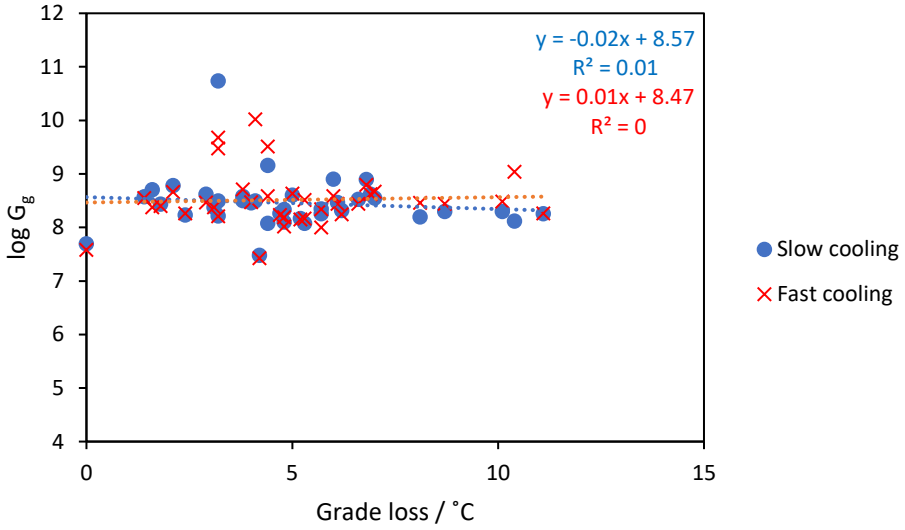

Figure 4.18: log G_g correlation with grade loss for both slow and fast cooling.

4.3.3.4 Rheological Index (R_m)

Figure 4.19 shows that R_m does not have correlations with LLTPG for slow cooling conditions since R^2 values are extremely low. Hence, replacing the LLTPG with R_m at slow cooling is not effective due to a lack of correlations.

However, for fast cooling conditions, there is an R^2 value of 0.50, which indicates R_m has a moderate correlation with LLTPG. Worthy of note is the gradient of fast cooling (0.08), which is less than one that indicates that when compared with the LLTPG, the R_m is less sensitive. Even though there are R^2 values with moderate correlations for fast cooling for the variation of R_m with LLTPG, the sensitivity is lower for R_m compared to LLTPG.

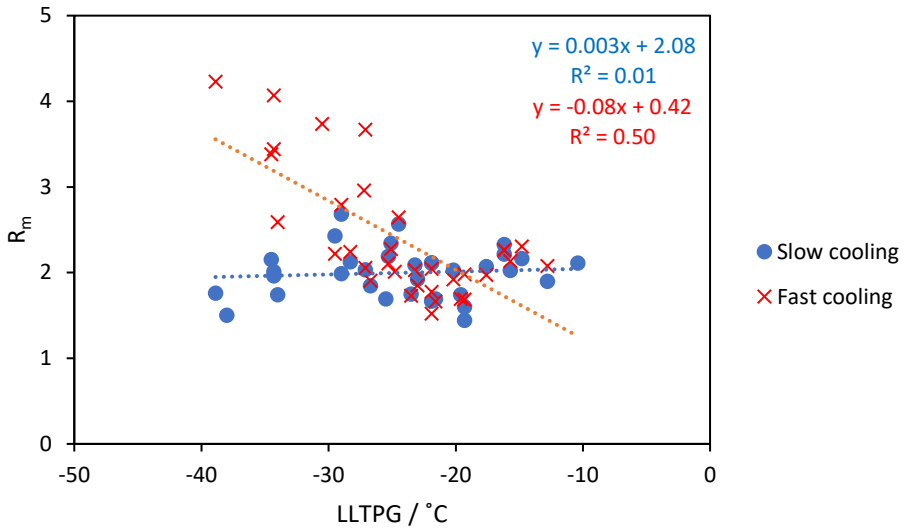

Figure 4.19: R_m correlation with LLTPG for both slow and fast cooling.

According to Figure 4.20, R_m for both slow and fast cooling conditions shows no correlation with grade loss, in which R^2 values are very low. Due to the lack of correlations, R_m is not suitable to replace grade loss. Further testing might be required to confirm this.

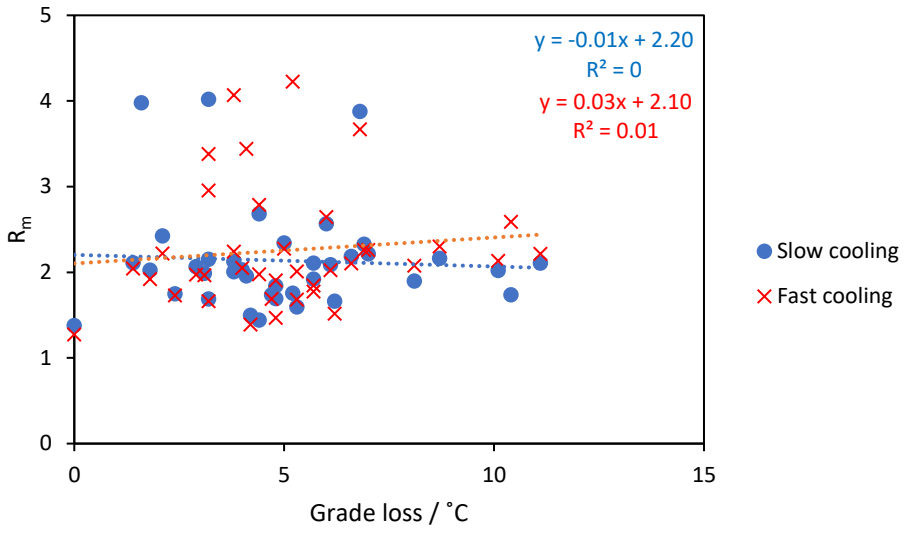

Figure 4.20: R_m correlation with grade loss for both slow and fast cooling.

4.4 Correlation Analysis of Fracture Performance with DSR

The DENT test is used to evaluate the ductile and brittle properties of asphalt binders. It is based on work done by Cotterell and Reddel on the theory of the essential work of fracture. The DENT test measures the essential work of failure in asphalt binders, the plastic work of failure, and the CTOD. This method provides a good distinction between poorly performing asphalt binders and superior ones [14].

The CTOD offers a means of measuring strain tolerance in the ductile state under high degrees of constraint and is closely linked to the essential work of fracture. It predicts the resistance of an asphalt binder to fatigue cracking. In essence, CTOD determines the maximum amount of stretching that an asphalt binder fiber may undergo before it fails. This has an inverse relationship with the amount of distress. Compared to the plastic work of failure, CTOD also gives a much more precise measure of fatigue cracking resistance. The higher the CTOD value, the better the strain tolerance and the lower the susceptibility to fatigue cracking [14].

The DENT test requires more labor, time, and samples, in contrast with the DSR test. Hence, if the CTOD indicator obtained from DENT can be replaced with DSR indicators, it would be more advantageous. Thus, in this investigation, the results from the DENT test were correlated with the results from the DSR test for USA samples from three regions under different cooling rates (slow and fast).

4.4.1 Correlation of Limiting Temperatures with DENT Data

Figure 4.21 shows the strong correlations of $T_{\delta=30^\circ}$ with CTOD for both slow and fast cooling conditions. $T_{\delta=30^\circ}$ for slow cooling conditions more correlates with CTOD, with an R^2 value of 0.81. The R^2 value is 0.77 for $T_{\delta=30^\circ}$ for fast cooling. The gradient of slow cooling (0.67 ± 0.06) is almost equal to that of fast cooling (0.62 ± 0.06), which shows that $T_{\delta=30^\circ}$ of slow and fast cooling rates have the same sensitivity. It is important to note that the gradients of both slow and fast cooling are less than one, which indicates that, when compared with the CTOD, the $T_{\delta=30^\circ}$ is less sensitive at both cooling conditions. Though $T_{\delta=30^\circ}$ has strong correlations with CTOD, in terms of sensitivity, the latter is best.

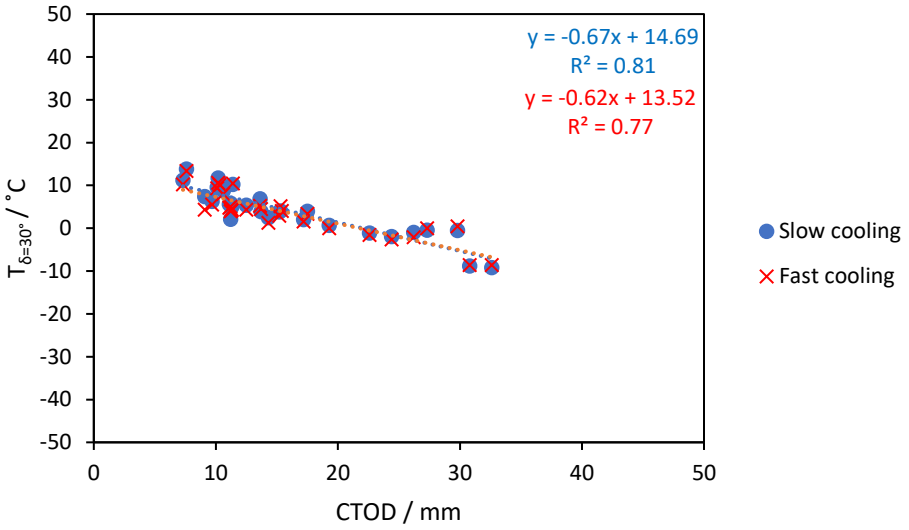

Figure 4.21: $T_{\delta=30^\circ}$ correlation with CTOD for both slow and fast cooling.

The correlations of $T_{\delta=45^\circ}$ with CTOD for both slow and fast cooling conditions are shown in Figure 4.22. $T_{\delta=45^\circ}$ for both slow and fast cooling conditions show a moderate correlation with CTOD with R^2 values of 0.57 and 0.62, respectively. Fast cooling has a higher correlation than slow cooling. The gradients of slow cooling and fast cooling are almost the same, as the values are 0.73 ± 0.12 and 0.70 ± 0.10, respectively, which shows that $T_{\delta=45^\circ}$ of slow and fast cooling have almost the same sensitivity. It is important to note that the gradients of both slow and fast cooling are less than one, which indicates that when compared with the CTOD, the $T_{\delta=45^\circ}$ is less sensitive at both cooling conditions. Despite the availability of R^2 values with moderate correlations for both slow and fast cooling for $T_{\delta=45^\circ}$ with CTOD, $T_{\delta=45^\circ}$ is less sensitive than CTOD.

The $T_{\delta=30^\circ}$ (Figure 4.21) has strong correlations compared to $T_{\delta=45^\circ}$ at both cooling conditions. When $T_{\delta=30^\circ}$ is compared with $T_{\delta=45^\circ}$, the latter has higher sensitivity due to the higher gradient. However, both have less sensitivity relative to CTOD.

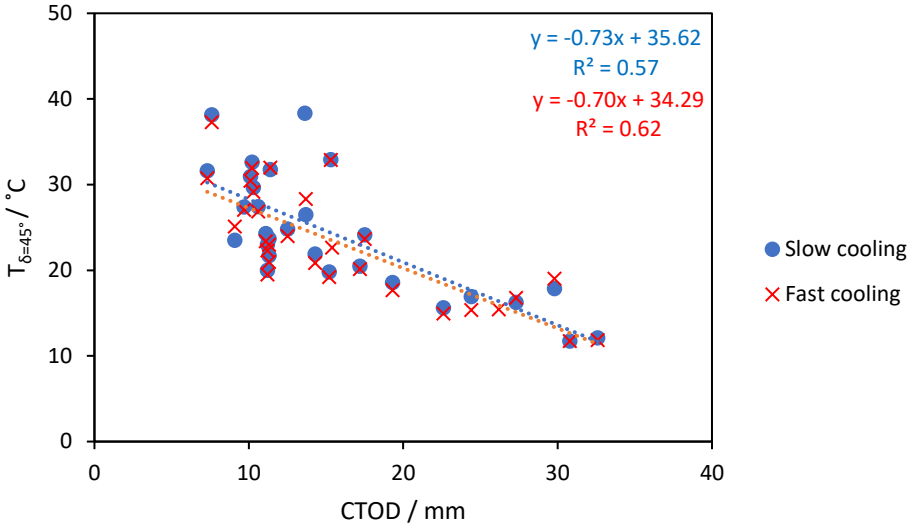

Figure 4.22: $T_{\delta=45^\circ}$ correlation with CTOD for both slow and fast cooling.

4.4.2 Correlation of ITPG with DENT Data

The correlations between ITPG and CTOD for both slow and fast cooling conditions are shown in Figure 4.23. ITPG for both slow and fast cooling conditions shows a moderate correlation with CTOD, with R^2 values of 0.55 and 0.56, respectively. The gradients of slow cooling and fast cooling are almost the same, as the values are 0.54 ± 0.09 and 0.52 ± 0.09, which shows that the ITPG of slow and fast cooling has almost the same sensitivity. Notably, the gradients of both fast and slow cooling are less than one, indicating that the ITPG is less sensitive under both cooling rates when compared to the CTOD. The ITPG and CTOD have moderate correlations for both slow and fast cooling. But ITPG is less sensitive than CTOD.

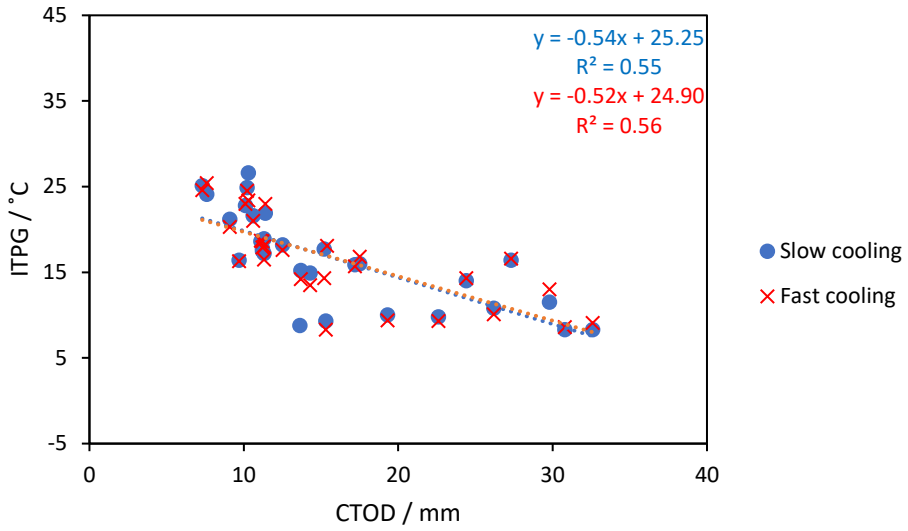

Figure 4.23: ITPG correlation with CTOD for both slow and fast cooling.

4.4.3 Correlation of Master Curve Parameters with DENT Data

4.4.3.1 Crossover Frequency (ω_c)

The relationships between log ω_c and CTOD for both slow and fast cooling conditions are displayed in Figure 4.24. The log ω_c for the slow cooling condition shows a strong correlation with CTOD, with an R^2 value of 0.70, while the fast cooling condition shows a moderate correlation with CTOD, with an R^2 value of 0.66. The gradients of slow cooling and fast cooling are the same, with a value of 0.08 ± 0.01, which indicates that the log ω_c of slow and fast cooling have the same sensitivity. It is important to note the gradients of both slow and fast cooling, which are extremely less than one, which indicates that when compared with the CTOD, the log ω_c is less sensitive at both cooling conditions. Even though the presence of R^2 values with strong and moderate correlations, respectively, for slow and fast cooling for log ω_c with CTOD considering the sensitivity, CTOD is better.

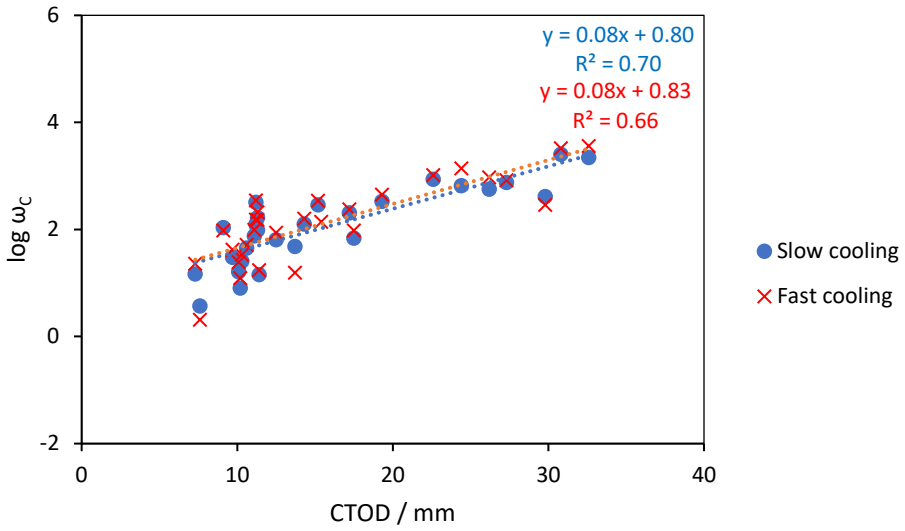

Figure 4.24: log ω_c correlation with CTOD for slow and fast cooling.

4.4.3.2 Crossover Modulus (G_c)

The log G_c for both slow and fast cooling conditions shows no correlation with CTOD with extremely low R^2 values, according to Figure 4.25. Hence, the log G_c is not a possible alternative for the CTOD.

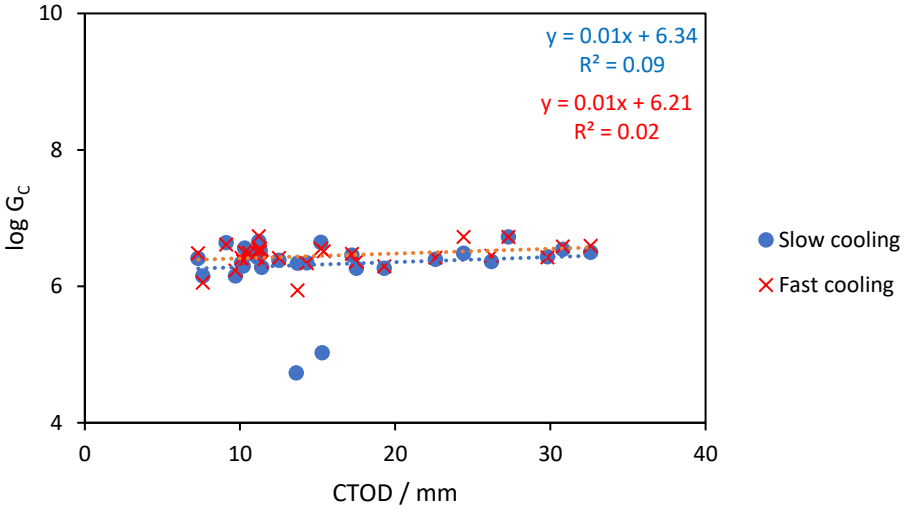

Figure 4.25: log G_c correlation with CTOD for slow and fast cooling.

4.4.3.3 Glassy Modulus (G_g)

Figure 4.26 shows that log G_g does not have correlations with CTOD for slow cooling conditions since the R^2 value is 0.17. Hence, replacing the CTOD with log G_g is not effective at slow cooling due to a lack of strong correlation.

However, for fast cooling conditions, there is an R^2 value of 0.52, which indicates log G_g has a moderate correlation with CTOD. However, since the gradient for fast cooling is extremely low (0.06), the sensitivity of log G_g is extremely lower compared to CTOD from the DENT test. Hence, log G_g at fast cooling is not suitable for surrogate CTOD.

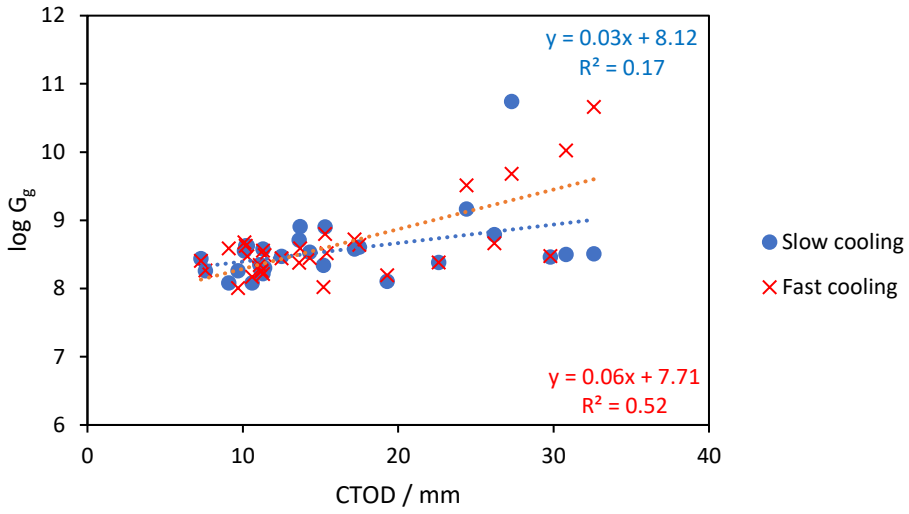

Figure 4.26: log G_g correlation with CTOD for slow and fast cooling.

4.4.3.4 Rheological Index (R_m)

Figure 4.27 shows that R_m does not have correlations with CTOD for slow cooling conditions since R^2 values are extremely low (0.05). Hence, replacing the CTOD with R_m at slow cooling is not effective due to a lack of correlations. However, for fast cooling conditions, there is an R^2 value of 0.47, which indicates R_m has a weak correlation with CTOD. Worthy of note is that the gradient of both fast and slow cooling is extremely low (0.05), which is less than one that indicates that when compared with the CTOD, the R_m is less sensitive. Hence, R_m is not an alternative to the CTOD.

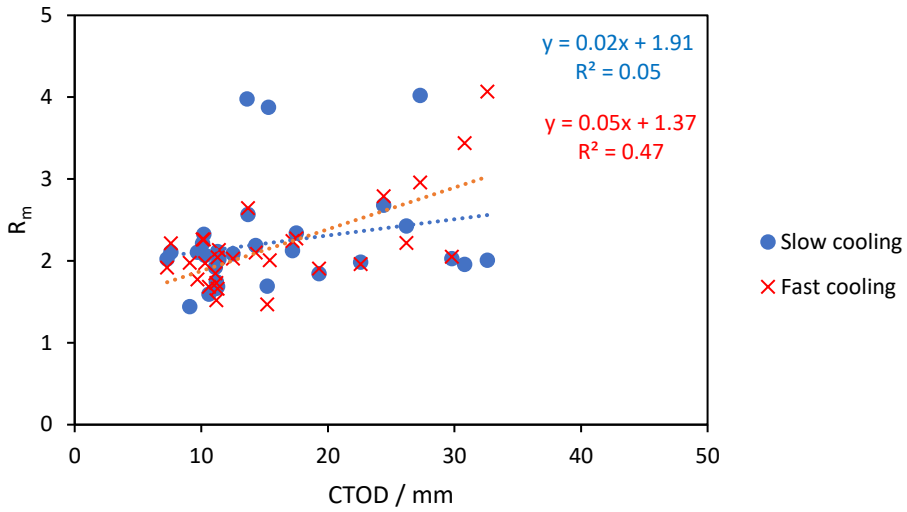

Figure 4.27: R_m correlation with CTOD for slow and fast cooling.

4.5 Analysis of Black Space Diagrams

An effective tool for comprehending the rheological behavior of asphalt samples is a Black space diagram. It aids in distinguishing a heterogeneous binder with multiple phases from one with a homogenous composition. Black space diagrams are simple rheological plots of the logarithm of G* versus δ. Rheological simplicity and homogeneity are indicators of a Black space diagram's smooth and continuous evolution of curves corresponding to various temperatures. As an example, a binder with a heterogeneous composition and multiple phases correlates to a Black space diagram with discontinuities among curves and anomalous behavior [61].

Previous studies have shown that cracking and the associated failure mechanisms that often accompany highly oxidized asphalt can be better predicted by using location on Black space diagrams at lower temperatures. According to the study, the Black space diagram of a binder is a critical performance measure for cracking. The wax crystallization in the asphalt binder, which has been known to cause physical hardening, is one of the phase changes that the diagrams also take into account [80].

4.5.1 Analysis of Binders from Different Origin Using the Black Space Diagrams

Generally, when the δ increases, the G* should decrease. Depending on the level of modification of asphalt binder, there might be deviations from the above mentioned behavior of G* and δ. Thus, looking at the Black space diagrams, it could be possible to figure out the modified and unmodified binders. Nine agencies in the USA, comprising the West, Mid-West, and North-East regions, are represented by the Black space diagrams for asphalt

binders below, Figure 4.28. One example from each agency is included here since samples from the same agency exhibit identical behavior.

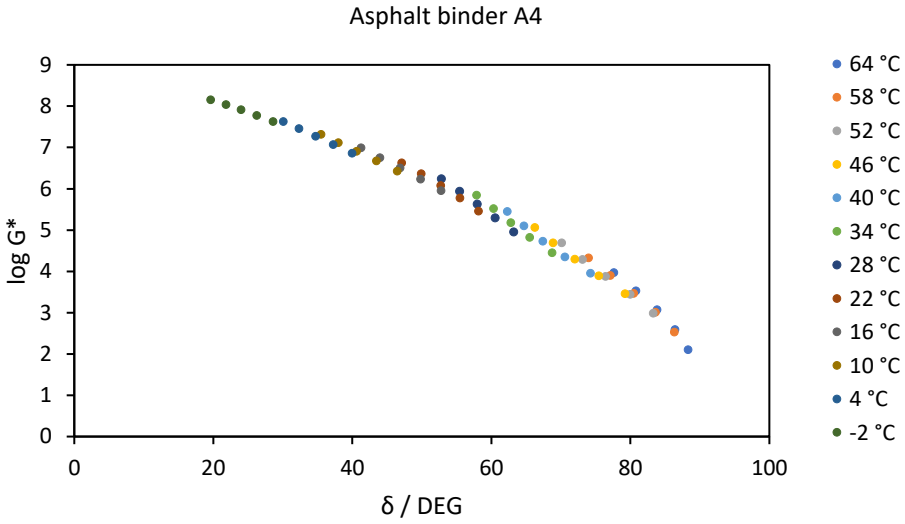

(a)

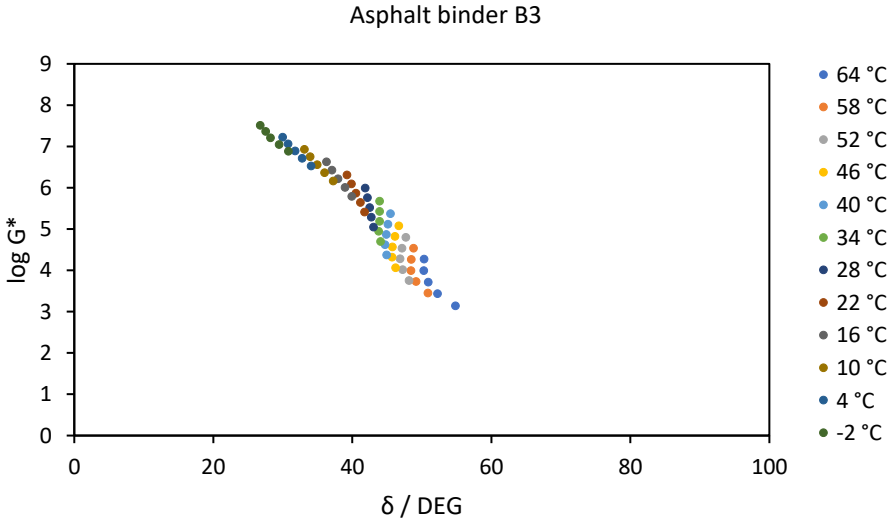

(b)

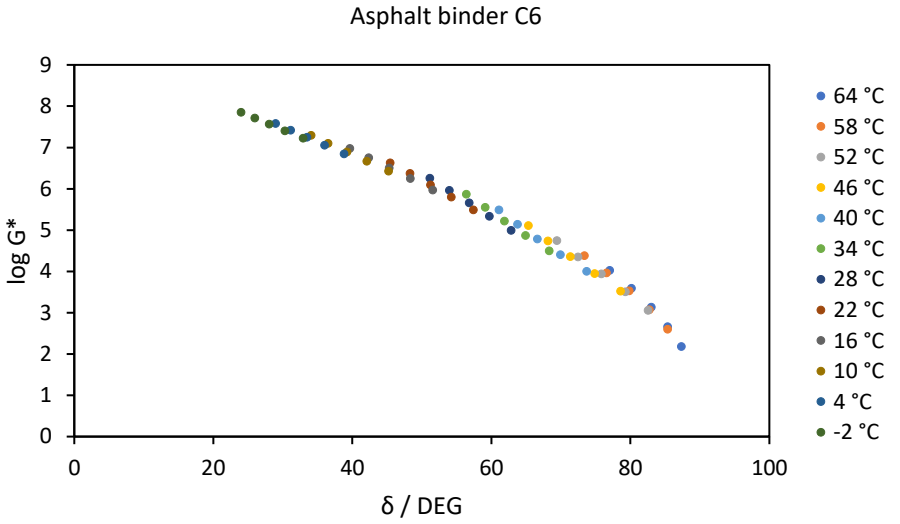
Asphalt binder C6
log G*
δ / DEG
0
1
2
3
4
5
6
7
8
9
0
20
40
60
80
100
64 °C
58 °C
52 °C
46 °C
40 °C
34 °C
28 °C
22 °C
16 °C
10 °C
4 °C
-2 °C

(c)

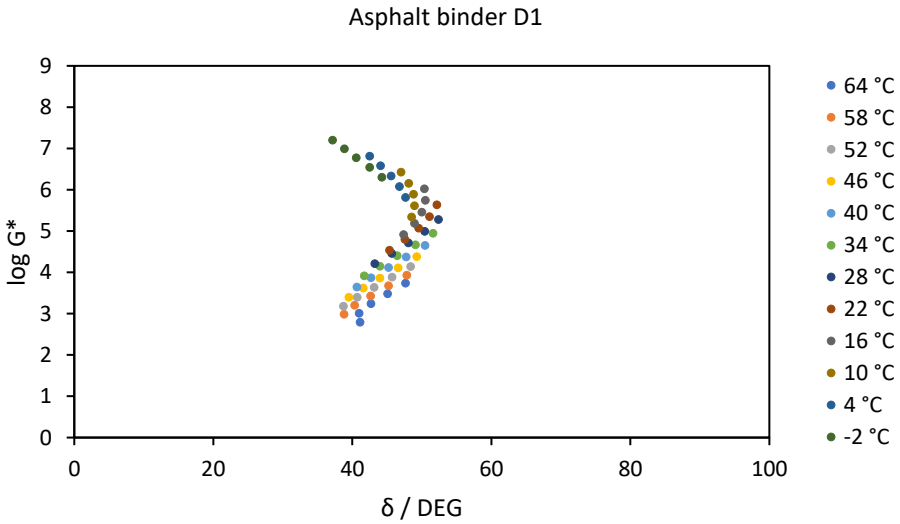
Asphalt binder D1
log G*
δ / DEG
0
1
2
3
4
5
6
7
8
9
0
20
40
60
80
100
64 °C
58 °C
52 °C
46 °C
40 °C
34 °C
28 °C
22 °C
16 °C
10 °C
4 °C
-2 °C

(d)

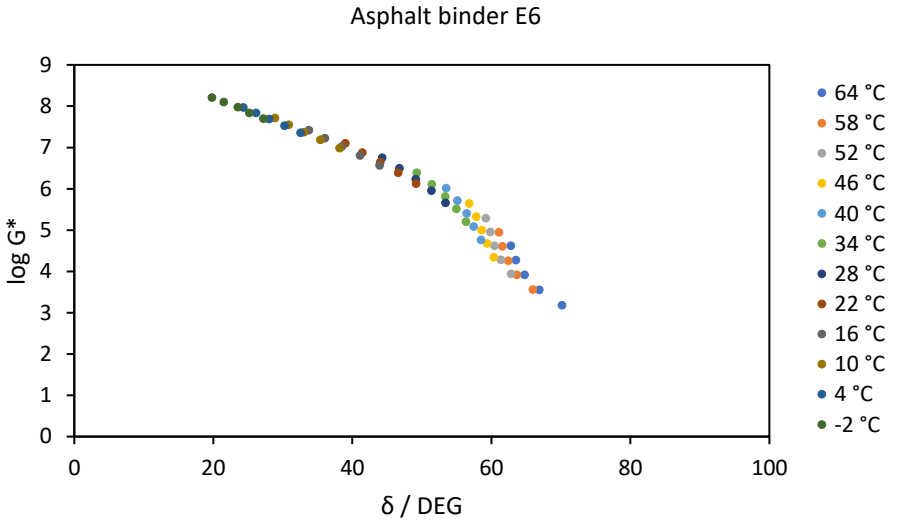
Asphalt binder E6
log G*
δ / DEG
0
1
2
3
4
5
6
7
8
9
0
20
40
60
80
100
64 °C
58 °C
52 °C
46 °C
40 °C
34 °C
28 °C
22 °C
16 °C
10 °C
4 °C
-2 °C

(e)

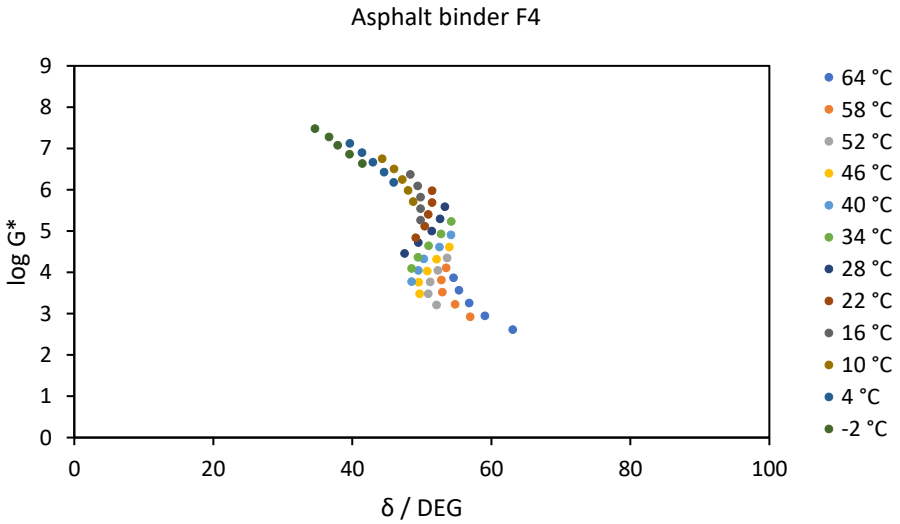
Asphalt binder F4
log G*
δ / DEG
0
1
2
3
4
5
6
7
8
9
0
20
40
60
80
100
64 °C
58 °C
52 °C
46 °C
40 °C
34 °C
28 °C
22 °C
16 °C
10 °C
4 °C
-2 °C

(f)

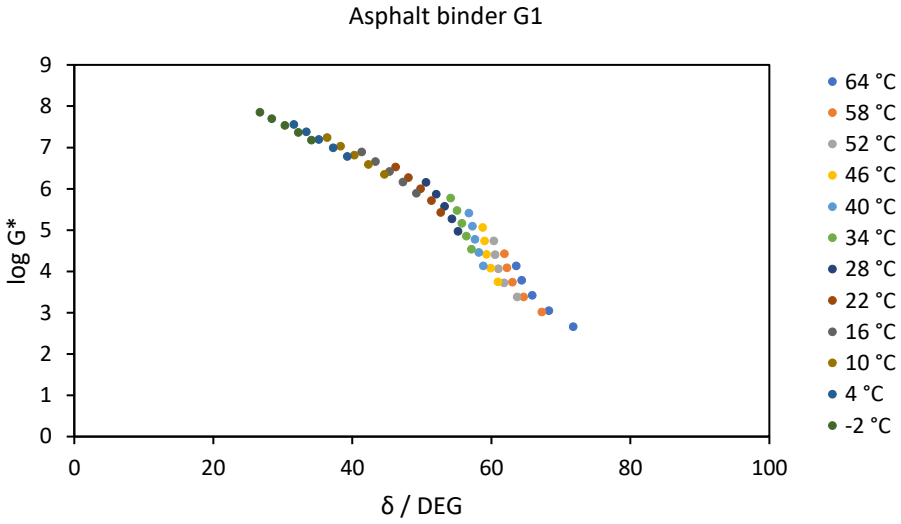
Asphalt binder G1
log G*
δ / DEG
0
1
2
3
4
5
6
7
8
9
0
20
40
60
80
100
64 °C
58 °C
52 °C
46 °C
40 °C
34 °C
28 °C
22 °C
16 °C
10 °C
4 °C
-2 °C

(g)

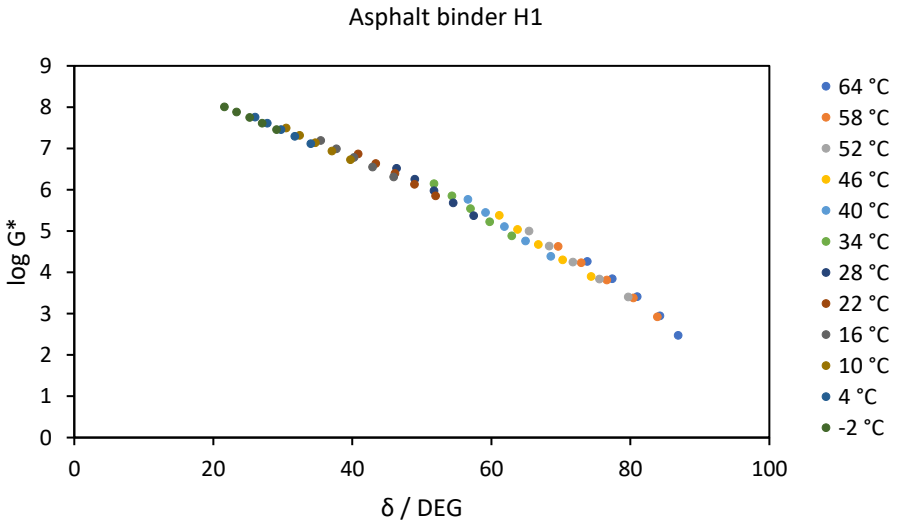
Asphalt binder H1
log G*
δ / DEG
0
1
2
3
4
5
6
7
8
9
0
20
40
60
80
100
64 °C
58 °C
52 °C
46 °C
40 °C
34 °C
28 °C
22 °C
16 °C
10 °C
4 °C
-2 °C

(h)

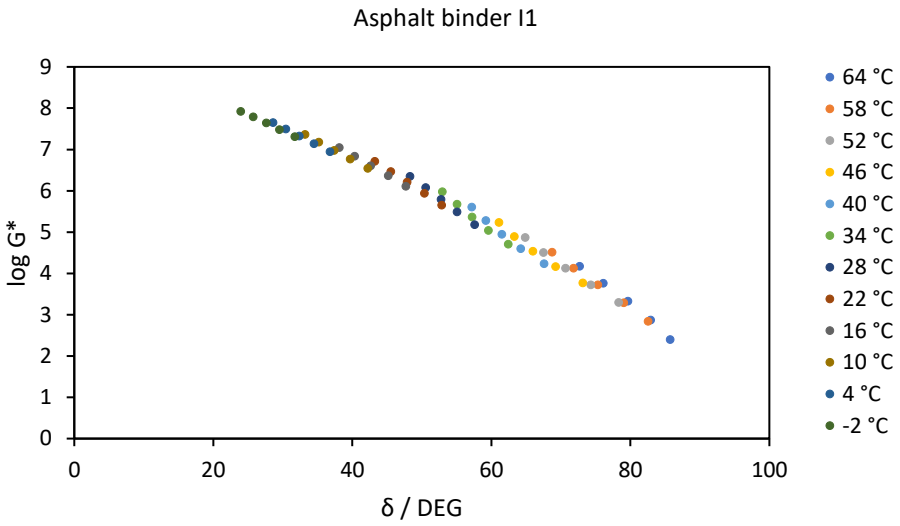

(i)

Figure 4.28: Black space diagrams for asphalt binders from different origins at different temperatures.

4.5.2 Comparison of Black Space Diagrams for Slow and Fast Cooling Rates

If Black space diagrams overlap each other, this indicates that the asphalt sample shows almost the same stiffness and stress relaxation abilities at different cooling conditions. Hence, Black space diagrams could be used to compare the performance similarities between slow and fast cooling. According to Figure 4.29, plots for slow and fast cooling conditions overlap with each other. Two tested samples were used to demonstrate how slow and fast cooling rates affect Black space diagrams because all the tested samples show behavior that is similar to either of the figures. Figure 4.29 (a) represents the less modified binders, while Figure 4.29 (b) represents the highly modified binders. Eventually, these observations validated the ability to use either slow or fast cooling conditions for DSR testing.

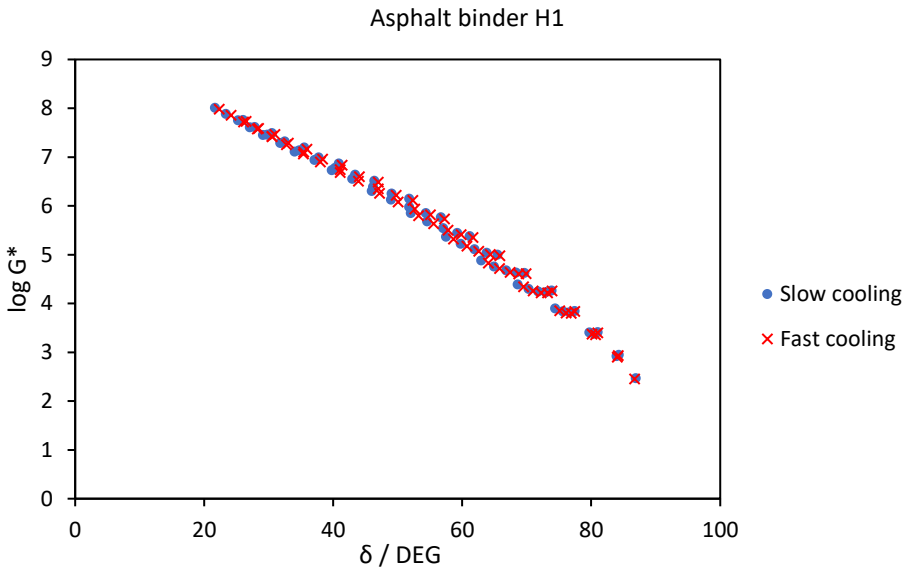

(a)

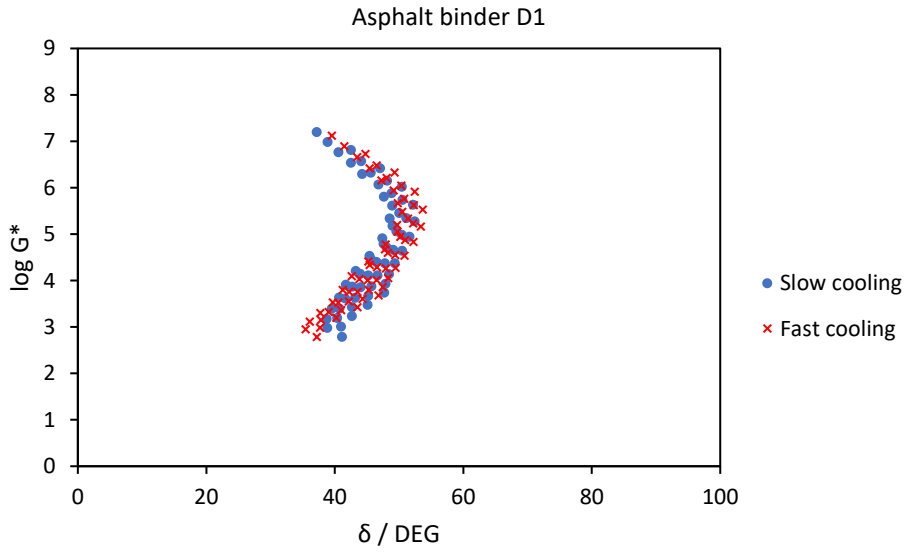

(b)

Figure 4.29: Black space diagrams for asphalt binders from different origins at different temperatures for slow and fast cooling.

4.6 Chemical Characterization

One of the key elements influencing the duration that asphalt pavement lasts is the quality of the asphalt binder. Researchers have attempted, but have been unable, to establish a direct correlation between the chemical composition of asphalt and its quality. This was mostly caused by the complex nature of the chemical composition

of asphalt and a lack of thorough knowledge regarding the classification of the chemical composition of asphalt. Here, asphalt binders from the USA have been tested with XRF, NMR, and FTIR spectroscopy for chemical characterization.

4.6.1 XRF Spectroscopy Analysis

In this research, asphalt binder samples from three different regions of the USA undergo XRF analysis to discover and compare the relative amounts of heavy metals present in each of these samples. The presence of heavy metals, especially zinc and molybdenum, was indicative of the presence of recycled engine oil bottoms (REOB) as an additive in the asphalt binders. The presence of REOB was inferred to be the cause of increased chemical and physical hardening of asphalt binders. The heavy metals in REOB destabilize the asphaltenes in the asphalt binder, causing changes in chemical properties, which in turn affect its rheological performance badly. Also, the paraffinic nature of REOB leads to increased precipitation of asphaltenes, causing a decrease in the adhesive strength of the asphalt binder to the aggregate [14].

For a very long time, researchers have studied the colloidal sol/gel nature of asphalt cement, and significant findings have been published regularly. A gelled material behaves in a non-Newtonian fashion with significant elasticity, delayed elasticity, and non-linearity in viscoelastic characteristics, while a sol substance behaves in a largely Newtonian manner. The literature is generally in agreement that materials that are excessively blown, gelled, or elastic should not be used for paving applications. In sol-type asphalts, thermal stresses can be released, but in gel-type asphalts, they are retained, which frequently causes excessive premature cracking [68].

The use of REOB has become popular because it probably offers the most economical means of extending the Superpave grade span. Profits rise when more waste oil residue is added because it sells for significantly less than regular asphalt cement. Binders high in asphaltenes become more susceptible to both chemical and physical hardening as the amount of REOB increases. This takes place due to the decreasing solubility of the asphaltene portion in the maltene continuous phase to generate gel-type binders. The resulting binders exhibit delayed elasticity, high zero shear viscosity, an extensive degree of non-Newtonian flow, and low stiffness. These binders are more prone to cracking at low-temperatures because they are less able to relax thermal stresses.

4.6.1.1 Analysis of Zinc and Molybdenum Present in Asphalt Binders from Different Origins

The majority of the examined asphalt binders, as shown in Figure 4.30, contain zinc. The samples belonging to B agency from the West region had significantly more zinc in their asphalt binders than the other samples, according to the results. Zinc content is highest in binder B3, with a value of more than 18,000 counts per second. Zinc levels in asphalt binders from agencies A, D, and E are extremely low. The remaining agencies all have modest zinc levels. The zinc concentration is less than 2,000 counts per second in most of the binders. The presence of REOB in the USA samples is indicated by zinc detection. Hesp and Shurvell state that zinc is expected to be present in REOB in rather constant proportions since zinc dialkyldithiophosphate (ZDDTP) is a universal and deliberate antioxidant and anti-wear additive used in engine oil [68]. Thus, most of the examined asphalt binders contain zinc, which indicates the addition of REOB in the USA.

X-ray analysis was done by Hesp and Shurvell on asphalt binders from 26 distinct asphalt pavement contracts in Ontario. The findings indicated that substantial levels of zinc were present in the asphalt binders of 12 out of 15 poorly performing asphalt pavements. Zinc did not, however, appear in any of the eleven asphalt pavements with superior performance. They concluded that the collapse of road networks, which is mostly caused by the increasing physical hardening and reduced resiliency of asphalt pavements, is caused by the presence of REOB in asphalt pavements [68]. The above mentioned findings of Hesp and Shurvell should be validated for the USA asphalt pavements, which are constructed with REOB modified asphalt binders.

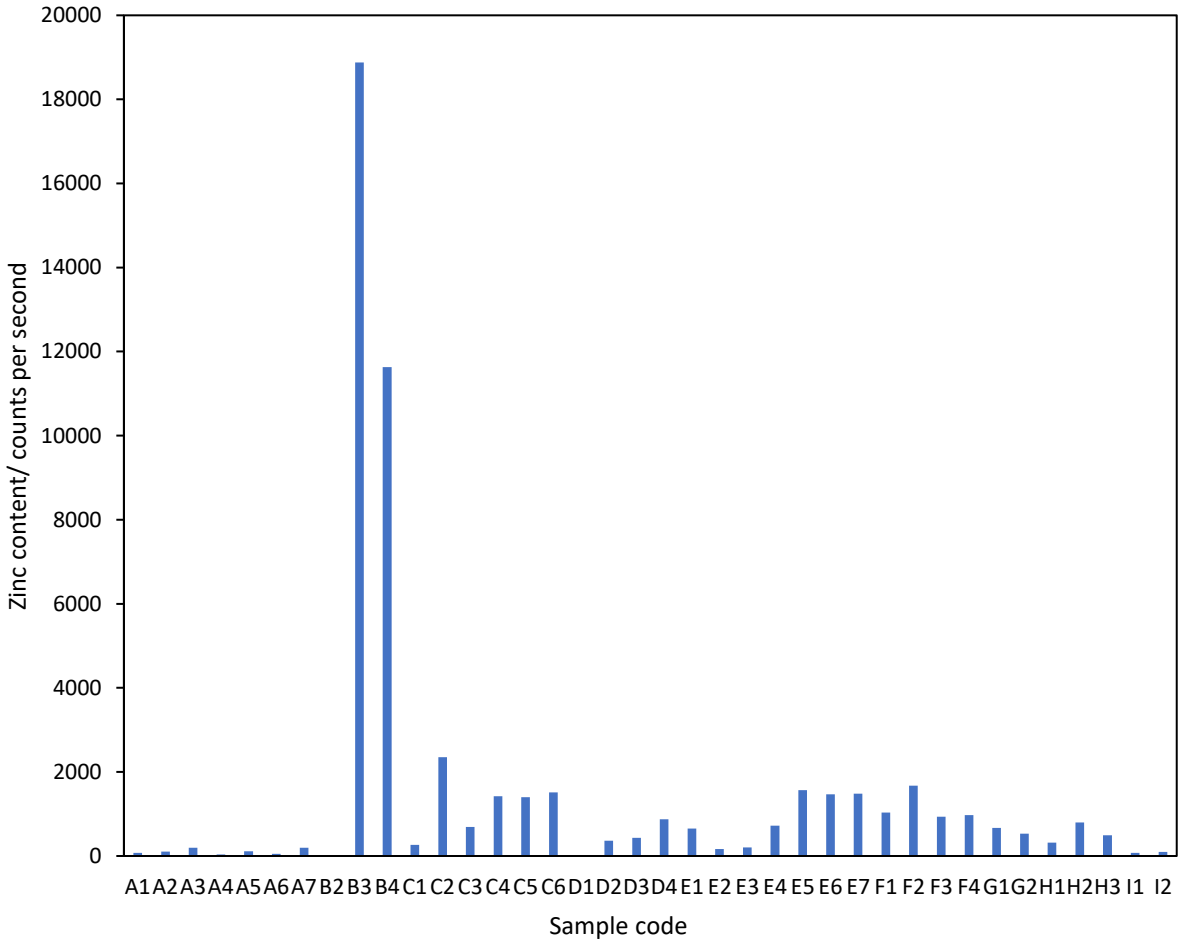

Figure 4.30: Zinc content of asphalt binders with different origins.

The presence of molybdenum suggests that REOB is being used in asphalt cement as a modifier. Thus, it is crucial to compare the molybdenum content of asphalt samples from various USA agencies since this can reveal information about the relationship between differences in molybdenum concentration and the performance of the asphalt binder relative to the content of REOB. All binders from various USA regions consisted of molybdenum, as seen in Figure 4.31. The molybdenum content varies significantly across samples. Binder B3, which is in the West, has the highest molybdenum content, reaching close to 3,000 counts per second. Many other samples have significantly lower molybdenum contents, with many below 1,000 counts per second. The D state, which is in the West, has extremely low amounts of molybdenum. Hesp and Shurvell claim that molybdenum was discovered in asphalt cement, which has undergone premature failure, while superior grade asphalt cement was discovered to be free of molybdenum. Thus, it can be concluded that since USA asphalt binders consist of molybdenum as a result of

the REOB addition, premature failure might occur, and excessive cracking of roads may occur due to the increased physical hardening and reduced strain tolerance this additive causes in asphalt pavements in the USA [67].

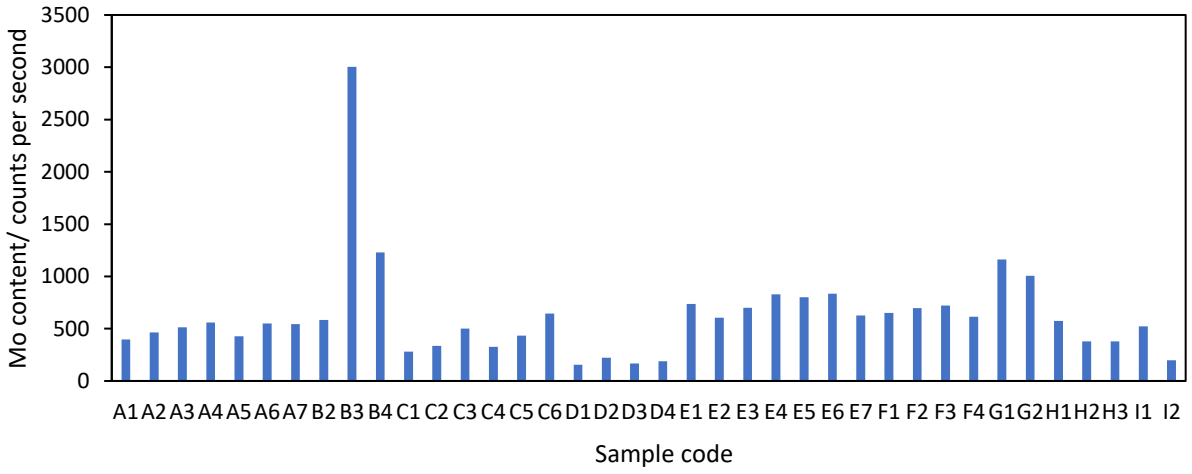

Figure 4.31: Molybdenum content of asphalt binders with different origins.

4.6.1.2 Analysis of XRF Spectra for Asphalt Binder

The emission of radiation is detected by the XRF analyzer, and the presence of various heavy elements can be determined both quantitatively and qualitatively by plotting the intensity against the X-ray energy. Peak heights in the spectrum offer a quantitative indicator of the existence of metals, but to enable absolute comparisons between metals, calibrations for each metal are needed. Several unique peaks in the spectra suggest the existence of several metals of interest. Since concern is paid toward the determination of REOB, the zinc peaks at 8.6 and 9.6 keV and the molybdenum peak at 17.4 keV are considered.

For a comparison of zinc and molybdenum levels in asphalt binders, Figure 4.32 provides an XRF spectrum for 0 % REOB, 16 % REOB, and asphalt binder B3. When considering the XRF spectrum for 0 % REOB (Figure 4.32 (a)), specific peaks for zinc and molybdenum are not significant. Comparatively, in the XRF spectrum for 16 % REOB (Figure 4.32 (b)), peaks for zinc and molybdenum are seen. It is worth noting the XRF spectrum of the B3 binder (Figure 4.32 (c)) since Figures 4.30 and 4.31 have the highest zinc and molybdenum contents, respectively, for binder B3. Thus, comparing the XRF spectrum of the B3 binder to 0 % REOB and 16 % REOB is important. Peaks with higher intensities for zinc at 8.6 and 9.6 keV and for the molybdenum peak at 17.4 keV confirm that the B3

binder contains a higher amount of zinc and molybdenum. Hence, binder B3 has been highly modified with the addition of REOB.

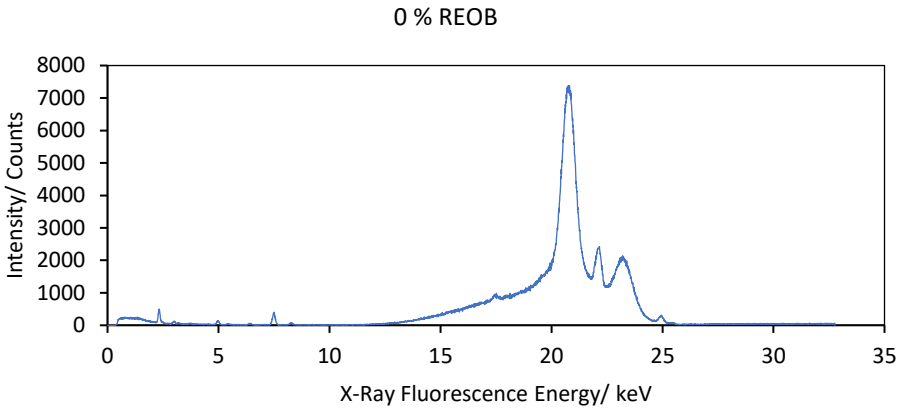

(a)

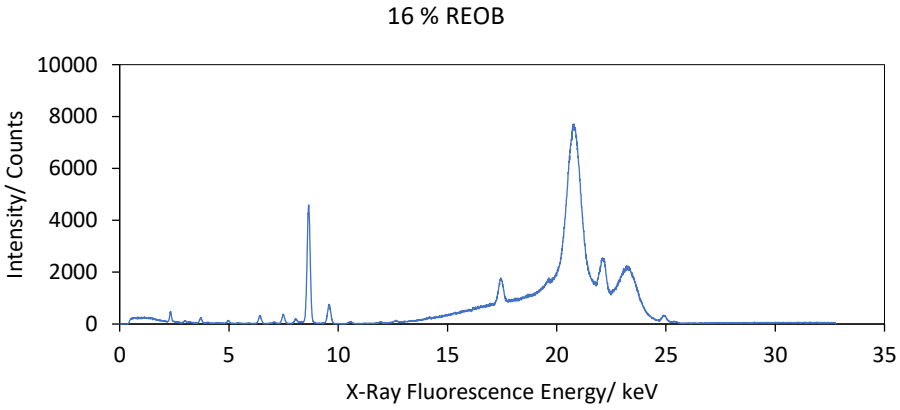

(b)

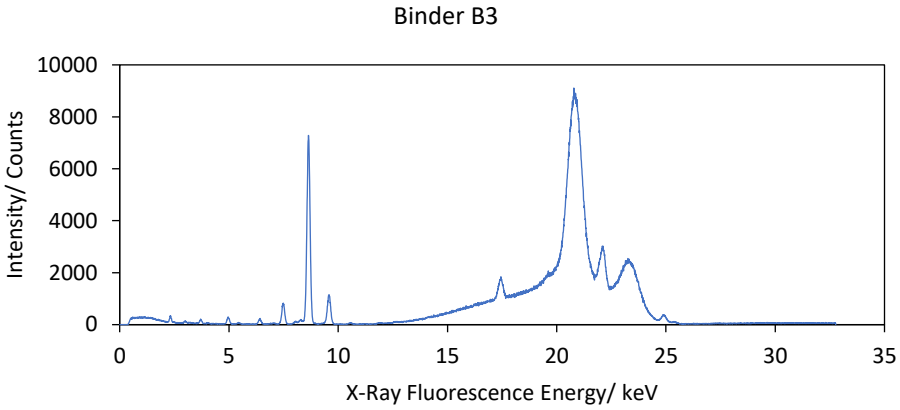

(c)

Figure 4.32: X-ray fluorescence spectra for a) 0 % REOB b) 16 % REOB, and c) binder B3.

4.6.2 Analysis of NMR Spectroscopy Data

To better understand the evolving trends in the crystalline components of asphalt binders, tests were conducted on asphalt binders from the USA with varying degrees of oxidation (unaged and PAV aged). These asphalt binders, in different oxidation states, were characterized using NMR spectroscopy in the liquid state. Among the chemical constituents of asphalt, wax plays a significant role in influencing the low-temperature service performance. Wax is generally considered to be a material that primarily consists of saturated long linear hydrocarbons and crystallizes in asphalt at 25 °C. Most wax compositions are made up of normal alkanes and isomeric alkanes, with the former having the most detrimental effect on asphalt performance [69].

4.6.2.1 ^{13}C NMR and DEPT-135 Spectra of Asphalt Binders

In the ^{13}C NMR spectra, carbons in aliphatic chains and naphthenic rings are responsible for the peaks between 10-40 ppm. Both the unaged and PAV aged versions of binder D1 exhibit five distinct major peaks in their ^{13}C NMR spectra, as shown in Figure 4.33. The spectra for all tested asphalt binders were nearly identical. Therefore, only the spectrum of one representative binder is presented. The peak at 14.1 ppm is due to the methyl carbons of aliphatic side chains, and the peaks at 22.7, 31.9, and 29.1 ppm correspond to carbons in methylene units progressively further from the methyl group. The most significant peak in the aliphatic carbon area, at 29.7 ppm, is caused by the internal methylene carbons of long paraffinic chains.

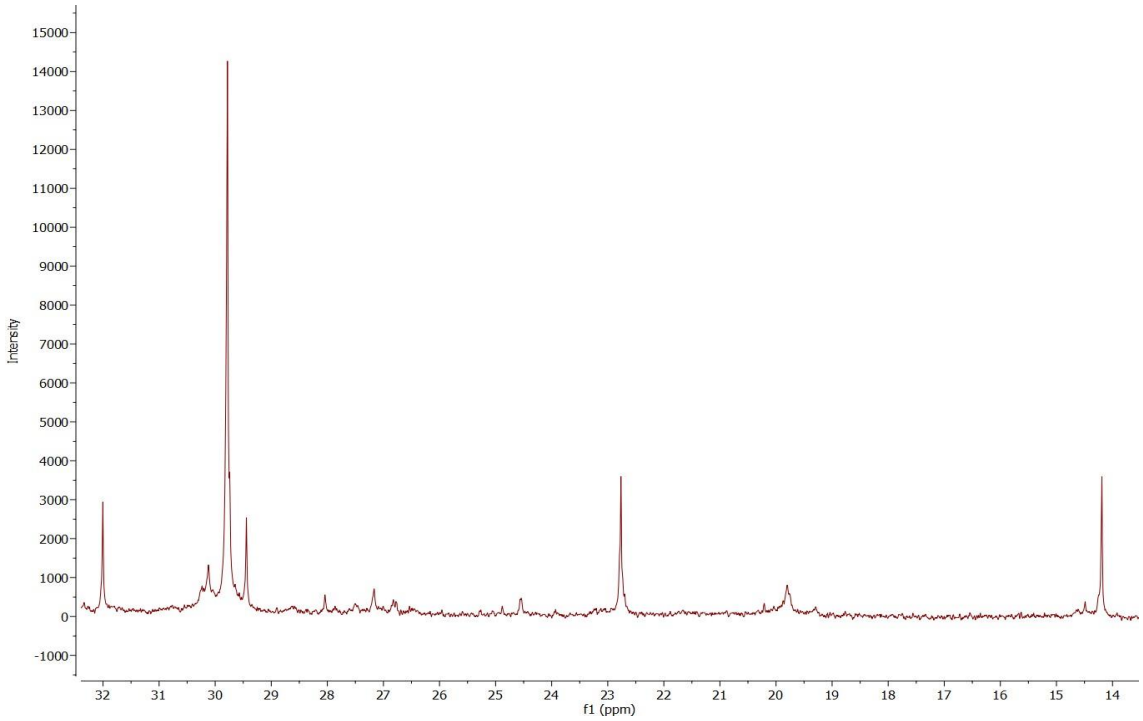

(a)

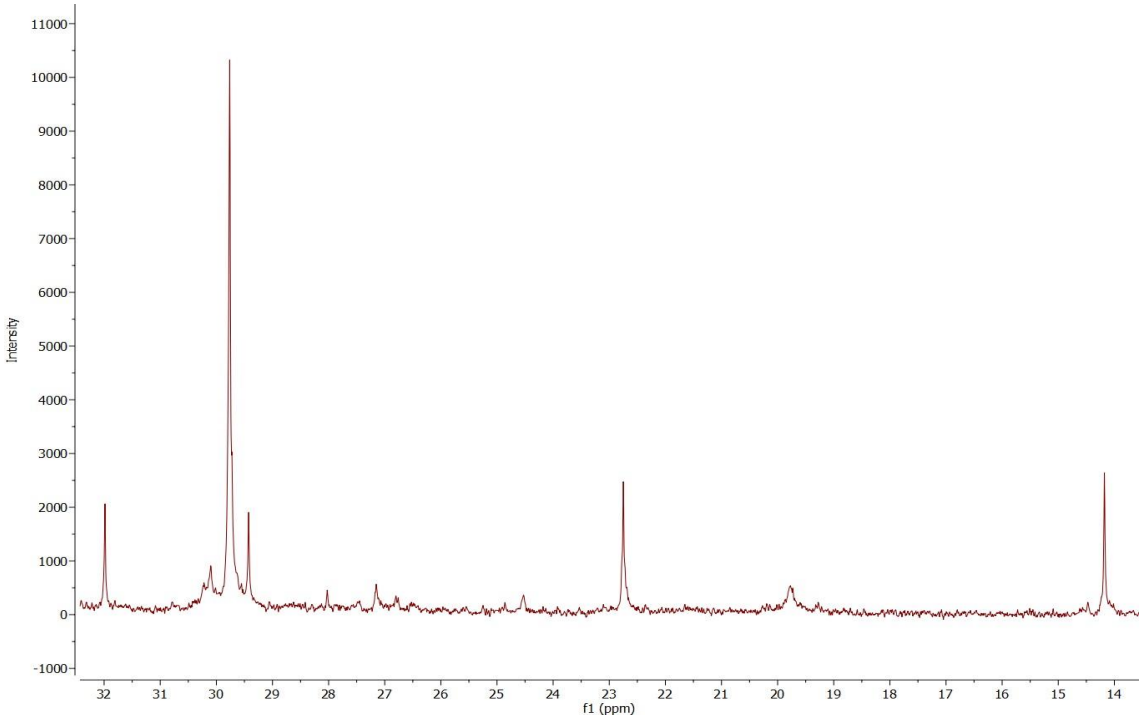

(b)

Figure 4.33: ^{13}C NMR spectrum of asphalt binder D1 (a) Unaged, and (b) PAV aged.

Clarifying the aliphatic region in ^{13}C spectra and differentiating between the methyl (CH_3), methylene (CH_2), and methine (CH) groups are the primary purposes of the DEPT test. Figure 4.34 displays the DEPT-135 spectra of binder D1 in two different oxidation states: unaged and PAV aged. Since the spectra for all tested asphalt binders were nearly identical, only the spectrum of one representative binder is presented. As predicted, the carbons in the methylene units at 22.7, 31.9, 29.1, and 29.7 ppm of long paraffinic chains are downward. The peaks at 14.1 ppm and 19.71 ppm correspond to methyl peaks, and methyl branches on a straight methylene backbone are upward.

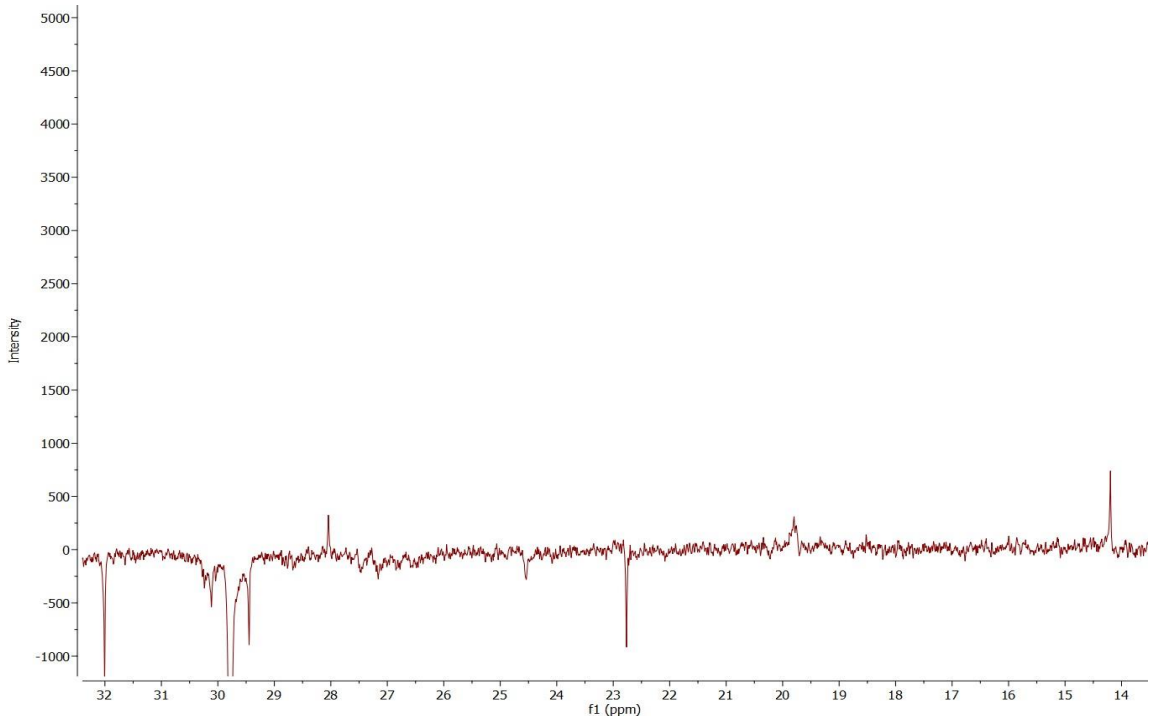

(a)

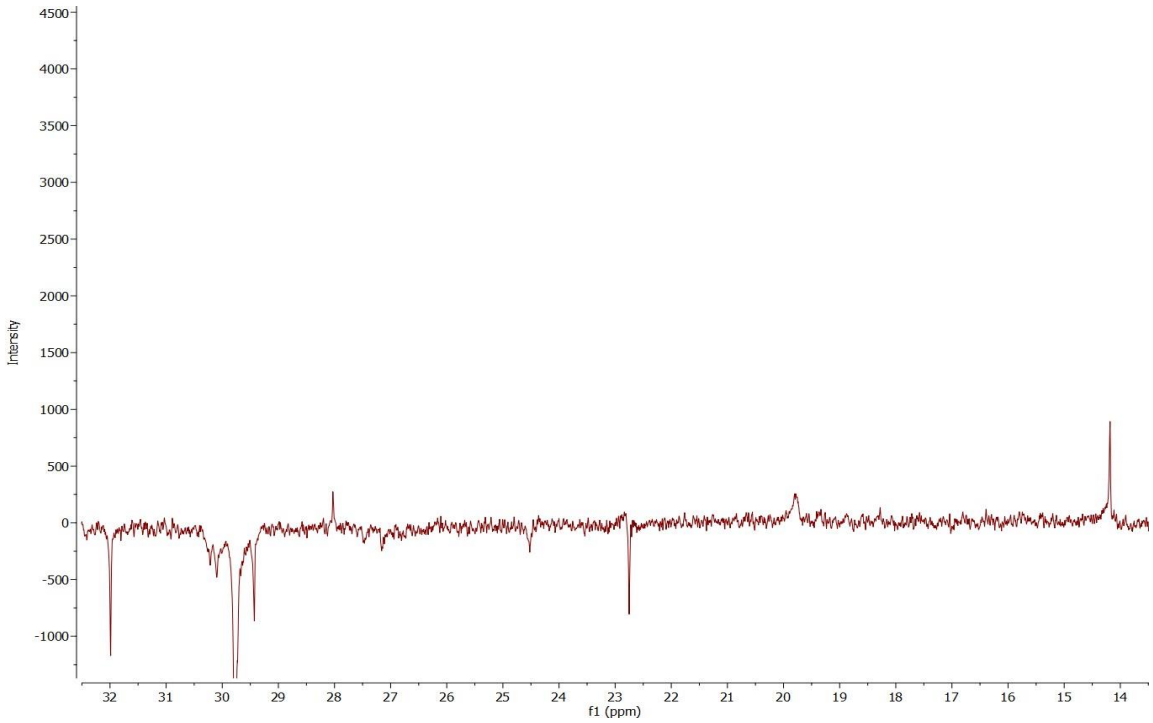

(b)

Figure 4.34: DEPT-135 NMR spectrum of asphalt binder D1 (a) Unaged, and (b) PAV aged.

4.6.2.2 Comparison and Analysis of NMR Data

Identifying the differences between the ^{13}C spectra of different asphalt binders and assessing the impact of the binder aging on the ^{13}C chemical shift is challenging when using only the naked eye. As a result, Figure 4.35 displays the ratio of methylene at various positions to the 14.1 ppm methyl peak. The ratio represents the relative average length of a methyl group terminated straight methylene chain.

In ^{13}C NMR spectroscopy, the intensity of a particular peak does not directly correspond to the number of such nuclei in the molecule. This means that the area under the peak is not proportional to the quantity of these nuclei present in the molecule. This phenomenon is due to the Nuclear Overhauser Enhancement (NOE) Effect, which occurs by the influence of adjacent ^{1}H on ^{13}C, leading to a substantial alteration in sensitivity. However, its effect on different types of carbon is inconsistent and could result in the spectrum's intensity that is not proportional to the carbon amount. Therefore, the average length derived from ^{13}C NMR for a methyl group terminated straight methylene chain is a relative measure, not an absolute one.

According to Figure 4.35, in the average molecular structure of the asphalt binder, oxidative aging has less of an impact on the contents of methylene carbons next to the methyl functional group than it does on the internal methylene carbons of long paraffinic chains. Furthermore, the content of internal methylene carbons in long paraffinic chains amongst different asphalt binders varies significantly when compared to other carbon types. The difference brought about by oxidation, however, was noticeably less than the difference brought about by the source of the asphalt binder. The use of the NMR technique was unable to establish a definitive pattern regarding the impact of oxidation on the crystallizable fractions in the asphalt binder.

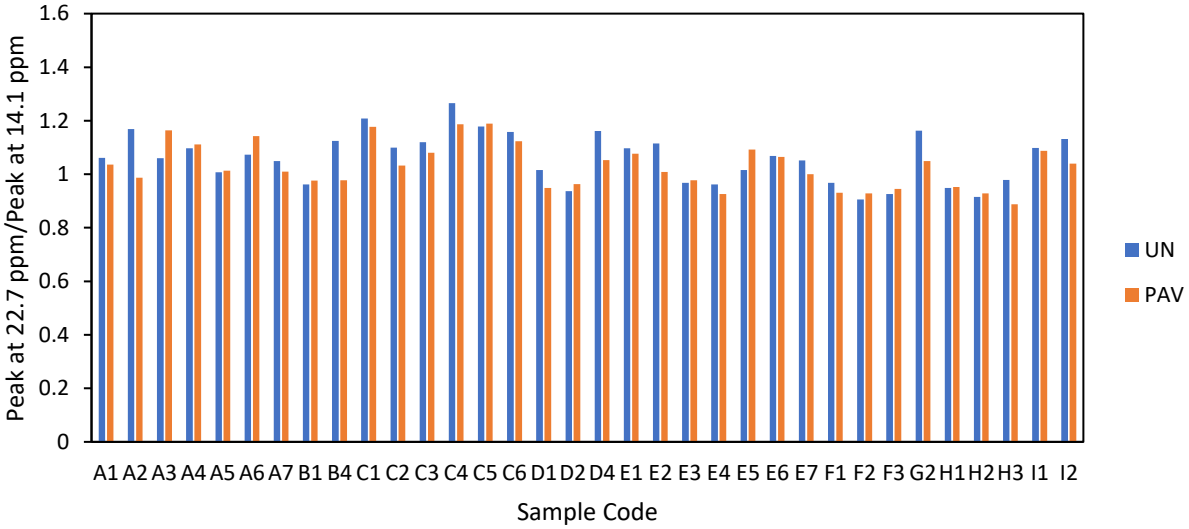

(a)

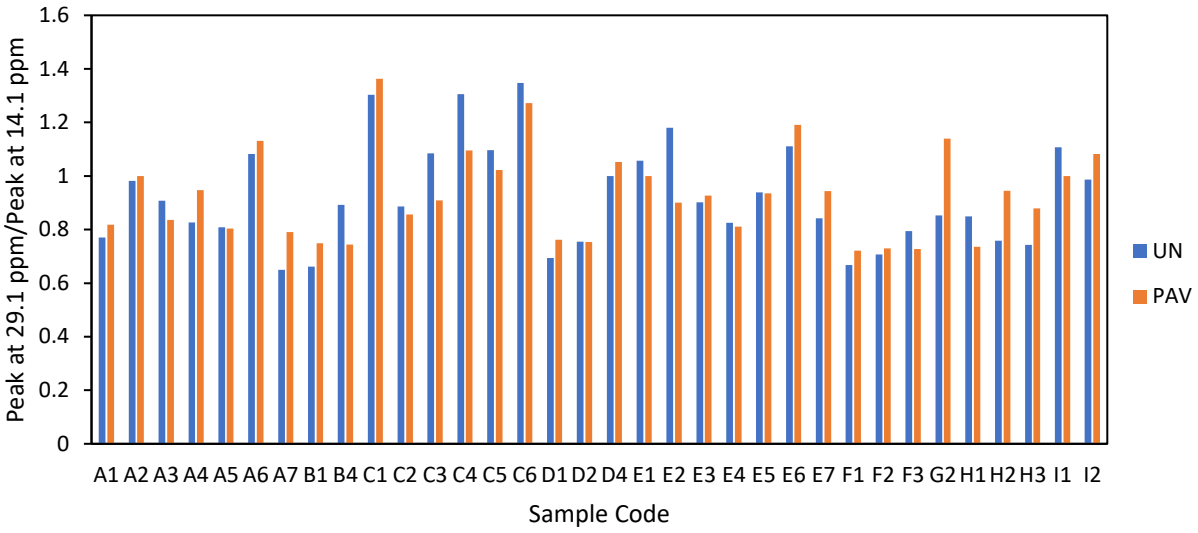
Peak at 29.1 ppm/Peak at 14.1 ppm
1.6
1.4
1.2
1
0.8
0.6
0.4
0.2
0
A1 A2 A3 A4 A5 A6 A7 B1 B4 C1 C2 C3 C4 C5 C6 D1 D2 D4 E1 E2 E3 E4 E5 E6 E7 F1 F2 F3 G2 H1 H2 H3 I1 I2
Sample Code
UN
PAV

(b)

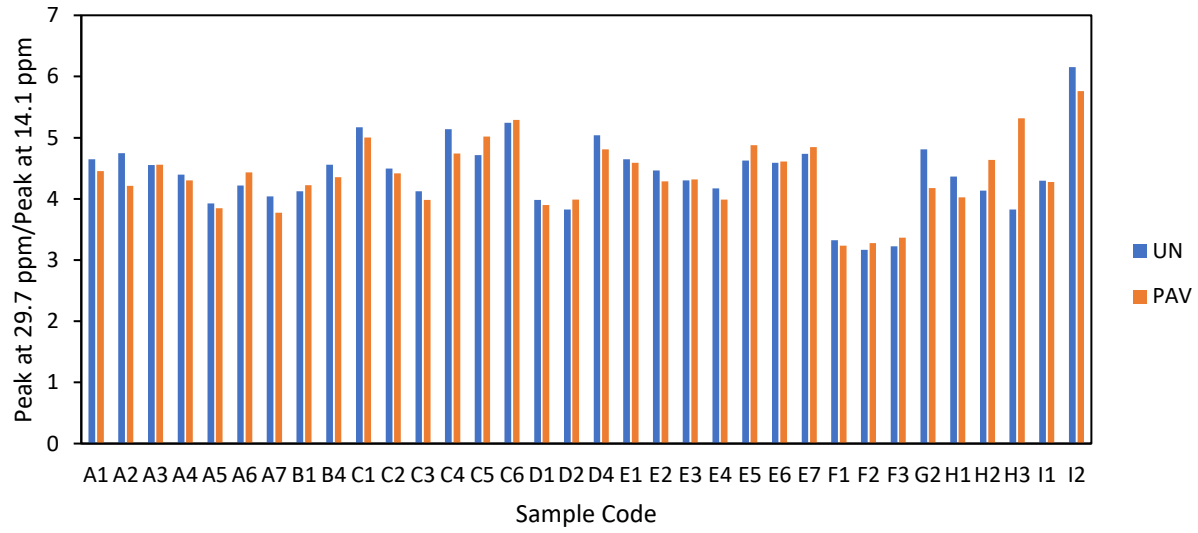
Peak at 29.7 ppm/Peak at 14.1 ppm
7
6
5
4
3
2
1
0
A1 A2 A3 A4 A5 A6 A7 B1 B4 C1 C2 C3 C4 C5 C6 D1 D2 D4 E1 E2 E3 E4 E5 E6 E7 F1 F2 F3 G2 H1 H2 H3 I1 I2
Sample Code
UN
PAV

(c)

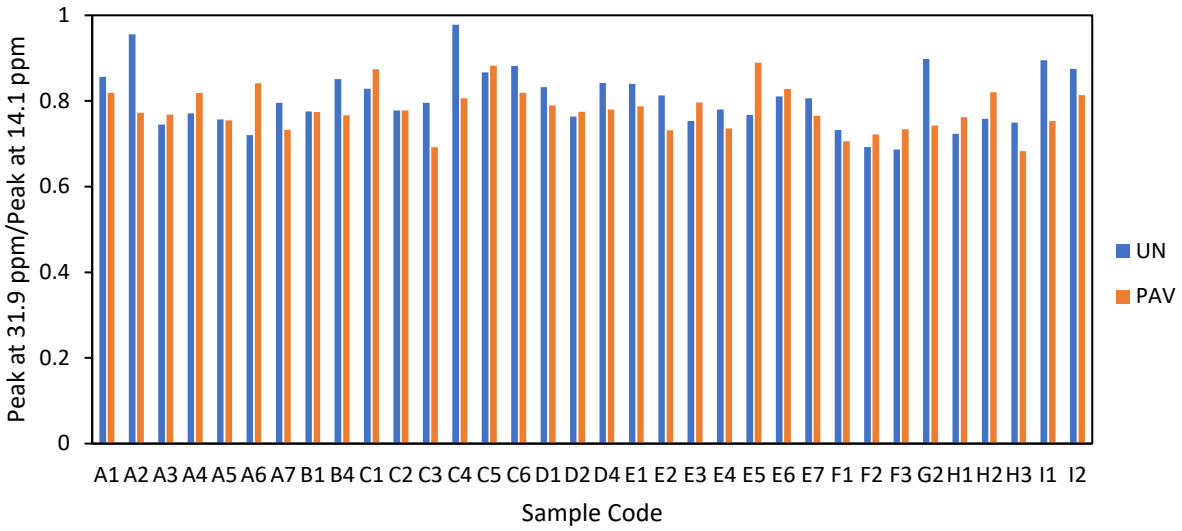

(d)

Figure 4.35: Ratio of carbons from 13C NMR for asphalt binders. (a) Peak at 22.7 ppm/Peak at 14.1 ppm (b) Peak at 29.1 ppm/Peak at 14.1 ppm (c) Peak at 29.7 ppm/Peak at 14.1 ppm (d) Peak at 31.9 ppm/Peak at 14.1 ppm.

4.6.2.3 Correlation Analysis of NMR Results with BBR, EBBR, and DENT Tests

Figure 4.36 is employed to examine if there is a correlation between the relative average length of a long paraffinic internal methylene chain, as determined by NMR, and indicators obtained from the BBR, EBBR, and DENT test methods. A moderate correlation (R^2 value of 0.52) is observed between the NMR signal and the LTPG from the BBR method (Figure 4.36 (a)). The LLTPG obtained from the EBBR method has a lower correlation (R^2 value of 0.45) with the relative average length of the internal methylene chain obtained from NMR (Figure 4.36 (b)). The CTOD from the DENT test shows the least correlation (R^2 value of 0.37) (Figure 4.36 (c)).

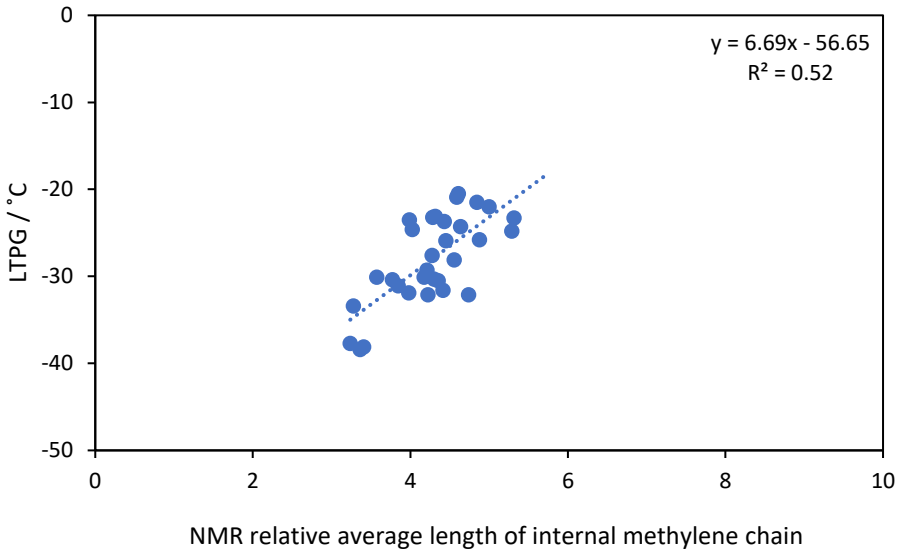
y = 6.69x - 56.65
R² = 0.52
LTPG / °C
0
-10
-20
-30
-40
-50
0
2
4
6
8
10
NMR relative average length of internal methylene chain

(a)

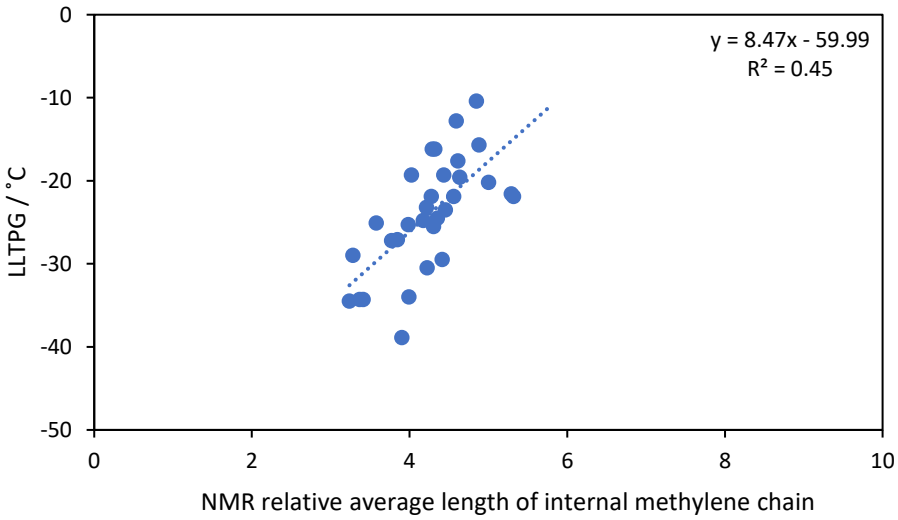
y = 8.47x - 59.99
R² = 0.45
LLTPG / °C
0
-10
-20
-30
-40
-50
0
2
4
6
8
10
NMR relative average length of internal methylene chain

(b)

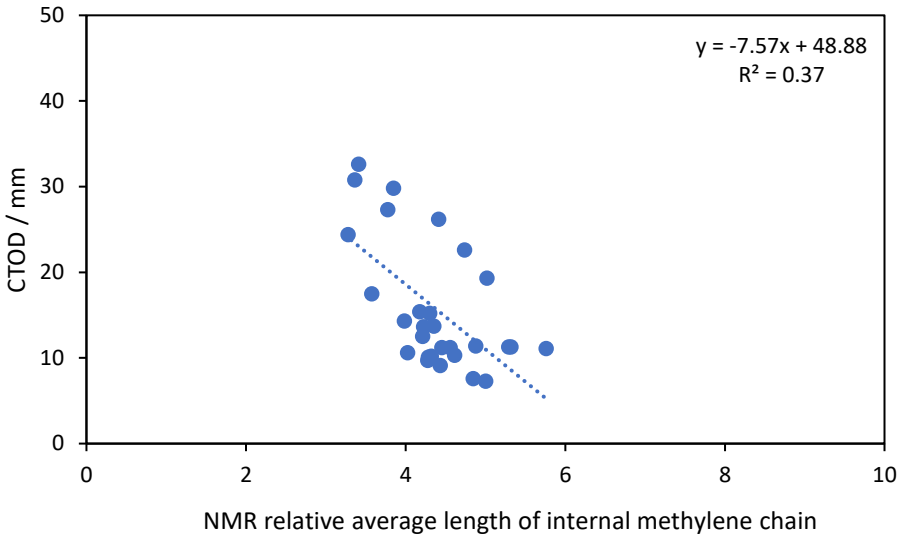

(c)

Figure 4.36: Comparison between the relative average length of straight internal methylene carbon of a long paraffinic chain terminated by a methyl group and other test parameters a) LTPG b) LLTPG c) CTOD.

4.6.3 Analysis of FTIR Spectroscopy Data

FTIR spectroscopy analyzes functional groups present in asphalt, such as carbonyl, sulfoxide, aromatic, butadiene, and styrene to indicate oxidation and polymer addition. In Figure 4.37, the carbonyl, sulfoxide, aromatic, butadiene, and styrene indexes of unaged and PAV aged binders are compared.

The carbonyl functional group is an immediate product of oxidation and thus a strong indicator of oxidative hardening. It is significant to see in Figure 4.37 (a), that for all the binders, carbonyl indexes are higher in PAV aged binders compared to unaged binders. Sulfoxides are another product of oxidation; however, they do not harden asphalt. It is important to note that for all the binders, sulfoxide indexes are higher in PAV aged binders compared to unaged binders. For all the tested binders, sulfoxide indexes (Figure 4.37 (b)) are greater than the carbonyl indexes (Figure 4.37 (a)), which is associated with the high content of sulfur in the binder [73, 81]. The formation of carbonyl and sulfoxide is associated with the increase in viscosity of the binder [9]. It has therefore been an accepted criterion for monitoring oxidative hardening [28].

High aromatic levels in asphalt, which are the lowest molecular weight naphthenic aromatic compounds, contribute positively to pavement performance. They form a major part of the dispersion medium for peptized asphaltenes [61]. As illustrated in Figure 4.37 (c), some binders have higher aromatic indexes in PAV aged samples, while others

have higher indexes in unaged samples. This observation suggests that the aging process impacts the aromatic indexes of asphalt binders differently. During PAV aging, the aromatic index is expected to decrease. However, some asphalt binders exhibit an increased aromatic index after PAV aging, which is unexpected. This behavior can be attributed to the calculation of these indexes relative to the methylene content in the binder. At elevated temperatures, methylene is more volatile than aromatic compounds. Consequently, during PAV aging, the loss of methylene is relatively higher compared to the loss of aromatics. As a result, the aged binders contain a relatively higher proportion of aromatic functional groups, resulting in a rise in the aromatic index after aging. It is important to note that the absolute quantity of aromatics may still be lower in these binders. Figure 4.37 (c) shows that most PAV samples have more aromatics than sulfoxides. Low aromatic levels are responsible for oxidative hardening in asphalt due to asphaltene precipitation from a continuous maltene phase when waste engine oil is added. However, a high aromatic content enhances the properties of the asphalt binder.

FTIR spectroscopy is a valuable tool for determining the levels of polymer modifiers, such as styrene butadiene styrene (SBS) and styrene butadiene (SB), in asphalt binders. The presence of these polymers is associated with improved performance of the asphalt binder. SBS, a common asphalt modifier, is known to enhance the elasticity of asphalt, thereby preventing rutting and cohesive failure [1, 61,81]. Figures 4.37 (d) and 4.37 (e) reveal the presence of butadiene and styrene in most of the tested asphalt binders from the USA, suggesting that most samples contain styrene-butadiene type polymers. However, with PAV aging, the butadiene index has decreased for the majority of tested binders, and the styrene index has decreased for half of them. The added butadiene and styrene degrade with PAV aging. However, the increase in styrene and butadiene indexes observed in some of the asphalt binders after PAV aging is attributed to the calculation of these indexes relative to the methylene quantity in the binder. At higher temperatures, the volatility of methylene is significantly greater compared to that of styrene and butadiene. Consequently, the loss of methylene during PAV aging is relatively high compared to the loss of styrene and butadiene. This results in a relatively higher quantity of styrene and butadiene in the aged binders. However, the absolute quantity might be lower for these functional groups. When compared to carbonyl, sulfoxide, and aromatic indexes, the butadiene and styrene indexes are lower for the tested asphalt binders. Thus, aging may lead to a reduced in-service performance of the binder, which implies reduced durability.

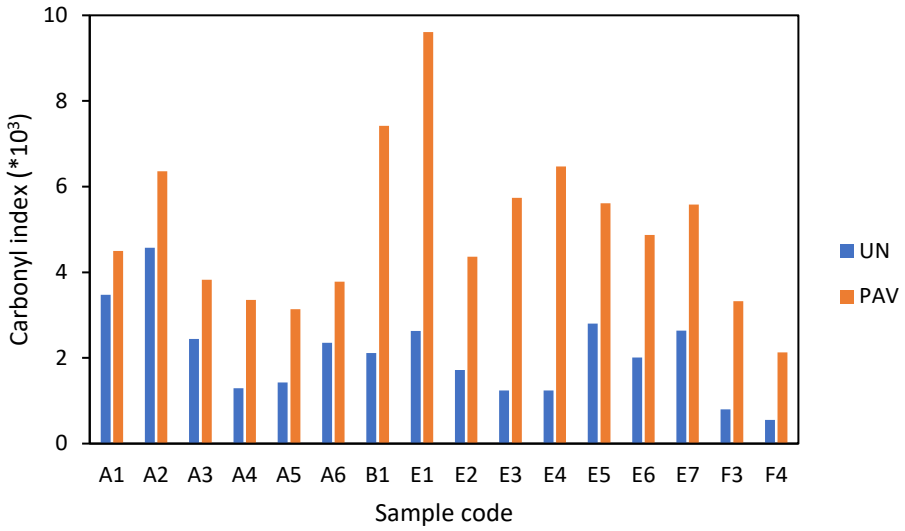
10
8
6
4
2
0
Carbonyl index (*10³)
A1 A2 A3 A4 A5 A6 B1 E1 E2 E3 E4 E5 E6 E7 F3 F4
Sample code
UN
PAV

(a)

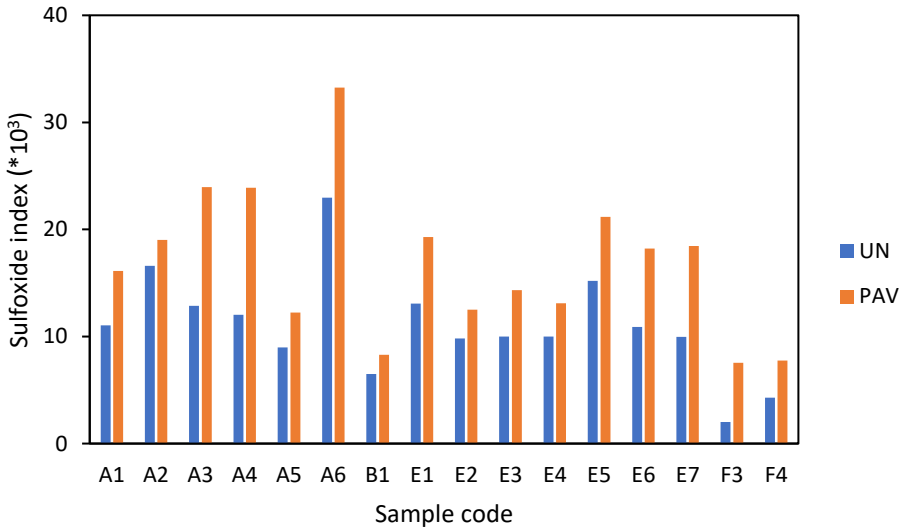
40
30
20
10
0
Sulfoxide index (*10³)
A1 A2 A3 A4 A5 A6 B1 E1 E2 E3 E4 E5 E6 E7 F3 F4
Sample code
UN
PAV

(b)

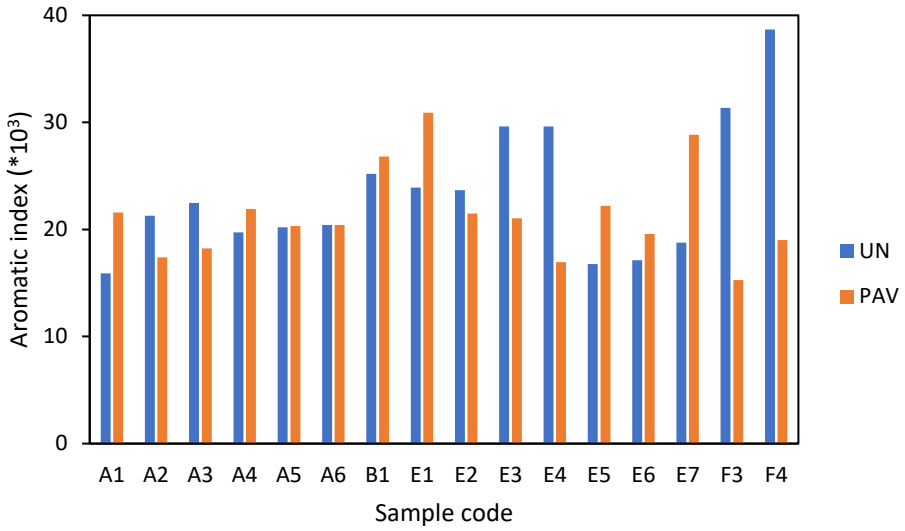
40
30
20
10
0
Aromatic index (*10³)
A1 A2 A3 A4 A5 A6 B1 E1 E2 E3 E4 E5 E6 E7 F3 F4
Sample code
UN
PAV

(c)

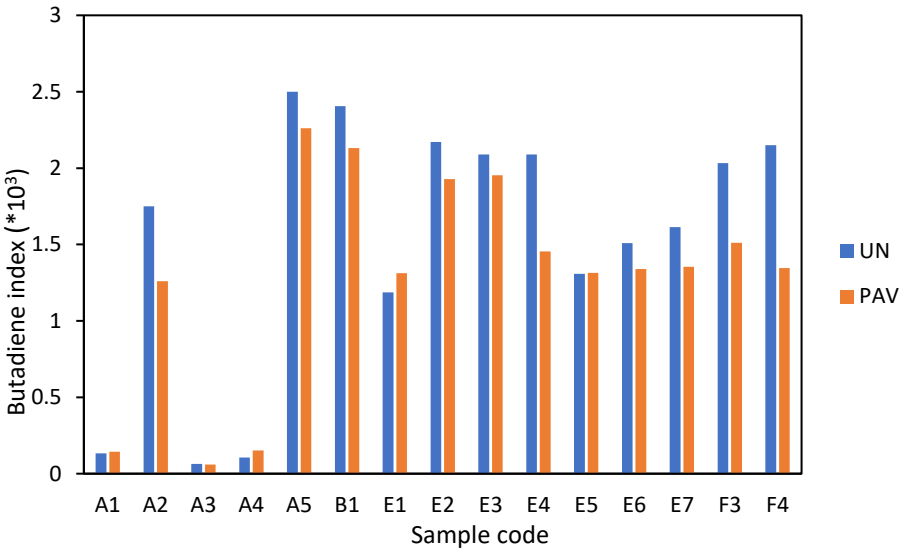
3
2.5
2
1.5
1
0.5
0
Butadiene index (*10³)
A1 A2 A3 A4 A5 B1 E1 E2 E3 E4 E5 E6 E7 F3 F4
Sample code
UN
PAV

(d)

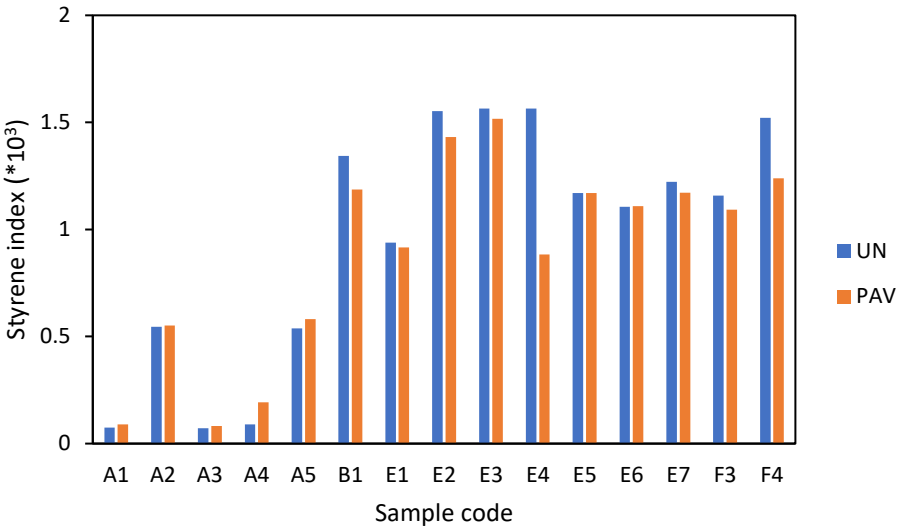

(e)

Figure 4.37: Effect of aging on a) carbonyl indexes b) sulfoxide indexes c) aromatic indexes d) butadiene indexes and e) styrene indexes.

Chapter 5

Summary and Conclusions

The summary and conclusions outlined below are a reflection of all that has been discussed in this study.

DSR test indicators such as $T_{\delta=30^\circ}$, $T_{\delta=45^\circ}$, $\Delta T_{c\delta}$, ITPG, ω_c, G_c, G_g, and R_m were obtained for asphalt samples at both slow and fast cooling rates. Each indicator had a higher correlation between slow and fast cooling rates, implying both methods are suitable for DSR testing. For $T_{\delta=30^\circ}$, $T_{\delta=45^\circ}$, $\Delta T_{c\delta}$, ITPG, ω_c, and R_m, both methods were almost equal in sensitivity. The fast cooling condition has higher sensitivity for G_c, and G_g. Considering the lower time consumption compared to slow cooling, fast cooling is more suitable for DSR testing.

$T_{\delta=30^\circ}$ and $T_{\delta=45^\circ}$ had stronger correlations for both slow and fast cooling conditions with LLTPG obtained from EBBR test. The sensitivity of $T_{\delta=30^\circ}$ and $T_{\delta=45^\circ}$ at both cooling rates was higher than that of LLTPG. Thus, $T_{\delta=30^\circ}$ and $T_{\delta=45^\circ}$ at both cooling rates are suitable to replace LLTPG for low-temperature performance grading. Since the sensitivity of fast cooling is higher than that of slow cooling, $T_{\delta=30^\circ}$ and $T_{\delta=45^\circ}$ under fast cooling condition are the more convenient specifications to replace LLTPG. ITPG had stronger correlations with LLTPG at both slow and fast cooling conditions. The sensitivity of ITPG at both cooling conditions was equal to the sensitivity of LLTPG. Thus, ITPG at both cooling conditions is suitable to replace LLTPG for low-temperature performance grading. Among the master curve parameters, only ω_c at both cooling conditions had strong colorations with LLTPG. However, the sensitivity of ω_c was lower compared to LLTPG. G_c and G_g did not correlate with LLTPG, while R_m for fast cooling had a moderate correlation with less sensitivity. Based on the observation above, none of the master curve parameters are suitable to replace LLTPG, which is used for low-temperature performance grading.

In past studies on Ontario binders, it was revealed that LLTPG from EBBR showed a high correlation with $T_{\delta=30^\circ}$, a moderate correlation with $T_{\delta=45^\circ}$, and no correlation with ITPG. Previously, it was not found that $T_{\delta=45^\circ}$ and ITPG were highly correlated with LLTPG. However, in this study, a different trend was observed for USA binders, where LLTPG was highly correlated with $T_{\delta=30^\circ}$, $T_{\delta=45^\circ}$, and ITPG. It is essential to note that these findings may not be directly applicable to Ontario binders. The observed deviation between USA and Ontario binders can be attributed to differences in hardness and stiffness, as USA binders are harder while Ontario binders are softer.

The $T_{\delta=45^\circ}$ property at both slow and fast cooling conditions has a moderate correlation with EBBR grade loss, while $T_{\delta=30^\circ}$ has weak correlations. The above behavior was different from the previous studies. The reason for the lack of stronger correlations for EBBR grade loss with $T_{\delta=30^\circ}$ and $T_{\delta=45^\circ}$ might be that the tested samples are only from USA, expanding the scope of asphalt binder elsewhere may lead to different conclusions. No correlations were observed for ITPG with EBBR grade loss. Among master curve parameters, ω_c at both cooling conditions had moderate colorations with EBBR grade loss, but the sensitivity of ω_c was less compared to EBBR grade loss. G_c, G_g, and R_M did not correlate with EBBR grade loss. These indicate that none of the master curve parameters can be used in place of EBBR grade loss, which is used for low-temperature performance grading.

The $T_{\delta=30^\circ}$ at both cooling rates has a strong correlation with CTOD from the DENT test, but the sensitivity of the $T_{\delta=30^\circ}$ was less compared to CTOD. $T_{\delta=45^\circ}$ and ITPG at both cooling conditions had moderate correlations with CTOD; however, the sensitivity of $T_{\delta=45^\circ}$ and ITPG was less compared to CTOD. The behavior mentioned above is different from earlier research which was conducted on Ontario asphalt binders. The reason for this deviation might be that the tested samples are from nine agencies in the USA, which represents a wider range of asphalt binders with modifications that are different from those in Canada. Stronger correlations were present at slow cooling conditions between ω_c and CTOD, while moderate correlations were present between ω_c and CTOD at fast cooling conditions. Compared to CTOD, the sensitivity of ω_c was less at both cooling conditions. G_c did not have correlations with CTOD. For G_g, slow cooling did not have correlations with CTOD, but fast cooling had a moderate correlation. But in terms of sensitivity, G_g was less sensitive. CTOD did not have reasonable correlations with R_m. Thus, none of the master curve parameters are suitable to surrogate CTOD to determine fracture performance. Further testing for a larger sample size in the USA might be helpful to confirm these observations.

Thermo-reversible aging of asphalt binders occurs due to oil exudation and can be monitored by EBBR, while DSR is unable to do so. During the EBBR test, liquid oily components are expelled from the asphalt beam into the ethanol bath through exudation, resulting in a grade loss. The grade loss indicator from the EBBR test enables monitoring the effect of thermo-reversible aging on asphalt binders. Moreover, this method is well suited for identifying low quality asphalt binders containing low molecular weight oils. Exudation experiments have shown that the exudable components of asphalt primarily comprise paraffinic oils, commonly employed as additives. In contrast, the DSR

test has a disadvantage in that it cannot assess thermo-reversible aging. This limitation arises because the DSR test is rapid and conducted between two metal plates, which hinders oil exudation during testing.

Overlapping Black space diagrams at slow and fast cooling conditions indicate that the asphalt sample shows almost the same rheological behavior at both cooling conditions. Hence, Black space diagrams could be used to compare the performance similarities between slow and fast cooling in DSR testing.

The collapse of road networks is mostly caused by the increasing physical hardening and reduced resiliency of asphalt pavements, which are caused by the presence of REOB in asphalt pavements. Most of the examined asphalt samples contain zinc and molybdenum, which indicates the addition of REOB in the USA. For cold regions in the USA, special attention is suggested to be paid to banning the use of REOB.

For all the tested asphalt samples, five distinct peaks were obtained for ^{13}C NMR. A moderate correlation was present between the LTPG parameters obtained from the BBR and the relative average length of a long paraffinic internal methylene chain obtained from NMR.

FTIR was used to determine the extent of chemical oxidation by checking for the presence of various functional groups. The carbonyls and sulfoxides in the unaged binders are relatively low, the main reason is that most of the binders are from loose asphalt mixtures collected from newly paved roads. By aging the binders, the levels of the carbonyl and sulfoxide functional groups start to increase, as PAV aging shows a higher amount. It can be concluded that the chemical oxidation was more significant after the PAV aging of the samples. Aromatic, butadiene, and styrene indexes showed no consistent trend with the PAV aging as these indexes are relative.

References

1) Ma, J.; Nivitha, M. R.; Hesp, S. A. M.; Murali Krishnan, J. Validation of Empirical Changes to Asphalt Specifications Based on Phase Angle and Relaxation Properties Using Data from a Northern Ontario, Canada Pavement Trial. *Construction and Building Materials* 2023, *363*, 129776. https://doi.org/10.1016/j.conbuildmat.2022.129776.

2) Li, Y.; Hesp, S. A. M. On the Use of Empirical Phase Angle Limits for the Grading of Asphalt Binder. *Construction and Building Materials* 2022, *346*, 128413. https://doi.org/10.1016/j.conbuildmat.2022.128413.

3) Assaf, E. I.; Liu, X.; Lin, P.; Erkens, S.; Nahar, S.; Liz. Studying the Impact of Phase Behavior in the Morphology of Molecular Dynamics Models of Bitumen. *Materials & Design* 2023, *230*, 111943-111943. https://doi.org/10.1016/j.matdes.2023.111943.

4) Sörensen, A.; Wichert, B. Asphalt and Bitumen. *Ullmann's Encyclopedia of Industrial Chemistry* 2009. https://doi.org/10.1002/14356007.a03_169.pub2.

5) Kishchynskyi, S.; Nagaychuk, V.; Bezuglyi, A. Improving Quality and Durability of Bitumen and Asphalt Concrete by Modification Using Recycled Polyethylene Based Polymer Composition. *Procedia Engineering* 2016, *143*, 119-127. https://doi.org/10.1016/j.proeng.2016.06.016.

6) Nawarathna, C. Use a Typical Asphalt Binders from Alberta Oils and Sources for the Effective Recycling of Asphalt Pavement. (Masters' Dissertation, Queen's University (Canada)) 2021.

7) Redelius, P.; Soenen, H. Relation between Bitumen Chemistry and Performance. *Fuel* 2015, *140*, 34-43. https://doi.org/10.1016/j.fuel.2014.09.044.

8) Goosen, E. S.; Jenkins, K. J. Understanding Bitumen Aging through Interrelationships and Aging Ratios. *Transportation Research Record* 2023, 1-26. https://doi.org/10.1177/03611981221147519.

9) Siroma, R. S.; Nguyen, M. L.; Huard, P.; Chailleux, E. A Literature Review of Bitumen Aging: From Laboratory Procedures to Field Evaluation. *Journal of Testing and Evaluation* 2022, *50 (2)*, 1023-1044. https:// doi.org/10.1520/JTE20210235.

10) Hunter, R. N. *The Shell Bitumen Handbook, 6th Edition*; 2015. https://doi.org/10.1680/tsbh.58378.

11) Lesueur, D. The Colloidal Structure of Bitumen: Consequences on the Rheology and on the Mechanisms of Bitumen Modification. *Advances in Colloid and Interface Science* 2009, *145* (1-2), 42-82. https://doi.org/10.1016/j.cis.2008.08.011.

12) Siroma, R. S.; Nguyen, M. L.; Huard, P.; Planche, J.-P.; Adams, J. J.; Rovani, J. F.; Kumbargeri, Y. S.; Hung, Y.; Nicolaï, A.; Ziyani, L.; Chailleux, E. Asphaltene Agglomeration through Physical-Chemical and Rheological Testing. *Roads Materials and Pavement Design* 2023, 1-14. https://doi.org/10.1080/14680629.2023.2221744.

13) Hesp, S. A. M.; Soleimani, A.; Subramani, S.; Phillips, T.; Smith, D.; Marks, P.; Tam, K. C. Asphalt Pavement Cracking: Analysis of Extraordinary Life Cycle Variability in Eastern and Northeastern Ontario. *International Journal of Pavement Engineering* 2009, *10* (3), 209-227. https://doi.org/10.1080/10298430802343169.

14) Somuah, M. Investigative Comparison of Tank and Recovered Asphalt Samples Though Physical Performance Testing and Chemical Analysis. (Masters' Dissertation, Queen's University (Canada)) 2016.

15) Du, Y.; Chen, J.; Han, Z.; Liu, W. A Review on Solutions for Improving Rutting Resistance of Asphalt Pavement and Test Methods. *Construction and Building Materials* 2018, *168*, 893-905. https://doi.org/10.1016/j.conbuildmat.2018.02.151.

16) Pan, Y.; Guo, H.; Guan, W.; Zhao, Y. A Laboratory Evaluation of Factors Affecting Rutting Resistance of Asphalt Mixtures Using Wheel Tracking Test. *Case Studies in Construction Materials* 2023, *18*, e02148. https://doi.org/10.1016/j.cscm.2023.e02148.

17) *Distress Identification Manual for the Long-Term Pavement Performance Program*; 2014. https://highways.dot.gov/media/4421.

18) Kaseer, F.; Martin, A. E.; Arámbula-Mercado, E. Relationship between Rheological Indices and Cracking Performance of Virgin, Recycled, and Rejuvenated Asphalt Binders and Mixtures. *Transportation Research Record: Journal of the Transportation Research Board* 2021, *2675* (9), 93-109. https://doi.org/10.1177/03611981211007479.

19) https://pavementinteractive.org/reference-desk/pavement-management/pavement-distresses/rutting/, 13/04/2023, at 12.40 PM.

20) Adeyeye, A. Evaluation of Phase Angle as a Practical Parameter for Low-Temperature Specification Grading of Asphalt Binders. (Masters' Dissertation, Queen's University (Canada)) 2021.

21) Christensen, D. W.; Tran, N.; National Cooperative Highway Research Program; Transportation Research Board; National Academies of Sciences, Engineering, and Medicine. Relationships between the Fatigue Properties of Asphalt Binders and the Fatigue Performance of Asphalt Mixtures; *Transportation Research Board*: Washington, D.C., 2021.

22) Cucalon, G. L.; Kaseer, F.; Arámbula-Mercado, E.; Epps Martin, A.; Morian, N.; Pournoman, S.; Hajj, E. The Crossover Temperature: Significance and Application towards Engineering Balanced Recycled Binder Blends. *Road Materials and Pavement Design* 2018, *20* (6), 1391-1412. https://doi.org/10.1080/14680629.2018.1447504.

23) https://www.researchgate.net/figure/Fatigue-cracking-encountered-on-pavement_fig6_305699066, 08/06/2023, at 2.10 PM

24) Yee, P.; Aida, B.; Hesp, S. A. M.; Marks, P.; Tam, K. K. Analysis of Premature Low-Temperature Cracking in Three Ontario, Canada, Pavements. *Transportation Research Record* 2006, *1962* (1), 44-51. https://doi.org/10.1177/0361198106196200106.

25) Isacsson, U.; Zeng, H. Relationships between Bitumen Chemistry and Low-Temperature Behaviour of Asphalt. *Construction and Building Materials* 1997, *11* (2), 83-91. https://doi.org/10.1016/s0950-0618(97)00008-1.

26) Brown, E.; Kandhal, P.; Zhang, J. *Performance Testing for Hot Mix Asphalt*; 2001. https://www.eng.auburn.edu/research/centers/ncat/files/technical-reports/rep01-05.pdf.

27) Zhang, J.; Airey, G. D.; Grenfell, J.; Apeagyei, A. K. Moisture Sensitivity Examination of Asphalt Mixtures Using Thermodynamic, Direct Adhesion Peel and Compacted Mixture Mechanical Tests. *Road Materials and Pavement Design* 2016, *19* (1), 120-138. https://doi.org/10.1080/14680629.2016.1249510.

28) Asiedu, E. Investigating and Understanding the Effects of Reclaimed Asphalt Pavement and Shingles on the Rheology and Performance Grading of Asphalt Cement. (Masters' Dissertation, Queen's University (Canada)) 2020.

29) Khusainov, Emil, Use of a Phase Angle in Lieu of Critical Crack Tip Opening Displacement for Asphalt Binder Specification. (Masters' Dissertation, Queen's University (Canada)) 2021.

30) Test Method for Softening Point of Bitumen (Ring-And-Ball Apparatus), 2014. https://doi.org/10.1520/d0036_d0036m-14e01.

31) Ou Zhao, M.; Hesp, S. A. M. Performance Grading of the Lamont, Alberta C-SHRP Pavement Trial Binders. *International Journal of Pavement Engineering* 2006, *7* (3), 199-211. https://doi.org/10.1080/10298430600715667.

32) Khan, A. N.; Hesp, S. A. M. Comparison between Thermal, Rheological and Failure Properties for the Performance Grading of Asphalt Cements. *Construction and Building Materials* 2019, *220*, 196-205. https://doi.org/10.1016/j.conbuildmat.2019.05.187.

33) Li, Y.; Romero, P.; Sudbury, D. S.; Allen, C. Repeatability and Reproducibility of Low-Temperature Testing of Asphalt Mixtures Using a Modified Bending Beam Rheometer. *Cold Regions Engineering* 2015. https://doi.org/10.1061/9780784479315.020.

34) He, H.; Dyck, M. F.; Horton, R.; Li, M.; Jin, H.; Si, B. Distributed Temperature Sensing for Soil Physical Measurements and its Similarity to Heat Pulse Method. *Advances in Agronomy* 2018, 173-230. https://doi.org/10.1016/bs.agron.2017.11.003.

35) Khan, A. N.; Akentuna, M.; Pan, P.; Hesp, S. A. M. Repeatability, Reproducibility, and Sensitivity Assessments of Thermal and Fatigue Cracking Acceptance Criteria for Asphalt Cement. *Construction and Building Materials* 2020, *243*, 117956. https://doi.org/10.1016/j.conbuildmat.2019.117956.

36) Ding, J.; Jeong, J.; Lee, K.; Underwood. B. S.; Kim. Y. R.; Castorena, C. Repeatability and Reproducibility Analysis for Functional Test Results from Asphalt Mixture Performance Tester Cyclic Fatigue Test. *Transportation Research Record* 2023, *2677* (9), 539-554. https://doi.org/10.1177/03611981231159409.

37) Villegas-Villegas, R. E.; Baldi-Sevilla, A.; Aguiar-Moya, J. P.; Loria-Salazar, L.; Arguello, F. M. Relationship between Crossover Modulus and Asphalt Chemistry to Oxidation Process Based on the RHEO^{+} Method. *Road Materials and Pavement Design* 2023, 1-12. https://doi.org/10.1080/14680629.2023.2203758.

38) Anderson, D.; Christensen, D.; Bahia, H.; Dongre, R.; Sharma, M.; Antle, C.; Button, J. *Binder Characterization and Evaluation Volume 3: Physical Characterization* 1994 https://onlinepubs.trb.org/onlinepubs/shrp/SHRP-A-369.pdf.

39) Paliukaitė, M; Assuras, M.; Silva, S. C.; Ding, H.; Gotame, Y.; Nie, Y.; Ubaid, I; Hesp, S. A. M. Implementation of the Double-Edge-Notched Tension Test for Asphalt Cement Acceptance. *Transportation in Developing Economies* 2017, *3* (1). https://doi.org/10.1007/s40890-017-0034-0.

40) Ling, M.; Luo, X.; Gu, F.; Lytton, R. L. Time-Temperature-Aging-Depth Shift Functions for Dynamic Modulus Master Curves of Asphalt Mixtures. *Construction and Building Materials* 2017, *157*, 943-951. https://doi.org/10.1016/j.conbuildmat.2017.09.156.

41) Airey, G. D. State of the Art Report on Ageing Test Methods for Bituminous Pavement Materials. *International Journal of Pavement Engineering* 2003, *4* (3), 165-176. https://doi.org/10.1080/1029843042000198568.

42) Airey, G. Factors Affecting the Rheology of Polymer Modified Bitumen (PMB). *Elsevier eBooks* 2011, 238-263. https://doi.org/10.1533/9780857093721.2.238.

43) https://pavementinteractive.org/reference-desk/testing/binder-tests/pressure-aging-vessel/, 10/07/2023, at 1.30 PM.

44) Newman, J. K.; Freeman, R. B. *Evaluation of Strategic Highway Research Program (SHRP) Products for Application to Airport Pavements*. ROSA P. https://rosap.ntl.bts.gov/view/dot/41756.

45) Mukandila, E. M.; Loots, H.; P Dlamini. Principle of Dynamic Shear Rheometer Testing of Non-Standard Samples for Cohesion and Adhesion of Bituminous Road Seal Materials. *Conference on Asphalt Pavements for Southern Africa (CAPSA15), 11th, 2015, Sun City, South Africa* 2015.

46) Yusoff, N. I. M.; Chailleux, E.; Airey, G. D. A Comparative Study of the Influence of Shift Factor Equations on Master Curve Construction. *International Journal of Pavement Research and Technology* 2011, *4* (6).

47) Carret, J. C.; Falchetto, A. C.; Marasteanu, M; Benedetto, H. D.; Wistuba, M. P.; Sauzéat, C. Comparison of Rheological Parameters of Asphalt Binders Obtained from Bending Beam Rheometer and Dynamic Shear Rheometer at Low Temperatures. *Road Materials and Pavement Design*, 2015, *16* (sup1), 211-227. https://doi.org/10.1080/14680629.2015.1029696.

48) A Basic Introduction to Rheology, *Rheology and Viscosity*; 2016. https://cdn.technologynetworks.com/TN/Resources/PDF/WP160620BasicIntroRheology.pdf.

49) Kortschot, M. T.; Woodhams, R. T. Torsional Braid Analysis of Bitumen-Liquid Rubber Mixtures. *Polymer Engineering and Science* 1984, *24* (4), 252-258. https://doi.org/10.1002/pen.760240404.

50) Baumgardner, G. L.; Rowe, G. M.; Rossiter, W. J.; Wallace, T. J.; Dean, S. W. Specifications for Roofing and Industrial Asphalts Using Dynamic Shear Rheometry (DSR). *Journal of Astm International* 2007, *4* (8), 101044-101044. https://doi.org/10.1520/jai101044.

51) Soleimani, A.; Walsh, S.; Hesp, S. A. M. Asphalt Cement Loss Tangent as Surrogate Performance Indicator for Control of Thermal Cracking. *Journal of the Transportation Research Board* 2009, *2126* (1), 39-46. https://doi.org/10.3141/2126-05.

52) Abedali, A. H. Predicting Complex Shear Modulus Using Artificial Neural Networks. *Journal of Civil Engineering and Construction Technology* 2015, *6* (3), 15-26. https://doi.org/10.5897/jcect2015.0357.

53) Asgharzadeh, S. M.; Tabatabaee, N.; Naderi, K.; Partl, M. N. Evaluation of Rheological Master Curve Models for Bituminous Binders. *Materials and Structures* 2013, *48* (1-2), 393-406. https://doi.org/10.1617/s11527-013-0191-5.

54) Fried, A.; Castorena, C. Practical Methods to Construct Asphalt Binder Master Curves and Calculate Christensen–Anderson Model Parameters. *Journal of the Transportation Research Board* 2023, 036119812311692-036119812311692. https://doi.org/10.1177/03611981231169274.

55) Morian, N.; Zhu, C.; Hajj, E. Y. Rheological Indexes. *Journal of the Transportation Research Board* 2015, *2505* (1), 32-40. https://doi.org/10.3141/2505-05.

56) Yin, Y.; Huang, W.; Lv. J.; Ma, X.; Yan, J. Unified Construction of Dynamic Rheological Master Curve of Asphalts and Asphalt Mixtures. *International Journal of Civil Engineering* 2017, *16* (9), 1057-1067. https://doi.org/10.1007/s40999-017-0256-x.

57) Pellinen, T.; Witczak, M. W.; Bonaquist, R. Asphalt Mix Master Curve Construction Using Sigmoidal Fitting Function with Non-Linear Least Squares Optimization. 2003. https://doi.org/10.1061/40709(257)6.

58) Linden, M. A.; Turner, T. F.; Planche, J.-P.; Schabron, J. F.; Harnsberger, P. M. Evolution of the Crossover Modulus with Oxidative Aging. *Journal of the Transportation Research Board* 2013, *2370* (1), 76-83. https://doi.org/10.3141/2370-10.

59) Chailleux, E.; Ramond, G.; Such, C.; Roche, C. D. L. A Mathematical Based Master Curve Construction Method Applied to Complex Modulus of Bituminous Materials. *Road Materials and Pavement Design* 2006, *7* (sup1), 75-92. https://doi.org/10.1080/14680629.2006.9690059.

60) Hesp, S. A. M.; Subramani, S. Another Look at the Bending Beam Rheometer for Specification Grading of Asphalt Cements. trid.trb.org. https://trid.trb.org/view/899119.

61) Ubaid, I. Physical and Chemical Performance Testing of Ontario Asphalt Pavements. (Masters' Dissertation, Queen's University (Canada)) 2016.

62) https://pavementinteractive.org/reference-desk/testing/binder-tests/bending-beam-rheometer/, 23/07/2023 at 3.50 PM.

63) Zhai, H.; Salomon, D. Evaluation of Low-Temperature Properties and the Fragility of Asphalt Binders with Non-Arrhenius Viscosity–Temperature Dependence. *Journal of the Transportation Research Board* 2005, *1901* (1), 44-51. https://doi.org/10.1177/0361198105190100106.

64) Shurvell, H; Subramani, S.; Hesp, S.; Genin, S.; Scafe, D. W. Five Year Performance Review of a Northern Ontario Pavement Trial: Validation of Ontario's Double-Edge-Notched Tension (DENT) and Extended Bending Beam Rheometer (BRR) Test Methods. 2009.

65) Campbell, S.; Ding, H.; Hesp, S. A. M., Double-Edge-Notched Tension Testing of Asphalt Mastics. *Construction and Building Materials* 2018, *166*, 87-95. https://doi.org/10.1016/j.conbuildmat.2018.01.094.

66) Andriescu, A.; Hesp, S. A. M.; Youtcheff, J. S. Essential and Plastic Works of Ductile Fracture in Asphalt Binders. *Transportation Research Record: Journal of the Transportation Research Board* 2004, *1875* (1), 1-7. https://doi.org/10.3141/1875-01.

67) Hesp, S. A. M.; Shurvell, H. F. Waste Engine Oil Residue in Asphalt Cement. 2012. https://www.researchgate.net/publication/288719991.

68) Hesp, S. A. M.; Shurvell, H. F. X-Ray Fluorescence Detection of Waste Engine Oil Residue in Asphalt and Its Effect on Cracking in Service. *International Journal of Pavement Engineering* 2010, *11* (6), 541-553. https://doi.org/10.1080/10298436.2010.488729.

69) Wang, W.; Rahman, A.; Ding, H.; Qiu, Y. Assessment of Aging Impact on Wax Crystallization in Selected Asphalt Binders. *Materials* 2022, *15* (22), 8248-8248. https://doi.org/10.3390/ma15228248.

70) Ahmad, I.; Shakirullah, M.; Rehman, H. U.; Ishaq, M.; Khan, M. A.; Shah, A. A. NMR Analysis of Cracking Products of Asphalt and Assessment of Catalyst Performance. *Energy* 2009, *34* (2), 127-133. https://doi.org/10.1016/j.energy.2008.10.008.

71) Mendes, T.; Mcgrane, M. *Binder Characterization and Evaluation by Nuclear Magnetic Resonance Spectroscopy*. https://www.trb.org/publications/shrp/SHRP-A-335.pdf.

72) Hofko, B.; Porot, L.; Cannone, A. F.; Poulikakos, L.; Huber, L.; Lu, X.; Mollenhauer, K.; Grothe, H. FTIR Spectral Analysis of Bituminous Binders: Reproducibility and Impact of Ageing Temperature. *Materials and Structures* 2018, *51* (2). https://doi.org/10.1617/s11527-018-1170-7.

73) Martin, K. L.; Davison, R. R.; Glover, C. J.; Bullin, J. A. Asphalt Aging in Texas Roads and Test Sections. *Transportation Research Record* 1990, No. 1269.

74) https://m.indiamart.com/proddetail/x-ray-fluorescence-xrf-spectrometer-3898011833.html, 15/09/2023 at 5.15 PM.

75) https://www.fishersci.com/shop/products/c-700-sample-cups-cells-31-mm-single-open-ended/11022102, 09/02/2024 at 4.27 PM.

76) https://www.orgchemboulder.com/Technique/Procedures/IR/index.shtml, 10/03/2024 at 6.05 PM.

77) Zhang, J.; Ma, J.; Hesp, S. A. M. Development of a Simple and Quantitative Oil Exudation Test for Asphalt Binder. *Construction and Building Materials* 2024, 415, 135003-135003. https://doi.org/10.1016/j.conbuildmat.2024.135003.

78) Hesp, S. A. M.; Iliuta, S.; Shirokoff, J. W. Reversible Aging in Asphalt Binders. *Energy & Fuels* 2007, 21 (2), 1112-1121. https://doi.org/10.1021/ef060463b.

79) Hesp, S. A. M.; Kodrat, I; Scafe, D.; Soleimani, A.; Subramani, S.; Whitelaw, L. Rheological Testing of Asphalt Cements Recovered from an Ontario Pavement Trial. *Sixth International Conference on Maintenance and Rehabilitation of Pavements and Technological Control (MAIREPAV6) International Society for Maintenance and Rehabilitation of Transportation Infrastructure Transportation Research Board* 2009.

80) King, G; Anderson, M.; Hanson, D.; Blankenship, P. Using Black Space Diagrams to Predict Age Induced Cracking, *7th RILEM International Conference on Cracking in Pavements. Springer Netherlands*, 2012.

81) Lin, P.; Huang, W.; Li, Y.; Tang, N.; Amirkhanian, S. N. Investigation of Influence Factors on Low Temperature Properties of SBS Modified Asphalt. *Construction and Building Materials* 2017, *154*, 609-622. https://doi.org/10.1016/j.conbuildmat.2017.06.118.